

Fall 2012

Development of bio-optical algorithms to estimate chlorophyll in the Great Salt Lake and New England lakes using in situ hyperspectral measurements

Shane Richard Bradt
University of New Hampshire, Durham

Follow this and additional works at: <https://scholars.unh.edu/dissertation>

Recommended Citation

Bradt, Shane Richard, "Development of bio-optical algorithms to estimate chlorophyll in the Great Salt Lake and New England lakes using in situ hyperspectral measurements" (2012). *Doctoral Dissertations*. 683.
<https://scholars.unh.edu/dissertation/683>

This Dissertation is brought to you for free and open access by the Student Scholarship at University of New Hampshire Scholars' Repository. It has been accepted for inclusion in Doctoral Dissertations by an authorized administrator of University of New Hampshire Scholars' Repository. For more information, please contact nicole.hentz@unh.edu.

DEVELOPMENT OF BIO-OPTICAL ALGORITHMS TO ESTIMATE
CHLOROPHYLL IN THE GREAT SALT LAKE AND NEW ENGLAND LAKES
USING *IN SITU* HYPERSPECTRAL MEASUREMENTS

BY

SHANE RICHARD BRADT

BS in Biology, Nazareth College of Rochester, 1996

MS in Zoology, University of New Hampshire, 2000

DISSERTATION

Submitted to the University of New Hampshire

in Partial Fulfillment of

the Requirements for the Degree of

Doctor of Philosophy

in

Zoology

September, 2012

UMI Number: 3533713

All rights reserved

INFORMATION TO ALL USERS

The quality of this reproduction is dependent upon the quality of the copy submitted.

In the unlikely event that the author did not send a complete manuscript and there are missing pages, these will be noted. Also, if material had to be removed, a note will indicate the deletion.



UMI 3533713

Published by ProQuest LLC 2013. Copyright in the Dissertation held by the Author.

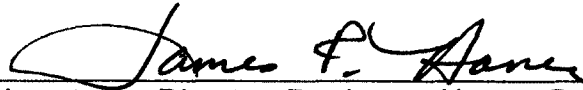
Microform Edition © ProQuest LLC.

All rights reserved. This work is protected against unauthorized copying under Title 17, United States Code.



ProQuest LLC
789 East Eisenhower Parkway
P.O. Box 1346
Ann Arbor, MI 48106-1346

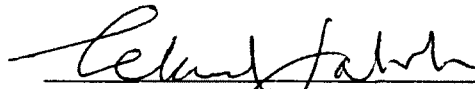
This dissertation has been examined and approved.



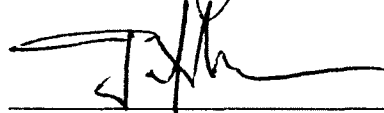
Dissertation Director, Dr. James Haney, Professor of Ecology, Evolution and Behavior and Marine, Estuarine and Freshwater Biology and Zoology



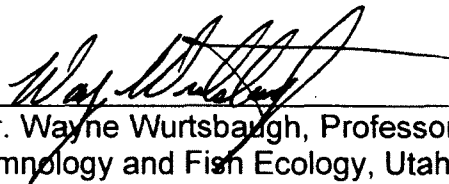

Dr. Janet Campbell, Research Professor of Marine Sciences



Dr. Leland Jahnske, Professor of Marine, Estuarine and Freshwater Biology and Plant Biology



Dr. Timothy Moore, Research Scientist, Ocean Process Analysis Lab



Dr. Wayne Wurtsbaugh, Professor of Aquatic Ecology, Limnology and Fish Ecology, Utah State University

August 14, 2012
Date

DEDICATION

This dissertation is dedicated to three groups of people, all of which had an important role in my life over the past 11 years:

To my parents, Jeana Bradt and Richard Bradt, who constantly offered their love and support, while also trying to explain my PhD over and over again to my cousins, aunts, etc.

To my advisor, Dr. James Haney, who set me adrift on this wild adventure, and who knew when to help steer the boat, and when to step back and let me paddle on my own.

To my family, my wife Gabby Bradt and my sons Charlie Bradt and Sam Bradt, for putting up my crazy schedule, for loving me and living with me every day, and for inspiring me to just finish the darn thing.

ACKNOWLEDGEMENTS

Funding for my PhD program and dissertation research was provided by:

New England Interstate Water Pollution Control Commission

National Science Foundation

NH Space Grant Consortium

Office of Naval Research / NASA

UNH Cooperative Extension

UNH Department of Zoology

UNH Graduate School

US EPA Region I Laboratory

US Geological Survey, Utah Water Science Center

Utah Division of Forestry, Fire & State Lands

Over the course of my dissertation research, a vast array of people have assisted my ways too numerous to count. I could not have gotten to this point without all of the help I received during the past 11 years, from vital courses I attended, to providing a way to get on a lake to collect measurements, to helping capture some of the very spectra I use in these pages. While I cannot possibly name all of the people and organizations to whom I am so indebted, I have listed below many of the key players who offered their assistance and support, making this dissertation possible. Thank you all, from the bottom of my heart.

Dr. James Haney – for providing the spark for and company along this journey

Dr. Timothy Moore – for your help with imagery, data processing and Matlab

Dr. Wayne Wurtsbaugh – for providing a “big lake” remote sensing study site

Dr. Janet Campbell – for starting (and continuing) my remote sensing education

Dr. Leland Jahnke – for vastly improving my understanding of algal physiology

Dr. David Naftz – for helping me visit the Great Salt Lake and Uzbekistan

Hilary Snook – for providing funding, encouragement and connections in Region I

Jeff Schloss – for your help with lakes, GIS, optics and lake management

Bob Craycraft – for help with sample processing, methods and getting on lakes

Dr. Gabriela Bradt – for hauling around the DRS and collecting so many spectra

Dr. Giorgio Dall’Olmo – for help with equipment, processing and for inspiration

Dr’s Emmanuel Boss, Curtis Mobley, Collin Roesler – for kicking my optical butt

Dr. Richard Blakemore – for not hesitating to provide funds for critical equipment

Dr. Doug Vandemark – for providing access to and parts for my first radiometer

Amanda Murby – for help with data, logistics and keeping the cyano torch lit

Sonya Carlson – for keeping the Haney lab spirit alive and well over the years

Travis Godkin – for ensuring I never had to take care of the Haney Lab *Daphnia*

Dr. Russell Congalton – for helping me learn how the other half (land) people live

TABLE OF CONTENTS

Dedication	iii
Acknowledgements	iv
Table of Contents	vi
List of Tables	xii
List of Figures	xv
Abstract	xix
Chapter I: Introduction	1
Importance of chlorophyll	2
Chlorophyll as a biological indicator	2
Chlorophyll and real-world impacts	4
Remote sensing of chlorophyll	6
Algorithm approaches	6
Sensor selection	7
Algorithm development	9
“On-lake” remote sensing	10
Ocean chlorophyll algorithms	11
Ocean color – blue to green ratio	12
Fluorescence Line Height	13
Maximum Chlorophyll Index	14
Floating Algal Index	14

Semi-analytical.....	15
Lake chlorophyll algorithms	16
Red to near-infrared band ratios	16
Chapter II: General Methodology	18
Limnology	18
Lake water sampling	18
Chlorophyll profile	19
Analysis	19
Chlorophyll concentration	19
Colored Dissolved Organic Matter	21
On-lake spectral measurements.....	21
Single radiometer.....	22
Single-radiometer field data collection	22
Single-radiometer post-processing	24
Hydrolight modeling to estimate the factor p	24
Dual radiometers	25
Dual-radiometer data collection	25
Dual-radiometer post-processing	27
Algorithms using on-lake spectra	31
Hyperspectral band ratios.....	31
Ocean color algorithms.....	32
Simulated 709 nm band in MODIS	33
Maximum Chlorophyll Index	34

Satellite 2-band algorithms	35
Algorithms not used	35
Algorithm performance analyses	36
Linear versus log-log regression.....	36
Linear regressions	37
Log-log regressions	37
Chapter III: Chlorophyll algorithms for New England lakes	52
Introduction.....	52
General description.....	52
Methodology	53
Sampling.....	53
Chlorophyll a.....	53
Dual-radiometer data collection/processing.....	55
Single-radiometer data collection/processing	56
Results.....	57
Spectral measurements.....	57
Description of dual-radiometer spectra	57
Description of single-radiometer spectra	58
Chlorophyll a.....	58
Evaluation of algorithms	59
Dual radiometer – hyperspectral band algorithms	59
Dual radiometer – MERIS algorithms	59
Dual radiometer – MODIS algorithms	60

Dual radiometer – SeaWiFS algorithms.....	60
Comparison of single- and dual-radiometer algorithms	61
Discussion	62
General observations.....	62
Round robin chlorophyll methods	62
Single- vs. dual-radiometer spectra	62
Algorithms.....	64
Hyperspectral algorithms	64
Satellite sensor algorithms.....	65
Chapter IV: Chlorophyll Algorithms for the Great Salt Lake	86
Introduction.....	86
Methodology	89
Sampling.....	89
Chlorophyll a.....	89
Dual-radiometer data collection/processing.....	90
Results.....	92
Spectral measurements.....	92
Description of dual-radiometer spectra	92
Spectral data collected under adverse conditions	92
Chlorophyll a.....	93
Evaluation of algorithms	93
Hyperspectral band algorithms	94
MERIS algorithms.....	94

MODIS algorithms	95
SeaWiFS algorithms	95
Discussion	96
General observations.....	96
Spectral data collected under adverse conditions	96
Algorithms.....	96
Hyperspectral algorithms	96
Satellite sensor algorithms.....	97
Chapter V: Summary and Conclusions	114
Ocean color algorithm band selection	114
Simulated 709 nm band for MODIS.....	116
Maximum Chlorophyll Index	119
Improved estimation of chlorophyll in study regions.....	121
Appendices.....	127
Appendix A: Remote Sensing Basics.....	128
Remote sensing as a concept	128
Spatial resolution	130
Description	130
Importance	130
Temporal Resolution.....	131
Description	131
Importance	132
Spectral resolution	133

Description	133
Importance	133
Radiometric resolution	134
Description	134
Importance	135
Appendix B: Hydrolight Settings	137
Appendix C: Chlorophyll Algorithms for New England Lakes	139
Hyperspectral linear	139
MERIS linear	140
MODIS linear	141
Single- and dual-radiometer comparison	142
Coefficients for log-log analyses	142
Appendix D: Chlorophyll Algorithms for the Great Salt Lake	143
Hyperspectral linear	143
MERIS linear	144
MODIS linear	145
Coefficients for log-log analyses	146
Literature Cited	162

LIST OF TABLES

Table 1.	Spectral and radiometric characteristics for sensors to simulate for algorithm development in the current study	17
Table 2.	Type of integrated sampling for whole lake water by project.	39
Table 3.	Details for all chlorophyll analytical methods used in this study.....	40
Table 4.	Details for chlorophyll algorithms used in this study based on hyperspectral measurements.....	41
Table 5.	Details for chlorophyll algorithms used in this study based on currently deployed satellite sensors.	42
Table 6.	Chlorophyll values for each lake site from different laboratories in the New England Lakes and Ponds project.....	67
Table 7.	Comparison of chlorophyll values from different laboratories in the New England Lakes and Ponds project.	68
Table 8.	Algorithms run with spectra from New England lakes.	69
Table 9.	Log-log regression models for predicting chlorophyll concentrations in the New England lakes sorted by RMS.	70
Table 10.	Comparison of log-log algorithms for determining chlorophyll concentrations in New England lakes analyzed with only dual-radiometer spectra and a combined data set of single- and dual-radiometer spectra.	71
Table 11.	Algorithms run with Great Salt Lake spectra.....	98
Table 12.	Log-log regression models using all spectra for predicting chlorophyll concentrations in the Great Salt Lake sorted by RMS.....	99

Table 13.	Log-log regression models using a dataset without spectra collected in the open water of Gilbert Bay on May 19-20, 2006 for predicting chlorophyll concentrations in the Great Salt Lake sorted by RMS.....	100
Table 14.	Linear regression models for predicting chlorophyll concentrations in the New England lakes using dual-radiometer spectra sorted by RMS (all chlorophyll and chlorophyll > 5.0 $\mu\text{g L}^{-1}$).....	147
Table 15.	Comparison of the best linear fit algorithms for New England lakes for each sensor type and chlorophyll range.....	148
Table 16.	Coefficients for log-log regressions for relating spectral measurements to chlorophyll concentration in New England lakes	149
Table 17.	Linear regression models for predicting chlorophyll concentrations in New England lakes using dual-radiometer spectra sorted by RMS (chlorophyll < 50 $\mu\text{g L}^{-1}$ and 5.0 $\mu\text{g L}^{-1}$ < chlorophyll < 50 $\mu\text{g L}^{-1}$).....	150
Table 18.	Comparison of linear algorithms for determining chlorophyll concentrations in New England lakes analyzed with only dual-radiometer spectra and a combined data set of single- and dual-radiometer spectra.	151
Table 19.	Linear regression models for predicting chlorophyll concentrations in the Great Salt Lake sorted by RMS (all chlorophyll and chlorophyll > 1.5 $\mu\text{g L}^{-1}$)	152
Table 20.	Comparison of the best linear fit algorithms for the Great Salt Lake for each sensor type and chlorophyll range.	153
Table 21.	Linear regression models for predicting chlorophyll concentrations in the Great Salt Lake sorted by RMS (chlorophyll < 80 $\mu\text{g L}^{-1}$ and 1.5 $\mu\text{g L}^{-1}$ < chlorophyll < 80 $\mu\text{g L}^{-1}$).....	154

Table 22. Coefficients for log-log regressions for relating spectral measurements to chlorophyll concentration the Great Salt Lake..... 155

LIST OF FIGURES

Figure 1.	Left half of schematic flow diagram for data collection and calculations for dual-radiometer measurements.....	43
Figure 2.	Right half of schematic flow diagram for data collection and calculations for dual-radiometer measurements.....	44
Figure 3.	Simulated satellite bands were produced for each reflectance spectra for use in algorithm development.....	45
Figure 4.	Algorithm band locations for several 2-band hyperspectral algorithms (Table 4, A-C).	46
Figure 5.	Algorithm band locations for several 2-band hyperspectral algorithms (Table 4, D-G).	47
Figure 6.	Algorithm band locations for 3-band hyperspectral algorithms (Table 4, H-K).	48
Figure 7.	Algorithm band locations for operationally deployed ocean chlorophyll algorithms (Table 5, L-N).....	49
Figure 8.	Relationship between MERIS bands at 754 nm and 709 nm.	50
Figure 9.	Algorithm band locations for the Maximum Chlorophyll Index (MCI) algorithms (Table 5, O-S).	51
Figure 10.	Sampling sites for New England Lakes from 2002 to 2009.	72
Figure 11.	Comparison of chlorophyll concentrations determined by the Vermont Department of Environmental Conservation (VT) and the University of New Hampshire (UNH).	73
Figure 12.	Comparison of single-radiometer and dual-radiometer spectra using three chlorophyll algorithms.	74

Figure 13. Hyperspectral reflectance spectra taken in New England lakes with the dual-radiometer system from 2005 to 2009.	75
Figure 14. Average value and standard deviation for hyperspectral reflectance spectra taken of New England Lakes with the dual-radiometer system from 2005 to 2009.	76
Figure 15. Examples of spectra collected from CDOM-rich New England lakes.	77
Figure 16. Hyperspectral reflectance spectra taken in New England lakes with the single-radiometer system from 2002 to 2004.	78
Figure 17. Average value and standard deviation for hyperspectral reflectance spectra taken of New England Lakes with the single-radiometer system from 2002 to 2004.	79
Figure 18. Chlorophyll concentrations shown in $\mu\text{g L}^{-1}$ for New England Lake site visited from 2002 to 2009.	80
Figure 19. Histogram of extracted chlorophyll concentrations for lake sites on New England Lakes.	81
Figure 20. RMS values for chlorophyll estimation algorithms for New England lakes using hyperspectral bands and MERIS bands.	82
Figure 21. Best log-log regression models using hyperspectral bands for predicting chlorophyll concentrations in the New England lakes.	83
Figure 22. Best log-log regression models using satellite sensor bands for predicting chlorophyll in New England lakes.	84
Figure 23. RMS values for chlorophyll estimation algorithms for New England lakes using MODIS bands and SeaWiFS bands.	85
Figure 24. National Agriculture Imagery Program real color image of the Great Salt Lake captured in summer 2006 by aircraft and displayed at a resolution of 30 m.	101

Figure 25. Sampling sites on the Great Salt Lake in Farmington and Gilbert Bays from May 31 to June 3, 2005.	102
Figure 26. Sampling sites on the Great Salt Lake in Farmington and Gilbert Bays from May 17 to May 20, 2006.	103
Figure 27. Sampling sites on the Great Salt Lake in Farmington and Gilbert Bays from November 30 to December 2, 2006.	104
Figure 28. Hyperspectral reflectance spectra taken with the dual-radiometer system on the Great Salt Lake in 2005 and 2006.	105
Figure 29. Average value and standard deviation for hyperspectral reflectance spectra taken with the dual-radiometer system on the Great Salt Lake in 2005 and 2006.	106
Figure 30. Demonstration of the effect of excluding from algorithm development the open water Gilbert Bay spectra collected in May 2006.	107
Figure 31. Plot of RMS reduction produced when using restricted dataset compared to the same algorithms using all data for chlorophyll concentration estimation algorithms for Great Salt Lake for each sensor type.	108
Figure 32. Histogram of extracted chlorophyll concentrations for lake sites on the Great Salt Lake.	109
Figure 33. RMS values for chlorophyll estimation algorithms for The Great Salt Lake using hyperspectral bands and MERIS bands.	110
Figure 34. Best log-log regression models using 3 nm bands for predicting chlorophyll concentrations in the Great Salt Lake.	111
Figure 35. Best log-log regression models using satellite sensor bands for predicting chlorophyll in the Great Salt Lake.	112
Figure 36. RMS values for chlorophyll estimation algorithms for The Great Salt Lake using MODIS bands and SeaWiFS bands.	113

Figure 37. A comparison of the standard MODIS OC3 algorithm with a MODIS OC algorithm optimized for the Great Salt Lake using the restricted dataset.	124
Figure 38. A comparison of chlorophyll maps derived from a MODIS Aqua image of the Great Salt Lake from September 28, 2006 using standard MODIS OC3 algorithm and MODIS OC algorithm optimized for the Great Salt Lake.	125
Figure 39. Satellite-derived chlorophyll concentration estimates over time for five locations in the Great Salt Lake in 2006.	126
Figure 40. RMS values for linear chlorophyll estimation algorithms for New England lakes.	156
Figure 41. Best linear regression models using hyperspectral bands for predicting chlorophyll concentrations in New England lakes.....	157
Figure 42. Best linear regression models using satellite sensor bands for predicting chlorophyll concentrations in the New England lakes.	158
Figure 43. RMS values for linear chlorophyll estimation algorithms for the Great Salt Lake.	159
Figure 44. Best linear regression models using hyperspectral bands for predicting chlorophyll concentrations in the Great Salt Lake.....	160
Figure 45. Best linear regression models using satellite sensor bands for predicting chlorophyll concentrations in the Great Salt Lake.	161

ABSTRACT
DEVELOPMENT OF BIO-OPTICAL ALGORITHMS TO ESTIMATE
CHLOROPHYLL IN THE GREAT SALT LAKE AND NEW ENGLAND LAKES
USING *IN SITU* HYPERSPECTRAL MEASUREMENTS

by

Shane Richard Bradt

University of New Hampshire, September, 2012

Chlorophyll is widely used to evaluate lake water quality, effectively integrating the chemical, physical and biological state of a lake. Assessment of chlorophyll conditions in lakes can be greatly enhanced by the use of remote sensing, allowing information to be gathered at spatial and temporal scales not possible with traditional limnological sampling methods. In order for remote sensing methods to provide accurate estimates of chlorophyll concentration, algorithms need to be developed with high-quality spectral data paired with water quality measurements and optimized for regional lake differences.

In this study, *in situ* hyperspectral optical measurements were used to develop algorithms to estimate chlorophyll for the Great Salt Lake and New England lakes. The spectral data were used to mimic bands utilized by the MODIS, MERIS, and SeaWiFS sensors, as well as for a theoretical hyperspectral sensor

with 3-nm wide bands, providing the capability to evaluate algorithm performance in all of these sensors. In addition to the traditional bands used in these algorithms, alternate band combinations were examined for both ocean color chlorophyll (OC) and maximum chlorophyll index (MCI) algorithms. A simulated 709 nm band was created for MODIS using the 754 nm band, providing a method for testing MODIS with algorithms relying on the key 705 nm to 715 nm wavelength range.

In New England lakes, the most effective algorithm for hyperspectral bands (RMS = 0.206, in log decades) and MERIS (RMS = 0.218) was a version of MCI. For MODIS and SeaWiFS, the most effective algorithm used an OC approach with 489 nm as the blue band, yielding an RMS of 0.242 and 0.231, respectively. In the Great Salt Lake, the most effective algorithms for hyperspectral bands and MERIS were based on a single ratio of 709 nm / 675 nm, providing an RMS of 0.236 and 0.249, respectively. For MODIS and SeaWiFS, the most effective algorithm was the OC method using 489 nm as the blue band, which resulted in an RMS of 0.246 and 0.255, respectively.

CHAPTER I

INTRODUCTION

This study represents the first comprehensive chlorophyll algorithm development for both the Great Salt Lake and New England lakes. The use of on-lake remote sensing methodology, unfettered by clouds and atmospheric interference, is a tested, successful approach which proved useful for these study locations. In the approach used here, *in situ* hyperspectral measurements were used to both determine the optimal bands for chlorophyll algorithms in these lakes, as well as to simulate satellite bands (past, present and future) and test methods that can be employed in the field. The algorithms developed in this study for satellites can be used immediately as part of an imagery-processing program, while the algorithms developed using the hyperspectral bands can be deployed in on-lake systems or used to advocate for specific bands in future lake-focused satellite sensors. The techniques described in this work offer the potential to increase the spatial and temporal resolution of chlorophyll concentration data in the Great Salt Lake and New England Lakes, thus providing an opportunity to improve management of these important systems.

Importance of chlorophyll

Chlorophyll as a biological indicator

Lakes fill an important ecological role in our landscape, serving as a critical part of global water and climate cycles (Oki and Kanae 2006; Williamson et al. 2009), as well as an important source of biodiversity (Strayer and Dudgeon 2010; Vadeboncoeur et al. 2011). Lakes also have an important societal role, driving economic activity, by providing recreational opportunities and a source of drinking and irrigation water.

Due to the myriad array of important services provided by lakes, much effort has been put into creating metrics by which to judge their ecological health. The perfect environmental evaluation method would take into account all physical, chemical and biological conditions in a lake. However, logistical realities have caused researchers and managers to focus on characteristics which are relatively easy to sample, while providing maximal insight into lake conditions.

Lake ecosystem dynamics are driven both by top-down effects (such as fish predation) and bottom-up effects (such as the promotion of algal growth by nutrient additions). Most trophic status evaluation has been focused on the bottom-up effects of nutrients, including direct measurement of nutrient concentrations (especially phosphorus) and an assessment of the condition of

the first trophic layer (phytoplankton) (Carlson 1977; Wetzel 1983). Although much information could be obtained from detailed determination of phytoplankton communities for each lake sampling event, most sampling has instead relied on chlorophyll concentration to represent the quantity of algal biomass present in a lake. This approximation of biomass is relatively easy to collect, and can be analyzed in a standard laboratory setting without a high level of specialized knowledge.

Both the Carlson (1977) and Wetzel (1983) trophic indices use the same three lake characteristics to classify lakes: phosphorus concentration, chlorophyll concentration, and Secchi disk depth. Nutrient-poor lakes are classified as oligotrophic, nutrient-rich lakes as eutrophic, and lakes of intermediate nutrient levels as mesotrophic. Of the three measurements, chlorophyll is the only one directly related to the biological activity of the lake ecosystem, providing a direct window into both bottom-up (nutrients) and top-down (grazing) pressures flowing through the lake food web. Also, chlorophyll concentration has the advantage of being relatable to the non-scientists, an advantage when communicating between the limnologist and the public (Carlson 1977).

In addition to being used in scientific settings, chlorophyll concentration has been used widely in monitoring by governmental agencies. Under the Clear Water Act, the US Environmental Protection Agency uses chlorophyll as one of the primary drivers of lake management across the country, setting targets for lakes in each

region. These standards are used to monitor the degradation of lake health, and state governments are held accountable to the agency based on the results of routine monitoring. The use of chlorophyll concentration as a tool to monitor lake health is used by governments worldwide, and is also used by a wide range of volunteer and non-governmental groups.

Chlorophyll and real-world impacts

The extent of eutrophication, or nutrient enrichment, in lakes is a central focus of lake researchers, managers and governmental agencies. A eutrophic lake, characterized as having an abundance of nutrients, produces a greater standing crop of algal biomass than can be integrated efficiently into the higher trophic levels of the food web. While eutrophication of lakes can be due to natural conditions (i.e., soil chemistry) the majority of lake eutrophication worldwide can be attributed to human activities (inadequate sewage treatment, fertilizer runoff). Some of the causes of eutrophication are relatively easy to identify for a lake (river inflows), but others may be very difficult to identify precisely or to manage (lawn fertilizer). Once a lake becomes eutrophic, it can be quite difficult to remediate due to the potential of internal loading, in addition to the logistical difficulty of reducing human-provided nutrient inputs.

Many deleterious consequences can result once a lake becomes eutrophic. Due to the inability of the food web to process the extent of algal biomass,

phytoplankton can precipitate out of the upper layer of the lake (epilimnion), eventually reaching the lake's bottom layer (hypolimnion) where their decomposition can deplete oxygen. Once the hypolimnion becomes anoxic, the lake ecosystem can be substantially altered. Fish can no longer utilize the hypolimnion, and turnover events can release trapped hydrogen sulfide gas, producing a noxious or potentially harmful effect in areas surrounding the lake. In addition, the perceived water quality of a eutrophic lake as "less clean" can decrease property and rental values in lakeside properties.

As lakes become more eutrophic, phytoplankton assemblages become increasingly dominated by cyanobacteria (Chorus et al. 2000; Codd et al. 2005). Problems associated with these "blue-green algae" have been reported on every populated continent (Jones and Chorus 2001; Burgess 2001) and occurrence will likely increase in the future due to climate change (Paerl and Paul 2012).

Cyanobacteria can cause problems for recreational use of lakes due to unsightly blooms and complications for drinking water use as a result of the foul taste and odors associated with cyanobacteria (Izaguirre et al. 1983; Smith et al. 2002; Watson 2004). More importantly, cyanobacteria can produce three types of toxin (hepatotoxins, neurotoxins, dermatotoxins) which can directly affect human health (Codd 1995; Carmichael 2001). Toxic episodes have been described throughout North America (Repavich et al. 1990; Ouellette et al. 2006; Jacoby

and Kann 2007), and it is estimated that up to 95% of cyanobacterial blooms are toxic (Sivonen et al. 1990; Paerl and Paul 2012).

Low-level exposure to cyanobacterial toxins (such as microcystins) through consumption of lake water causes throat lesions and gastrointestinal illnesses (Slatkin et al. 1983; Turner et al. 1990), while long-term exposure to microcystin-contaminated drinking water can promote tumors and liver cancer (Falconer 1996; Ueno et al. 1996). High-level exposure to cyanobacterial toxins has resulted in human deaths (Ueno et al. 1996; Stewart et al. 2006). More recently, cyanobacterial toxins have been linked with neurodegenerative diseases such as amyotrophic lateral sclerosis (ALS) (Banack et al. 2010).

Remote sensing of chlorophyll

Algorithm approaches

Remote sensing is a powerful technology that can be used to assess environmental conditions in lakes over space and time. Spectral radiometry (“color”) can be measured remotely to estimate the chlorophyll content (“greenness”) of a lake. Algorithms are then used to estimate the chlorophyll concentration using the spectral measurements. (For a discussion of discipline-specific terminology, please see Appendix A)

Before remote sensing can be used reliably for estimating chlorophyll in lakes, efforts must be made to develop and test algorithms appropriate for the types of lakes found in a given region. The use of remote sensing methods without such regional validation may produce appealing satellite pictures, but any techniques applied without proper validation will not be quantitatively useful as a supplement or alternative to *in situ* monitoring.

The biggest challenge with using remote sensing to monitor lakes and ponds in the chosen study areas (the Great Salt Lake, New England lakes), is that most published algorithms for chlorophyll have been developed either for the ocean, or for lakes with much higher turbidity and more eutrophic conditions. Rather than assuming these algorithms can be effective in these previously untested lakes, I set out to determine which chlorophyll estimation algorithms perform best in each study area.

Sensor selection. A number of past and present satellite sensors have spectral bands in the visible and near infrared. However, when choosing a satellite sensor for estimating chlorophyll in lakes, several key characteristics must be considered. First and foremost, the sensor must possess the spectral bands necessary to measure wavelengths affected by the chlorophyll. The centers of the bands must not only be well positioned, but the width of the bands must be narrow enough to clearly distinguish key spectral patterns related to chlorophyll absorption from those caused by other in-water constituents. In addition to well-

positioned bands, the sensor must possess enough radiometric resolution to allow for the detection of changes of in-water optical properties. Because only about 10% of the signal received at the satellite is reflected from beneath the water surface, the radiometric resolution must be high enough to resolve variability in one-tenth of the available range. Together, spectral and radiometric resolution can be used to define sensors that are suited for lake measurements of chlorophyll. Spatial resolution is another critical aspect. If the pixels of a sensor are too big for a given lake, reflectance from the land will overwhelm the water signal, providing no clean measurement of the lake itself. The additional characteristics of temporal resolution, as well as swath width, serve to inform what type of lakes these sensors can be used to monitor, and how often measurements can be taken.

From the suite of currently deployed satellite sensors, MERIS, MODIS and SeaWiFS have been widely used for remote sensing of water (Table 1). All three sensors have appropriate spectral bands for the detection of chlorophyll in surface waters, and sufficient radiometric resolution to ensure the ability to measure small variations in those bands. While the relatively large size of the pixels on these satellites (~ 1 km) generally precludes the sensors from being used on most lakes, the short return times (1-3 days) and large image footprints (1,150-2,801 km²) make these sensors useful for regular monitoring programs of large lakes. In this study, algorithms were tested for all of these sensors (MERIS, MODIS and SeaWiFS) to determine the method which provided the best

performance for the measurement of chlorophyll in the Great Salt Lake and New England lakes.

In addition to examining current satellite sensors, the increasing availability of hyperspectral sensors (carried on boats, flown on planes, installed on fixed platforms, etc.) provides an expanding field of opportunity for the use of remote sensing in lake monitoring. While these sensors do not have the same capabilities as satellite-borne sensors to collect spectral data of many lakes simultaneously, they can still be used to provide details on spatial distribution of phytoplankton in an individual lake, or capture continuous estimates of chlorophyll concentration at a single site, in a way not possible with traditional limnological sampling. Each type of hyperspectral sensor has slightly different spectral band arrangement, thus there is no standard set of bands to simulate this type of sensor. To provide fine detail when testing algorithms, this study used 3-nm wide bands strategically chosen between 400 nm and 775 nm to explore the potential of hyperspectral sensors for the estimation of chlorophyll in lakes.

Algorithm development. Those not familiar with this field of research may envision the development of a chlorophyll algorithm through the coordination of lake sampling trips coincident with satellite overpasses. However, agencies such as NASA and the European Space Agency (ESA) rarely use this approach when initially developing remote sensing algorithms for oceans or inland waters (although it may be used for validation of derived products). Some of the

problems encountered when using satellite imagery for algorithm development are lags between image capture by the satellite and lake sampling, difficulty relating relatively large image pixels to water quality samples, variable cloud cover, variable bands for each satellite, and degradation of measurements due to atmospheric effects.

To avoid many of these issues, methods used to develop remote sensing algorithms focused on water bodies rely on data measured with a portable spectral radiometer carried on ship and used directly at the sampling location. Portable radiometers are used to collect highly detailed, hyperspectral measurements of lakes that are captured close in time with relevant water quality measurements. This *in situ* approach to measuring the spectral characteristics of surface water provides a detailed measurement of the light leaving the surface of the lake without having to worry about atmospheric interference. The hyperspectral nature of these measurements can be used to simulate any number and combination of satellite bands, thus ensuring the dataset can be used to develop and test chlorophyll algorithms for any satellite past, present or future.

“On-lake” remote sensing. In addition to providing spectral measurements for algorithm development, portable radiometers can be used as a remote monitoring system independent of satellites. Once the best algorithm for chlorophyll estimation has been determined, boat-mounted radiometers paired

with GPS devices can be used to rapidly survey a lake, providing spatial coverage similar to satellite imagery, while simultaneously providing immediate feedback on the most important areas of the lake for the collection of traditional limnological samples. Another approach for on-lake remote sensing would be the deployment of radiometers mounted to balloons, remote control aircraft or blimps. By elevating the sensor above the lake surface, and by providing for horizontal movement either by self-propulsion or towing from a boat, chlorophyll could be estimated across the entire surface of the lake. Radiometers pointed at the lake surface can be mounted on shore, providing a continuous estimation of chlorophyll over time at a given lake location. Radiometers can also be fitted onto submersible autonomous vehicles and used to collect measurements throughout a lake (Tedesco and Steiner 2011). Finally, radiometers could be mounted on buoys or moorings to provide near-continuous spectral data at a specific location on the lake.

Ocean chlorophyll algorithms

The ocean color remote sensing community has spent three decades developing satellite techniques for the accurate estimation of chlorophyll concentration in the ocean. The chlorophyll concentrations produced by these algorithms have been used to observe temporal and spatial variability in phytoplankton distributions at global and regional scales. Satellite-derived chlorophyll concentrations are also being used for estimating net primary productivity of the world's oceans,

providing invaluable information on the global carbon cycle and climate change (Behrenfeld et al. 2006; Polovina et al. 2008; Irwin and Oliver 2009). In addition, satellite-based estimates of chlorophyll have been used to track and monitor the occurrence of potentially toxic blooms in coastal areas (Hu et al. 2005; Ahn and Shanmugam 2006; Anderson 2009).

Ocean color - blue to green ratio. Launched in 1997 aboard the OrbView-2 satellite, the SeaWiFS sensor was developed through a private/public partnership between NASA and ORBIMAGE. More than a decade had passed since the first ocean color sensor, the Coastal Zone Color Scanner (CZCS), had ended its mission (1978-1986). Although the CZCS was a highly successful proof-of-concept mission, it had shortcomings, among which was inadequate spectral resolution. The SeaWiFS had six bands for pigment detection instead of three, and two infrared bands for atmospheric correction instead of one. SeaWiFS employed 2-band and 4-band algorithms for chlorophyll, named ocean chlorophyll 2 (OC2) and ocean chlorophyll 4 (OC4), respectively, (O'Reilly et al. 1998; 2000), that were developed using an *in situ* spectral and pigment dataset named the SeaWiFS Bio-optical Archive and Storage System (SeaBASS). The CZCS chlorophyll algorithm switched between two band ratios, using a higher wavelength band (520 nm / 550 nm) at chlorophyll > 1.5 $\mu\text{g L}^{-1}$, to avoid the lower and somewhat noisy blue band (443 nm / 550 nm) at high chlorophyll levels. The OC4 algorithm ($r^2 = 0.86$, RMS = 0.250 log decades) also employs band switching to estimate chlorophyll, but avoids a discontinuity at the switch by

selecting whichever ratio, 430 nm / 555 nm, 490 nm / 555 nm, or 510 nm / 555 nm, is greatest.

Similar band-switching algorithms have been developed for MODIS and MERIS sensors. Two MODIS sensors were launched by NASA, one aboard the Terra satellite in 1999, and one aboard Aqua in 2002. MODIS boasts many more bands than SeaWiFS (36 vs. 8). However, only 9 of the MODIS bands have the radiometric sensitivity required for ocean remote sensing, while the remaining bands are intended for remote sensing of the land and atmosphere. The MODIS chlorophyll algorithm (OC3: $r^2 = 0.86$, RMS = 0.255) relies on switching between two band ratios, 443 nm / 550 nm and 489 nm / 550 nm, instead of the three band ratios employed by OC4. MERIS was launched by the European Space Agency in 2002 aboard the ENVISAT satellite with bands specifically tailored for use in optically complex waters (i.e. lakes, coastal areas). A band switching algorithm for chlorophyll has been developed for MERIS bands (OC4E: $r^2 = 0.86$, RMS = 0.251), which utilizes three blue-to-green ratios, 443 nm / 560 nm, 489 nm / 560 nm, and 510 nm / 560 nm.

Fluorescence Line Height. The fluorescence line height (FLH) algorithm was first developed as a chlorophyll detection technique for airborne remote sensing over waters in which blue wavelength bands experienced reduced effectiveness (Gower 1980). Later, MODIS and MERIS were designed with bands in the red spectral region to capture the chlorophyll fluorescence peak, and the FLH

algorithm has been adapted and tested for MODIS (Letelier and Abbott 1996) and MERIS (Gower et al. 1999). The FLH algorithm utilizes three wavelengths, one centered on the chlorophyll fluorescence peak (677 nm) and two adjacent bands (665 nm, 746 nm) acting as anchors against which to measure the height of the peak. FLH has been employed to estimate chlorophyll concentration in a range of water types (Xing et al. 2007; He et al. 2008; Gons et al. 2008).

Maximum Chlorophyll Index. The Maximum Chlorophyll Index (MCI) algorithm is a baseline algorithm designed using MERIS bands to capture the spectral dynamics of the 709 nm band (Gower et al. 2005a), a wavelength not present in SeaWiFS or MODIS. A reflectance peak located between 690 nm and 710 nm is an important spectral feature of inland water bodies (Gitelson 1992; Rundquist et al. 1996), that provides a good frame of reference against which to measure the effects of chlorophyll absorption around 670 nm. This algorithm can be used with the MERIS sensor, hyperspectral sensors, and any sensor for which a band near 709 nm is available. MCI has been used successfully to measure floating algae (Gower et al. 2006) and phytoplankton dynamics in the ocean (Gower et al. 2008), as well as monitoring blooms of cyanobacteria in lakes (Binding et al. 2011; 2012).

Floating Algal Index. The floating algal index (FAI) has been developed to aid in the detection and quantification of floating algal mats which can characterize eutrophic and hypereutrophic lakes (Hu 2009). In addition to relying on a visible

wavelength (645 nm), the algorithm also utilizes two bands in the near infrared region (859 nm, 1240 nm or 1640 nm). The algorithm uses a similar method to both FLH and MCI, providing two anchor bands (645 nm, 1240 nm or 1640 nm) against which to measure the height of a third band (859 nm). In Lake Taihu, China, FAI was successfully applied to MODIS imagery to quantify the timing, location and duration of cyanobacteria blooms characterized by floating mats, but was determined to be of little use when cyanobacteria were present in the water column (Hu et al. 2010). In another study, FAI was used with both Landsat Enhanced Thematic Mapper Plus (ETM+) and PROBA/CHRIS to map seasonal seaweed in the Arabian Sea (Pauly et al. 2011). While the use of FAI with ETM+ provided clear detection of intertidal seaweeds, PROBA/CHRIS ultimately lacked the appropriate bands to accurately apply the algorithm.

Semi-analytical. Semi-analytical (SA) algorithms offer a different approach than those based on band ratios. The SA approach entails the parameterization of key inherent optical properties (i.e., the spectral shape of colored dissolved organic matter (CDOM) and chlorophyll absorption and scattering), which then allows reflectance measurements to be deconstructed to reveal the inherent optical properties, that are then related to the optically active constituent concentrations (i.e., CDOM, chlorophyll, and suspended sediments). While several such algorithms have been widely considered for use in ocean remote sensing (Maritorena et al. 2002), the effectiveness of this approach is largely controlled by the appropriateness of model parameterization. However, when these

algorithms function well, they provide information on the inherent optical properties of the study waters, not only estimates of chlorophyll concentration.

Lake chlorophyll algorithms

Red to near-infrared band ratios. Remote sensing algorithms for the estimation of chlorophyll in lakes have largely focused on the following features and wavelength ranges: 1) maximum chlorophyll absorption (665 nm to 675 nm), 2) scattering peak related to phytoplankton density (690 nm to 710 nm), and 3) areas not effected by chlorophyll absorption (720 nm to 754 nm). The blue range (400 nm to 500 nm) has been avoided in these algorithms because of the influence of CDOM which is frequently much higher than in oceanic water and strongly absorbs in the blue region. Initially, the chlorophyll algorithms were based on 2-band ratios, which focused on chlorophyll absorption and the scattering peak (Han and Rundquist 1997; Schalles et al. 1998; Gitelson et al. 2000). More recent investigations have further refined the position of band placement for 2-band ratios (Dall'Olmo and Gitelson 2005; 2006; Gurlin et al. 2011; Moses et al. 2012) and have explored the use of 3-band algorithms, involving the subtraction of two 2-band ratios (Gitelson et al. 2007; Duan et al. 2010; Yacobi et al. 2011a). A recent comprehensive review of lake chlorophyll band ratio algorithms has demonstrated that different techniques are best suited for different lake types, although much more agreement on useful bands and techniques has emerged in recent years (Gitelson et al. 2011b).

Table 1. Spectral and radiometric characteristics for sensors to simulate for algorithm development in the current study.

Sensor	Satellite	Agency	Launch	Bands	Radiometric	
					Resolution	Levels
MERIS	ENVISAT	ESA (Europe)	2002	15	16-bit	65536
MODIS	Aqua	NASA (USA)	2002	36	12-bit	4096
MODIS	Terra	NASA (USA)	1999	36	12-bit	4096
SeaWiFS	OrbView-3	NASA (USA)	1997	8	10-bit	1024

CHAPTER II

GENERAL METHODOLOGY

Limnology

Lake Water Sampling

Lake water was collected with an integrated sampling device at all sites. An integrated method is a more appropriate approach for remote sensing algorithm development than a grab sample, as it more closely mimics the integrated effects of the water column on upwelling and downwelling light fields. The type of integrated sampling device, and depth of the epilimnion sampled, varied with the coordinating agency with which each lake was sampled (Table 2). For lakes where the sample was taken from the entire epilimnion, a temperature profile was conducted prior to the sampling to determine the appropriate sampling depth. In these cases, care was taken to select an integration depth that would avoid inclusion of the metalimnion, and chlorophyll maximum that can occur from the accumulation of phytoplankton in that strata.

Immediately after collection, lake water was kept on ice and stored in the dark. For chlorophyll analysis, the water was filtered in the lab within 2 hours of

collection in New England, or within 24 hours in the Great Salt Lake. The filters were either frozen or stored in drying containers, depending on the methodology of the project. For colored dissolved organic matter (CDOM) analysis, lake water was filtered through 0.45 μm Millipore membrane filters and the filtrate poured into 500 ml opaque plastic bottles. These bottles were refrigerated until analyzed in the laboratory within one week.

Chlorophyll profile. For a subgroup of lakes sampled by the University of New Hampshire (UNH), a chlorophyll vertical profile was measured during daylight using a YSI 6600 V2 multi-parameter probe and a YSI-650 data logger (YSI Incorporated, Yellow Springs, OH). The chlorophyll fluorescence was logged every 3s as the probe was lowered throughout the entire water column at approximately 0.5 m min^{-1} . The chlorophyll fluorescence measured by the probe was converted to a chlorophyll concentration using a factor determined through field experiments relating average epilimnetic chlorophyll fluorescence determined by the probe and the UNH standard overnight chlorophyll a extraction method (see below).

Analysis

Chlorophyll concentration. Due to the wide range of projects under which this work was conducted, chlorophyll analyses were carried out through a variety of techniques (Table 3). All chlorophyll analyses for the Great Salt Lake stations

were conducted at Utah State University utilizing filter freezing, overnight ethanol extraction and the Welschmeyer fluorescence method (Welschmeyer 1994). Chlorophyll samples from New England lakes visited in 2002, 2003, 2004, 2005 and 2008 were analyzed by the Lakes Lay Monitoring Program at UNH using filter freezing, a 4-hour cold extraction with ethanol, and a spectrophotometric method (Lind 1985). Chlorophyll from New England lakes measured in 2007 and 2009 was analyzed at the EPA Region I Laboratory utilizing filter freezing, overnight ethanol extraction and the Welschmeyer fluorescence method (Welschmeyer 1994).

New England lakes sampled in 2006 were part of a regional lake study, known as the New England Lakes and Ponds project (NELP). NELP was coordinated by the US EPA Region I Laboratory and included the participation of five state laboratories in the region (Connecticut, Massachusetts, Maine, New Hampshire, and Vermont) and two universities (UNH and the University of Rhode Island). One goal of the NELP project was to compare the chlorophyll filtration/extraction methods from all seven of the project partners. As such, water collected from each lake was filtered and analyzed by each organization according to the chlorophyll methods employed by that organization.

In order to minimize the error introduced by using data produced by a number of analytical chlorophyll methods, chlorophyll values determined with the UNH method were used for 2006 samples whenever possible. However, the planned

round robin field techniques of the NELP were not carried through perfectly (i.e., appropriate filters were not available during every lake trip), and as such, numerous lakes did not have chlorophyll values determined with the UNH method. In addition, the sample storage technique for UNH samples was not always followed, as samples were sometimes exposed to sun more than prescribed by the method. For example, the filter preservation technique used by UNH relies on desiccation rather than freezing, and requires filter storage in complete darkness during the time between filtering and analysis. The greater than expected sun exposure of some filters may have possibly led to a degree of sample degradation on some filters, particularly those from chlorophyll-rich lakes.

A sum of squares method comparing the UNH chlorophyll concentrations to five of the other methods was used to determine which chlorophyll value to use for lakes with either missing UNH filters (and therefore no data) or lakes for which the greater than expected sun exposure caused suspicion of chlorophyll degradation (for more details, see Chapter IV).

Colored Dissolved Organic Material. Filtered lake water in opaque bottles was kept refrigerated between collection and analysis, and was analyzed for CDOM in the laboratory according to American Public Health standards (APHA et al. 1998). The refrigerated samples were warmed to room temperature, then poured into a quartz cuvette with a 5 cm path length. Spectral absorption measurements were recorded at 440 nm, 493 nm, 750 nm and 880 nm in a Milton Roy 1001+

spectrophotometer with a 2 nm bandwidth. The measured absorption values were converted to absorption coefficients (m^{-1}) using the cuvette path length.

On-lake spectral measurements

Single radiometer

Single-radiometer field data collection. Reflectance measurements were collected from a boat using a single Optical Coating Laboratory, Inc. (OCLI) MicroPac radiometer in the range 400-725 nm with a spectral resolution of 1.5 nm. The radiometer was mounted in a black case, and a 50-mm focal length fish-eye lens was used to concentrate incoming light on the radiometer slit.

Four separate spectral measurements were made at each sampling station, and the data were captured using the mmSoftpac1 software from OCLI. First, a measurement of the sensor's dark current was taken while the lens was completely covered, ensuring no light entered the radiometer. The value of the dark measurement at each wavelength was subtracted from each of the other three measurements in the post-processing phase before any calculations were made. Second, a measurement of downwelling radiance on a Kodak gray card (L_{dk}), assumed to be a Lambertian reflector at 18%, was taken at a zenith angle (Θ_z) of 135° and an azimuth angle (Θ_v) of 135° relative to the position of the sun (Mobley 1999). Third, a measurement of the downwelling radiance (L_s) was

made at $\Theta_z=45^\circ, \Theta_v=135^\circ$. Finally, a measurement of the upwelling radiance $\sim 1\text{m}$ above the surface of the lake (L_u) was made at $\Theta_z=135^\circ, \Theta_v=135^\circ$.

Single-radiometer post-processing. The remote sensing reflectance (R_{rs}) of a lake sampling station can be determined from two spectral quantities, downwelling irradiance (E_d) and water-leaving radiance (L_w) as shown below (λ has been left out for simplicity):

$$R_{rs} = \frac{L_w}{E_d} \quad (1)$$

Unfortunately, L_w is impossible to measure directly since L_u contains skylight reflected off the water surface. As such, we can approximate L_w by combining L_u and L_s as shown below:

$$L_w = L_u - L_s p \quad (2)$$

where L_u is the upwelling radiance measured above the surface of the water, L_s is the downwelling sky radiance, and p is a factor representing the percentage of skylight present in the L_u measurement. The R_{rs} equation can thus be rewritten as:

$$R_{rs} = \frac{L_u - L_s p}{E_d} \quad (3)$$

The measurement of downwelling sunlight impinging on the 18% Lambertian reflective Kodak gray card is used to approximate the total downwelling irradiance (E_d):

$$E_d = \frac{\pi L_{dK}}{0.18} \quad (4)$$

which then provides for the complete calculation of R_{rs} from the on-lake measurements as such:

$$R_{rs} = \frac{L_u - L_s p}{\frac{\pi L_{dK}}{0.18}} \quad (5)$$

Hydrolight modeling to estimate the factor p . Hydrolight 4.2 from Sequoia Scientific, Inc. was used to produce modeled spectra for each lake measured with the single-radiometer technique. Two modeled spectra were produced for each lake, one using the epilimnetic extracted chlorophyll concentration and another using the chlorophyll profile measured with the YSI probe. The Hydrolight routine designed for case 2 waters (ABCASE2) was run with the settings shown in Appendix B. The resultant Hydrolight spectra were then used for comparison with R_{rs} calculated with field data from each lake, allowing for an assessment of the best-fit value for the skylight contribution to the L_u signal.

Dual radiometers

Dual-radiometer field data collection. Dual-radiometer measurements were made using a methodology modeled on two previous studies (Dall'Olmo and Gitelson 2005; Doxaran et al. 2005). Reflectance measurements were collected from a boat using a pair of inter-calibrated Ocean Optics USB2000 radiometers. Data were collected in the range 380–850 nm at an interval of 0.4 nm. The downward-pointing radiometer was submerged and connected to a 2-meter long optical fiber with a 25° field-of-view. This radiometer was used to measure below-surface, nadir upward radiance, $L_u(z, \lambda)$. The upward-pointing radiometer was outfitted with a fiber optic cable and cosine collector mounted on a vertical beam or pole affixed to the boat and pointed at the sky. This radiometer was used to measure above-surface downwelling irradiance, $E_u(0^+, \lambda)$.

For the in-water radiometer, the optical fiber was held at depth on the sunny side of the boat through the use of a 2-m black pole with a 1-m black screw attached perpendicularly at the end. To allow accurate data collection from discrete depths, the screw was marked with tape at 5-cm increments relative to the location of the tip of the optical fiber when mounted on the pole. The effects of the fiber and pole on the light field were considered minor due to the small size of the fiber optic tip (~0.5 cm) and the non-reflective nature of the pole and screw onto which it was mounted.

Measurements of Lu_z at 3-6 depths (ranging from 5 cm to 80 cm) were made in triplicate at each lake to capture the attenuation of Lu_z in the water column. The depths at which each lake was measured were varied based on the optical characteristics of each water body. The depths measured in turbid, more productive lakes were clustered closer to the surface, whereas clearer, more oligotrophic lakes had measurements spread deeper into the water column. The vast majority of spectra were collected during periods of little or no wave activity, allowing for accurate depth placement of the fiber optic tip. When significant waves were present, all efforts were made to hold the tip at the correct depth by moving the pole against the direction of wave activity. When conditions were particularly challenging, extra measurements were taken to reduce the uncertainty in positioning of the fiber optic tip.

The radiometers were controlled during data collection using the CALMIT Data Acquisition Program (CDAP) from the Center for Advanced Land Management and Information Technologies (CALMIT) at University of Nebraska, Lincoln. Upon initiation of a measurement, CDAP made a pre-collection measurement of 3 ms in both the downward and upward-facing radiometers to assess the light environment. The intensity values of this quick measurement were then used to set the integration time of the two radiometers independently to maximize the use of the dynamic range of each detector in the light environment at the time of measurement. The integration time of the upward-facing radiometer was typically an order of magnitude shorter than that of the downward-facing radiometer.

However, the change in light field conditions can be assumed to be minor during the short time period of a single measurement, and any change in light condition would affect the light field equally for both the upwelling and downwelling measurements. CDAP was programmed to make six measurements at each depth in rapid succession, which were then averaged and stored as the final spectral data for that depth. All measurements were made over optically deep waters.

Dual-Radiometer Post-Processing. A schematic representation of the calculations described in this section can be found in Figures 1 and 2. The two figures represent the left half and right half of a two-page document, with the dotted lines showing the schematic flow from one side to the other. The digital numbers (DNs) collected by the radiometers can be denoted as follows (λ has been left out for simplicity):

$$DN_L = L_u(z)k_L \quad (6)$$

$$DN_E = E_d(0^+)k_E \quad (7)$$

where z is depth in meters, k represents a transformation coefficient specific to each radiometer, L stands for nadir radiance, and E stands for downward irradiance.

The first 25 detector elements of the USB2000 detectors were covered to prevent

light from impinging on the detectors, and as such, could be used to assess the dark current of the instrument. During each scan, CDAP used the values recorded by these 25 detector elements to determine the average value for the dark current of each radiometer, and subtracted this value from the measurements. The correction should be considered applied in all of the data discussed in the current work.

The ratio of equations (6) and (7) provides the equation shown below:

$$\frac{DN_L}{DN_E} = \frac{L_u(z) k_L}{E_d(0^+) k_E} \quad (8)$$

which depends upon both the radiance reflectance of the target, and the ratio of the transformation coefficients of the two instruments, k_L/k_E . To assess the stability of k_L/k_E over the course of field sampling, we collected measurements of a white Spectralon plaque of known irradiance reflectance, R_{ref} , at the initiation of data collection at each station, and thereafter, numerous times during data collection on a given day. Laboratory experiments demonstrated that the variation of k_L/k_E of an equivalent equipment setup did not exceed 2% over a period of four hours, thus confirming the stability of the measurement system (Dall'Olmo and Gitelson 2005). The collection of reference panel measurements allowed the determination of k_L/k_E as shown here:

$$\frac{k_L}{k_E} = \frac{DN_{L,ref} R_{ref}}{DN_{E,ref} \pi} \quad (9)$$

where $DN_{L,ref}$ and $DN_{E,ref}$ are the digital numbers recorded by the downwelling and upwelling radiometers, respectively, during the scan of the Spectralon plaque. The term π is used to transform the irradiance reflectance, R_{ref} , into a radiance assuming the Spectralon plaque is a Lambertian reflector. The calibration measurement of the Spectralon plaque during each field session was important to determine changes in k_L/k_E on a given day due to variations in the assembly of the sampling apparatus and connection of fiber optic cables.

The preliminary reflectance calculated by CDAP for each depth represented the following terms:

$$R_{CDAP} = \frac{DN_L}{DN_E} \frac{DN_{L,ref}}{DN_{E,ref}} R_{refCDAP} \quad (10)$$

where $R_{refCDAP}$ is the assumed reflectance of the plaque used by CDAP. CDAP incorrectly uses the value of 99 to represent 99% reflectance in the calculations $R_{refCDAP}$, instead of the appropriate 0.99, thus producing values two orders of magnitude higher than the actual values. This discrepancy is corrected in equation (16) by dividing the artificially inflated R_{rs} values by a factor of 100. After visual quality control inspection of the R_{CDAP} measurements, the valid spectra for each depth were averaged and regressed to determine the coefficient of attenuation, K , for each wavelength as shown below:

$$SS_{xy} = \sum_{i=1}^n \left((\ln R_{CDAP_i} - \overline{\ln R_{CDAP}}) (Z_i - \bar{Z}) \right) \quad (11)$$

$$SS_{yy} = \sum_{i=1}^n (Z_i - \bar{Z})^2 \quad (12)$$

$$K = \frac{SS_{xy}}{SS_{yy}} \quad (13)$$

where Z represents the depth in meters, i represents the depth intervals for each lake profile. Using R_{CDAP} and K , the intercept of the regression (b) was used to calculate R_{CDAP} at 0 cm beneath the surface of the lake:

$$R_{rs} = \frac{DN_L}{DN_E} \frac{DN_{ref,E}}{DN_{ref,L}} \frac{R_{ref}}{\pi} \frac{t}{n^2} F_i \quad (14)$$

$$R_{CDAP_{0^-}} = e^{\overline{\ln R_{CDAP}} - (K\bar{Z})} \quad (15)$$

Above water remote sensing reflectance (R_{rs}) was calculated using terms from equations (9) and (15):

$$R_{rs} = \left(\frac{R_{CDAP_{0^-}}}{\pi} \frac{t}{n_w^2} F_i \right) / 100 \quad (16)$$

where t is the radiance transmittance from water to air (~ 0.98) (Mobley 2004), n_w is the refractive index for water corrected for salinity and water temperature (Quan and Fry 1995), and F_i is the spectral immersion factor. Division by 100 is necessary due to an $R_{refCDAP}$ value of 99 used in equation (10). The equation for R_{rs} can be shown with all terms revealed as:

$$R_{rs} = \frac{DN_L}{DN_E} \frac{DN_{ref,E}}{DN_{ref,L}} \frac{R_{ref}}{\pi} \frac{t}{n^2} F_i \quad (17)$$

Algorithms using on-lake spectra

The performance of a wide range of chlorophyll algorithms was tested using reflectance measurements and extracted chlorophyll values (Tables 4, 5). Simulated satellite sensor bands were produced by averaging the hyperspectral data that corresponded to the range of each sensor band (Figure 3). Bands for hyperspectral algorithms were produced at 3-nm resolution by averaging the data within 1.5 nm on either side of the center band wavelength.

Hyperspectral band ratios

Algorithms developed for measuring chlorophyll in lakes using hyperspectral data commonly rely on two or three strategically chosen bands. One of these bands is chosen to capture the effects of chlorophyll absorption (between 665 nm and 675 nm), while the other band or bands are selected to provide contrasting anchor

points. In the case of algorithms (A), (B) and (C) (Table 4), the second band was positioned in an area of the spectrum (Figure 4), assumed to be free from the influence of chlorophyll absorption. In contrast, algorithms (D), (E), (F) and (G) (Table 4) pair the chlorophyll absorption band with a band located at the reflectance peak that appears between 690 nm and 710 nm with increasing chlorophyll concentration (Figure 5). It is believed that this peak is due to increased particulate scattering bounded by strong absorption by chlorophyll (~670 nm) and water (>720 nm). Algorithms (H), (I), (J) (K) (Table 4) utilize three bands to detail the scattering peak around 710 nm in contrast to the flat spectral region past 720 nm and maximal chlorophyll absorption region around 675 nm (Figure 6).

Ocean color algorithms

The operational ocean color algorithms for the SeaWiFS (L), MODIS (M) and MERIS (N) sensors (Table 5) all rely on a ratio of a blue band to a green band (Figure 7). These algorithms were designed for Case I waters, and operate on the assumption that all absorption in the blue region (bands at 443 nm, 489 nm, 510 nm) is due either to chlorophyll or CDOM which covaries with chlorophyll concentration (i.e., from cell lysis) (O'Reilly et al. 1998). The algorithm is designed to shift between multiple bands in the blue area of the spectrum, ensuring sensitivity through a range of chlorophyll values with increasing chlorophyll concentration. These algorithms are thought to perform poorly in

lakes due to the high variability of CDOM and suspended sediments, which often vary in concentration independently from chlorophyll (Morel and Prieur 1977).

When examining initial results of OC algorithms optimized for my study lakes, I noticed that the OC algorithms were not switching across all of the possible bands due to spectral characteristics of both New England lakes and the Great Salt Lake. Instead, the OC algorithms were always selecting the highest wavelength blue band for every spectrum, turning the switching algorithm into a simple band ratio. In order to investigate the influence of the blue band choice on the effectiveness of OC algorithms for my study lakes, I analyzed OC algorithm band ratios separately as stand alone algorithms, one for each blue band in the original switching algorithm.

Simulated 709 nm band in MODIS

One of the primary disadvantages of using MODIS for inland water bodies is the lack of a band to measure the scattering peak that lies in the 700 nm to 710 nm wavelength range. This area of the spectrum, which is captured by MERIS's 709 nm band, is used in nearly every algorithm for estimating chlorophyll in lakes, and without this band, the methods available to MODIS are limited. The usefulness of the peak that rises in this wavelength range with increasing chlorophyll concentration has been well documented (Gitelson 1992; Gitelson et al. 1999; Gower et al. 2005a; Dall'Olmo and Gitelson 2005; 2006; He et al. 2008;

Gitelson et al. 2009), but the exact nature of the peak is not fully understood. The major driver of the peak is likely increased backscattering as a result of increased phytoplankton density at higher chlorophyll concentrations, bounded on one side by strong absorption by chlorophyll (675 nm) and on the other by absorption by water. However, some portion of the peak is likely due to sun-stimulated fluorescence by photosystem I and/or II in phytoplankton (Harbinson and Rosenqvist 2003). Based on the assumptions that the primary source of the peak around 709 nm is backscatter from phytoplankton, and that nearly all of the signal around 750 nm is due to backscatter, I developed a relationship between simulated MERIS bands at 754 nm and 709 nm using the (Figure 8). This relationship was applied to the MODIS 748 nm band in order to create a simulated 709 nm band for use in algorithm development and potential employment with this sensor.

Maximum Chlorophyll Index

The Maximum Chlorophyll Index (MCI) algorithm was designed for the estimation of chlorophyll using satellite bands from MERIS. This algorithm uses two bands to draw a baseline, from which the height of another band is measured (Table 5; Figure 9). The traditional MCI (O) uses the bands at 681 nm and 754 nm to draw the baseline, and the band at 709 nm to measure against the baseline. A modified version of MCI (P) was also examined, testing the usefulness of the 665 nm band as one of the baseline endpoints. Although MODIS does not possess

the critical band for MCI (709 nm), both the traditional MCI (Q) and modified MCI (R) were analyzed for MODIS bands using a simulated 709 nm band (Figure 8). A final version of MCI (S) was explored, using strategically placed hyperspectral bands (S).

Satellite 2-band algorithms

Several of the 2-band algorithms that focused on the peak near 710 nm were adapted to the MODIS and MERIS satellite bands. One of the algorithms (T) was a simple use of the MERIS bands centered at the same location as the hyperspectral bands examined above. An adaptation of the same algorithm was developed with MODIS bands (U) with a simulated band at 709 nm. In addition, a further modified version of this approach utilized an average of the 665 nm and 681 nm bands from MERIS (V) as the indicator of the intensity of chlorophyll absorption. An equivalent approach was also used with MODIS bands 667 nm and 678 nm, along with a simulated 709 nm band (W). Finally, a 3-band algorithm based on hyperspectral algorithm (J) was adapted for use with MERIS (X) and MODIS (Y) bands.

Algorithms not used

Several of the chlorophyll estimation algorithms available in the literature were ultimately not used in this study. The FLH algorithm was attempted in the early

stages of analysis, but was abandoned due to poor results. The FAI was not possible to attempt due to the fact that radiometers used here did not collect data in all of the necessary spectral wavelengths (all data were below 775 nm). Semi-analytical algorithms were not attempted for I did not collect data on inherent optical properties of my study lakes in order to parameterize the models needed for these algorithms.

Algorithm performance analyses

Linear versus log-log regressions

All 2- and 3-band algorithms to estimate chlorophyll were explored using both linear and log-log regression analyses. In each case, the measured chlorophyll was regressed against a predictor variable (band ratio or ratio difference) derived from the corresponding spectral reflectance measurement. Measures of performance include the r^2 , relative absolute error (Rel Error), and root-mean-square (RMS) error. Since chlorophyll concentrations tend to vary by several orders of magnitude, log-log regressions are often used, such that best-fit regressions minimize *relative* error over the full range of chlorophyll concentration. In such cases, the RMS is measured in decades of log, and although it is not as easily understood as the RMS from a linear regression (which has units of $\mu\text{g L}^{-1}$), it is useful for comparing the relative performance of

different algorithms. As a benchmark, the best ocean color algorithms have RMS values of about 0.250 log decades (O'Reilly et al. 2000).

Linear regressions. To examine the effect of very low and very high chlorophyll concentrations on the linear analyses, each algorithm was run with four datasets: 1) all data, 2) only data above a low chlorophyll concentration, 3) only data below a high chlorophyll concentration, 4) only data between the low and high chlorophyll concentration. The values for the low and high chlorophyll concentrations were set for each study location (Great Salt Lake, New England) based on their own lake characteristics.

Log-log regressions. The primary analysis technique used to evaluate algorithms in this study was log-log regression. This approach was chosen in order to avoid the increased emphasis given to extreme low and high chlorophyll values when using linear regression analysis. For New England lakes, log-log analyses were conducted with the entire dataset. In the case of the Great Salt Lake, analyses were run both with the entire dataset, as well as with a restricted dataset in which suspect spectral data were excluded.

A problem was encountered when testing certain algorithms that involved ratio differences. Under some circumstances (low chlorophyll levels) the ratio differences were negative, and thus log transformation of the predictor variable was impossible. Unfortunately, the reliance on log-log regressions in this study

would have completely omitted these “negative” algorithms from consideration, in spite of the fact that some of these algorithms had been shown to be either highly useful for lakes based on published literature (in the case of 3-band, 2-ratio algorithms) or were being applied in a modified way and showed great promise (MCI).

In order to include algorithms which produced negative values in this study, a correction factor was added to the predictor variable in such cases before regression with extracted chlorophyll values. The factor was chosen in each case to ensure all predictor values used by the algorithm were positive, thus providing for the use of log-log analyses. This modification from the standard algorithms allowed for their evaluation compared with all of the other algorithms, without which they would have been completely excluded. Algorithms for which this modification was made are indicated by an asterisk in Tables 4 and 5.

Table 2. Type of integrated sampling for whole lake water by project.

Project	Coordinating Agency	Sites	Integrated sampling method
Great Salt Lake Synoptic Studies	Utah State University US Geological Survey	51	Sample collected 0-1 meter of epilimnion with peristaltic pump
New England Lakes and Ponds Project	US Environmental Protection Agency	40	Sample collected 0-2 meters with coring sampling device
National Lakes Assessment	US Environmental Protection Agency	16	Sample collected 0-2 meters with coring sampling device
NH Lakes Lay Monitoring Program	University of New Hampshire	11	Sample collected from entire epilimnion with tube sampling device (3-5 m)
UNH Center for Freshwater Biology	University of New Hampshire	53	Sample collected from entire epilimnion with tube sampling device (3-5 m)

Table 3. Details for all chlorophyll analytical methods used in this study. Laboratories are indicated as follows: CT - Connecticut Department of Energy and Environmental Protection, EPA - US Environmental Protection Agency Region I Laboratory, MA - Massachusetts Department of Environmental Protection, ME - Maine Department of Environmental Protection, NH - New Hampshire Department of Environmental Services, UM - University of Maine, UNH - University of New Hampshire, URI - University of Rhode Island, USGS - US Geological Survey Utah Water Science Center, VT - Vermont Department of Environmental Conservation. Fluor - fluorometric, Spec - spectrophotometric. All extractions used 90% acetone as a solvent.

Lab	Vol (ml)	Filter		Preservation	Analysis
		Type	Pore (μm)		
CT	250	GF/F	0.7	Frozen	Fluor
EPA	250	GF/F	0.7	Frozen	Fluor
MA	15	GF/C	1.2	Frozen	Fluor
ME	100	Membrane	0.45	Frozen w/ CaCO_3	Spec
NH	100	Membrane	0.45	Frozen	Spec
UM	250	GF/F	0.7	Frozen	Fluor
UNH	100	Membrane	0.45	Dried & Dark	Spec
URI	50	GF/F	0.7	Frozen w/ MgCO_3	Fluor
USGS	20	GF/C	1.2	Frozen	Fluor
VT	250	GF/F	0.7	Frozen	Fluor

Table 4. Details for chlorophyll algorithms used in this study based on hyperspectral measurements. Band values represent the center of the band used in the algorithm in nm. Bands were created by averaging the reflectance values from 1.5 nm on each side of the bands shown here. Hyper indicates 3-nm wide bands * indicates a correction factor was added to the predictor variable to ensure non-negative values.

	Sensor	Algorithm type	Bands
(A)	Hyper	2-band	$\frac{R_{rs735}}{R_{rs673}}$
(B)	Hyper	2-band	$\frac{R_{rs725}}{R_{rs665}}$
(C)	Hyper	2-band	$\frac{R_{rs720}}{R_{rs670}}$
(D)	Hyper	2-band	$\frac{R_{rs705}}{R_{rs673}}$
(E)	Hyper	2-band	$\frac{R_{rs710}}{R_{rs665}}$
(F)	Hyper	2-band	$\frac{R_{rs710}}{R_{rs670}}$
(G)	Hyper	2-band	$\frac{R_{rs703}}{R_{rs677}}$
(H)*	Hyper	3-band	$\frac{R_{rs740}}{R_{rs671}} - \frac{R_{rs740}}{R_{rs710}}$
(I)*	Hyper	3-band	$\frac{R_{rs730}}{R_{rs675}} - \frac{R_{rs730}}{R_{rs695}}$
(J)*	Hyper	3-band	$\frac{R_{rs754}}{R_{rs665}} - \frac{R_{rs754}}{R_{rs709}}$
(K)*	Hyper	3-band	$\frac{R_{rs754}}{R_{rs677}} - \frac{R_{rs754}}{R_{rs703}}$

Table 5. Details for chlorophyll algorithms used in this study based on currently deployed satellite sensors. Band values represent the center of the band used in the algorithm in nm. Bands were created by averaging the reflectance values over the width of the satellite band. MCI – Maximum Chlorophyll Index, Hyper - 3 nm-wide bands, * indicates a correction factor was added to the predictor variable to ensure non-negative values.

	Sensor	Algorithm type	Bands
(L)	SeaWiFS	OC	$\frac{\max [R_{rs,443}, R_{rs,489}, R_{rs,510}]}{R_{rs,555}}$
(M)	MODIS	OC	$\frac{\max [R_{rs,443}, R_{rs,489}]}{R_{rs,550}}$
(N)	MERIS	OC	$\frac{\max [R_{rs,443}, R_{rs,489}, R_{rs,510}]}{R_{rs,560}}$
(O)*	MERIS	MCI	$R_{rs,681}, R_{rs,709}, R_{rs,754}$
(P)*	MERIS	MCI (modified)	$R_{rs,665}, R_{rs,709}, R_{rs,754}$
(Q)*	MODIS	MCI	$R_{rs,678}, R_{rs,709(s)}, R_{rs,748}$
(R)*	MODIS	MCI (modified)	$R_{rs,667}, R_{rs,709(s)}, R_{rs,748}$
(S)*	Hyper	MCI (modified)	$R_{rs,677}, R_{rs,703}, R_{rs,754}$
(T)	MERIS	2-band	$\frac{R_{rs,709}}{R_{rs,665}}$
(U)	MODIS	2-band	$\frac{R_{rs,709(s)}}{R_{rs,667}}$
(V)	MERIS	3-band	$\frac{R_{rs,709}}{\text{mean} [R_{rs,665}, R_{rs,681}]}$
(W)	MODIS	3-band	$\frac{R_{rs,709(s)}}{\text{mean} [R_{rs,667}, R_{rs,678}]}$
(X)*	MERIS	3-band	$\frac{R_{rs,754}}{R_{rs,665}} - \frac{R_{rs,754}}{R_{rs,709}}$
(Y)*	MODIS	3-band	$\frac{R_{rs,748}}{R_{rs,667}} - \frac{R_{rs,748}}{R_{rs,709(s)}}$

Figure 1. Left half of schematic flow diagram for data collection and calculations for dual-radiometer measurements. Letters can be used to follow dotted lines onto the right half of the diagram (Figure 2). Numbers in parenthesis refer to the relevant equations in the methods text.

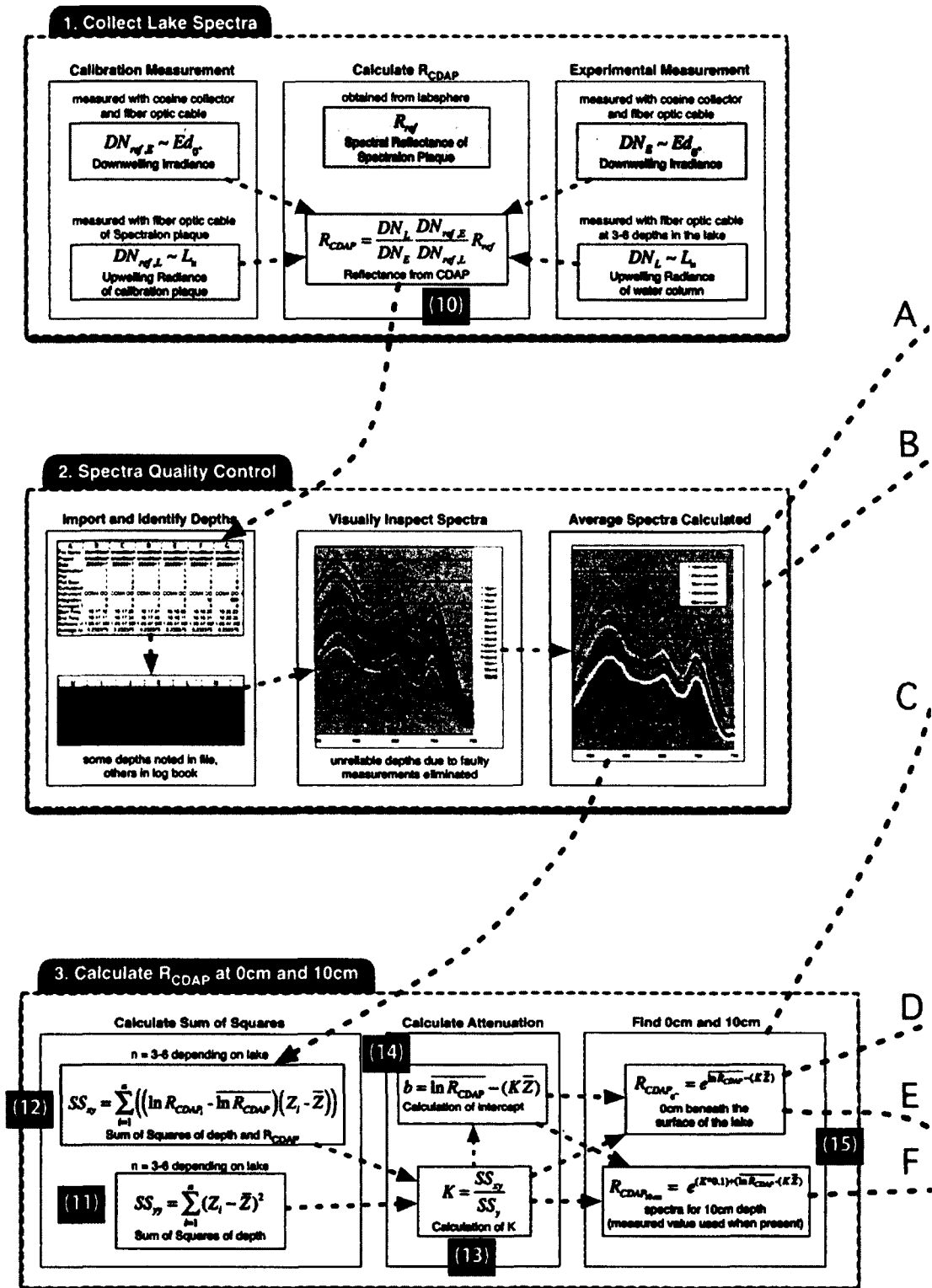


Figure 2. Right half of schematic flow diagram for data collection and calculations for dual-radiometer measurements. Letters can be used to follow dotted lines onto the left half of the diagram (Figure 1). Numbers in parenthesis refer to the relevant equations in the methods text.

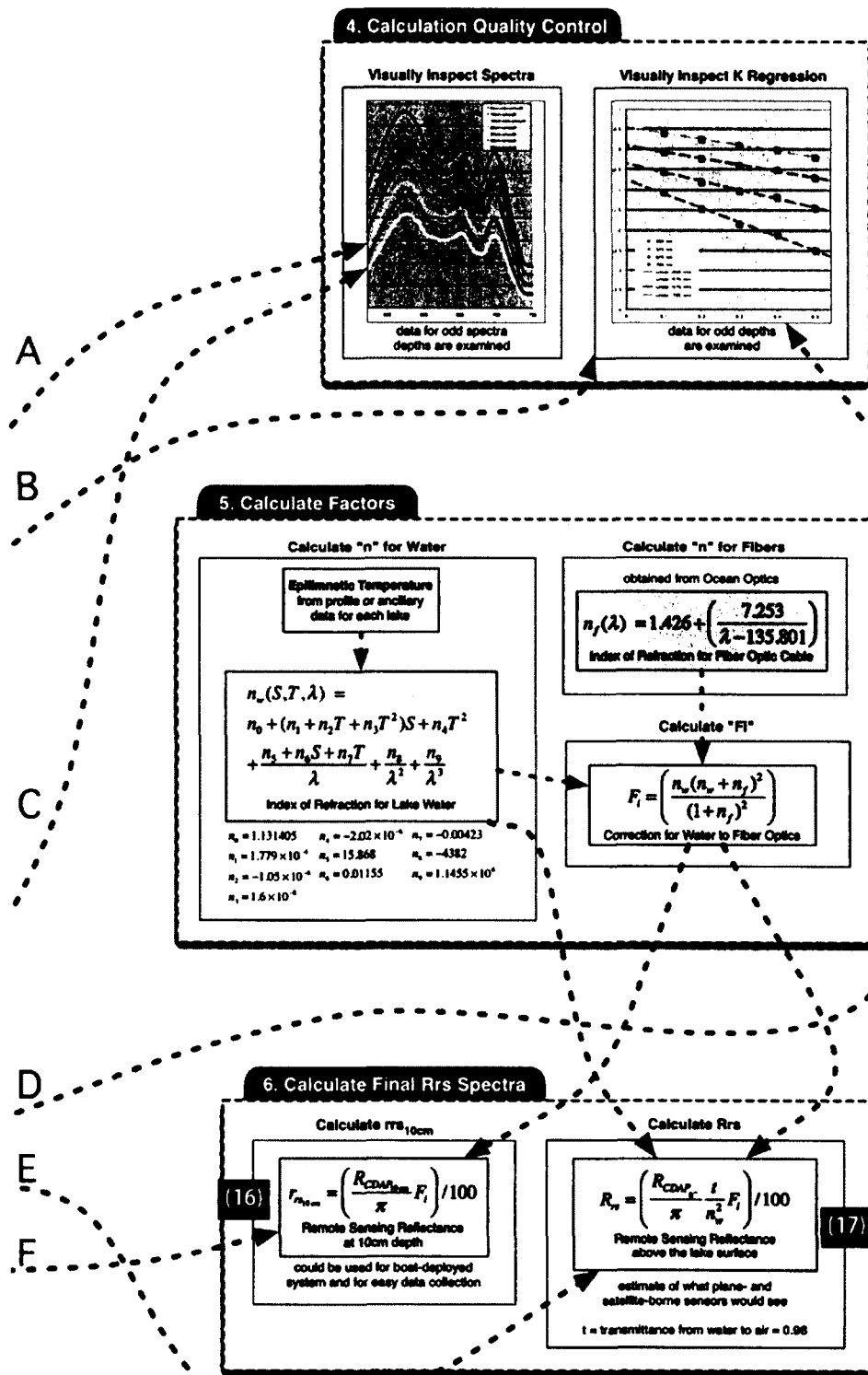


Figure 3. Simulated satellite bands were produced for each reflectance spectrum for use in algorithm development. The green bands below simulate the values of satellite bands on a high-chlorophyll lake ($36.6 \mu\text{g L}^{-1}$), while the blue bands represent the simulated bands on a low-chlorophyll lake ($5.7 \mu\text{g L}^{-1}$). The satellites sensors simulated here are (A) MERIS, (B) MODIS and (C) SeaWiFS.

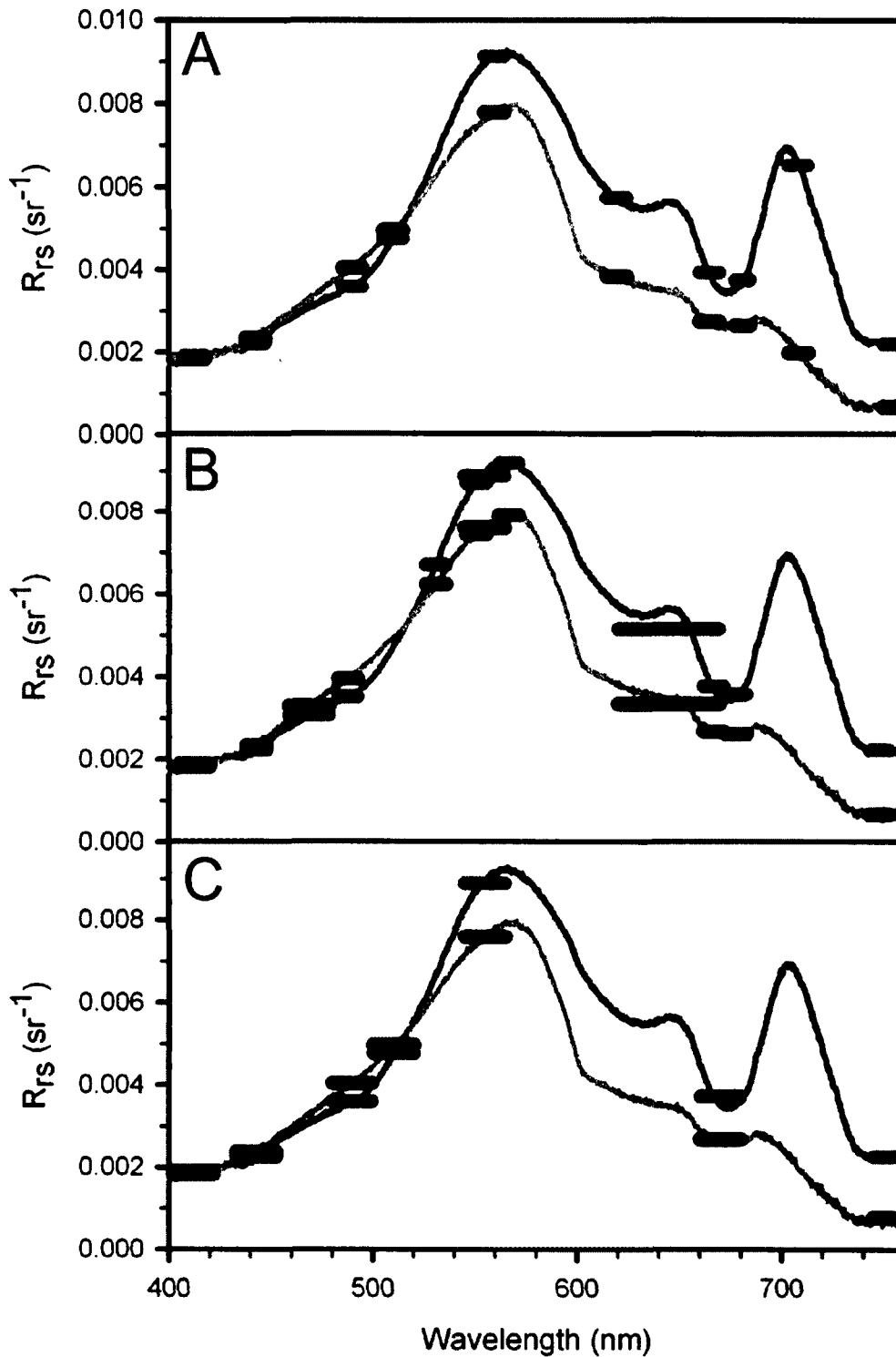
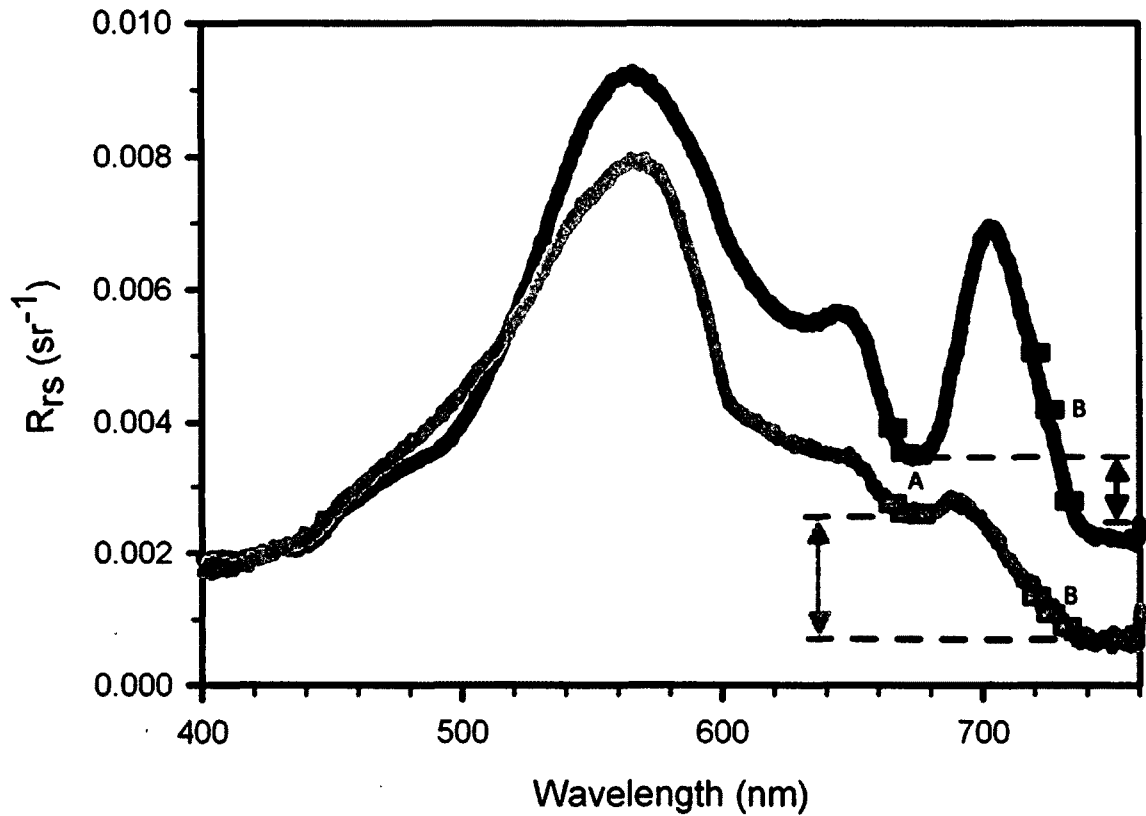
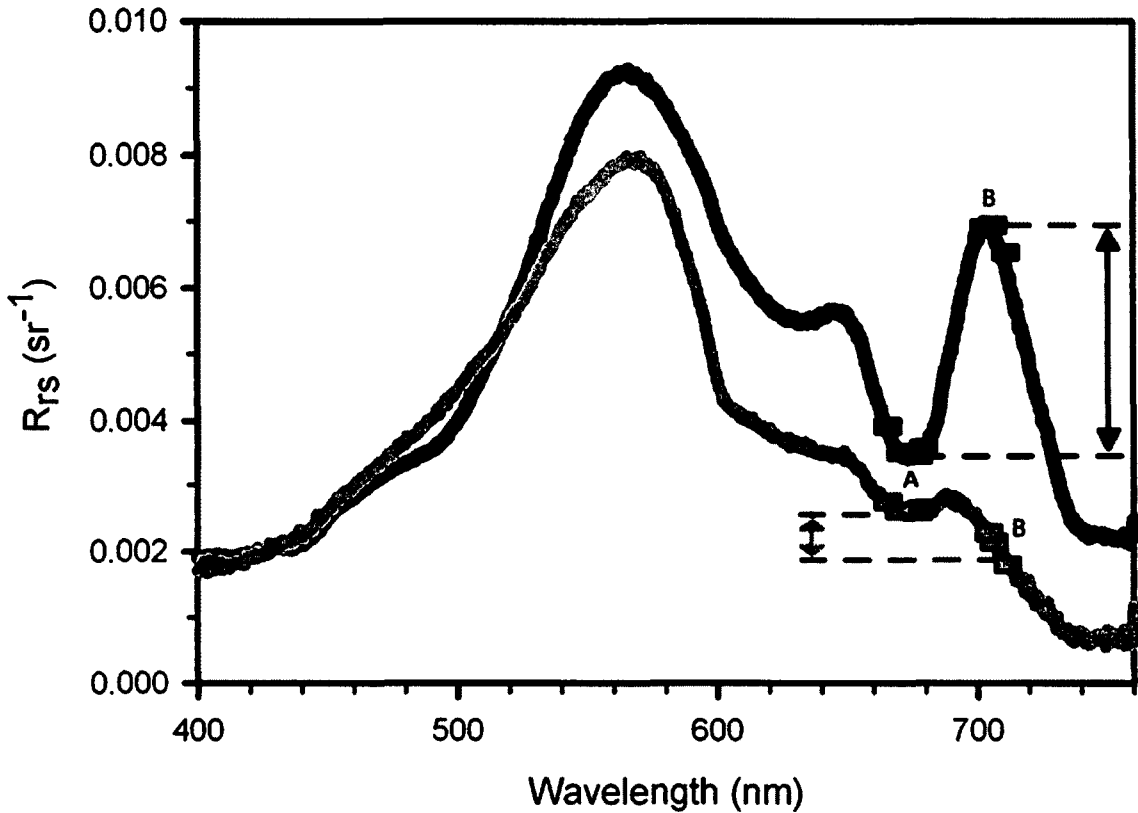


Figure 4. Algorithm band locations for several 2-band hyperspectral algorithms (Table 4, A-C). The A bands (665 nm, 670 nm, 673 nm) were chosen to measure the intensity of chlorophyll absorption. The B bands (735 nm, 725 nm, 720 nm) were chose as reference points in areas of the spectrum not directly affected by chlorophyll absorption. The light gray spectrum is typical of low chlorophyll lakes ($5.7 \mu\text{g L}^{-1}$). The dark gray spectrum is typical of high chlorophyll lakes ($36.6 \mu\text{g L}^{-1}$).



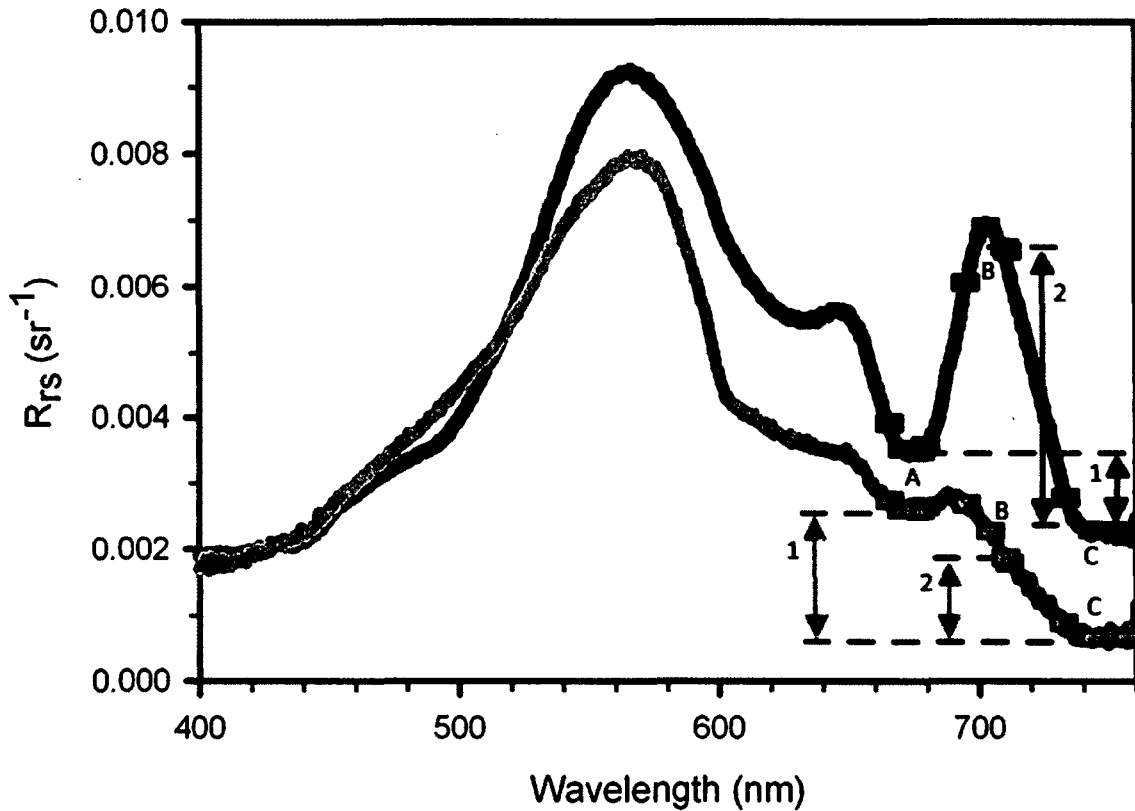
$$ratio = \frac{R_{rs}(\lambda_B)}{R_{rs}(\lambda_A)}$$

Figure 5. Algorithm band locations for several 2-band hyperspectral algorithms (Table 4, D-G). The A bands (665 nm, 670 nm, 673 nm, 677 nm) were chosen to measure the intensity of chlorophyll absorption. The B bands (703 nm, 705 nm, 710 nm) were chosen to characterize the peak which appears between 690 nm and 710 nm with increasing phytoplankton density. The light gray spectrum is typical of low chlorophyll lakes ($5.7 \mu\text{g L}^{-1}$). The dark gray spectrum is typical of high chlorophyll lakes ($36.6 \mu\text{g L}^{-1}$).



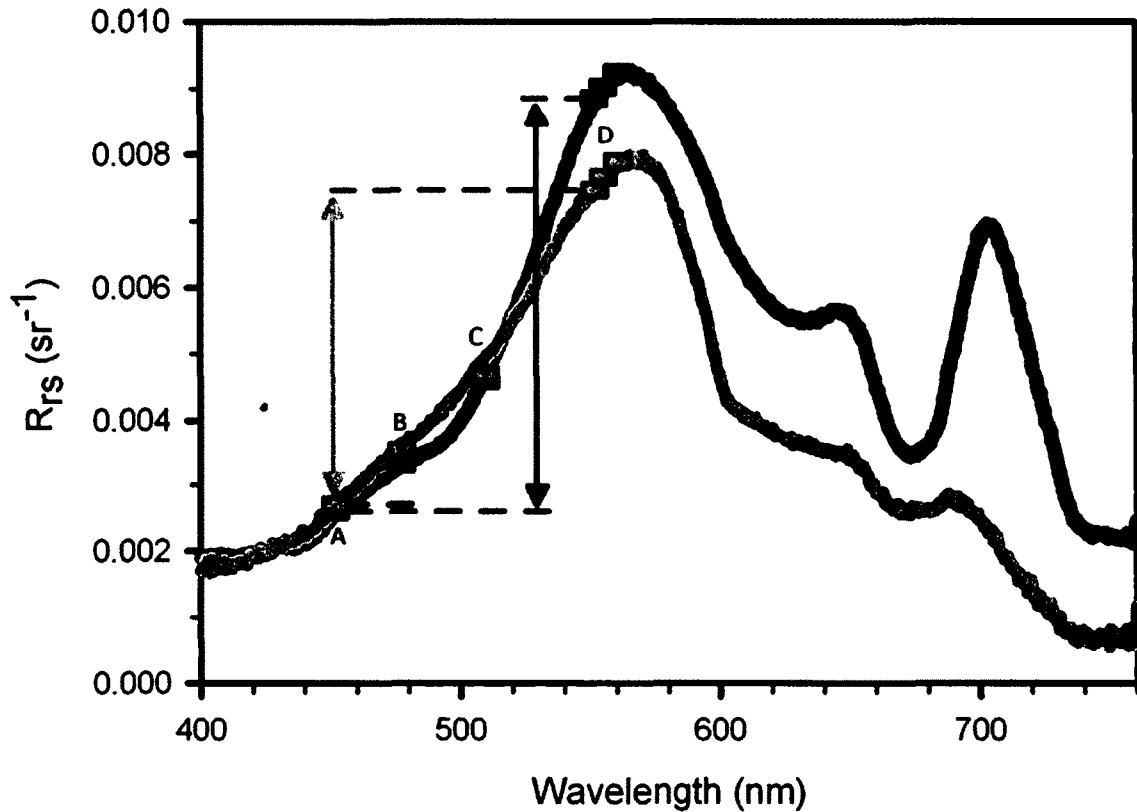
$$ratio = \frac{R_{rs}(\lambda_B)}{R_{rs}(\lambda_A)}$$

Figure 6. Algorithm band locations for 3-band hyperspectral algorithms (Table 4, H-K). The A band (665 nm, 671 nm, 675 nm, 677 nm) was chosen to measure the intensity of chlorophyll absorption. The B band (695 nm, 703 nm, 709 nm, 710 nm) was chosen to characterize the peak which appears between 690 nm and 710 nm with increasing phytoplankton density. The C band (730 nm, 740 nm, 754 nm) was selected to represent an area of the spectrum with little to no variation related to bio-optically active components. The light gray spectrum is typical of low chlorophyll lakes ($5.7 \mu\text{g L}^{-1}$). The dark gray spectrum is typical of high chlorophyll lakes ($36.6 \mu\text{g L}^{-1}$).



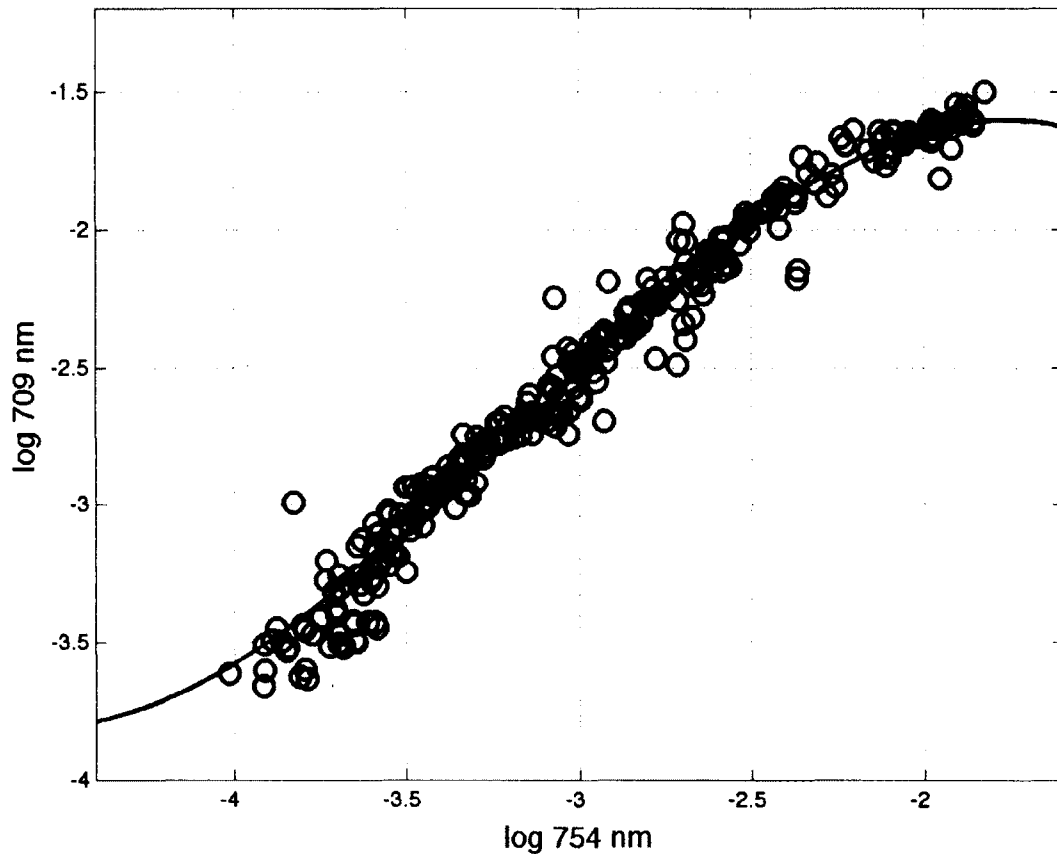
$$ratio = \frac{R_{rs}(\lambda_C)}{R_{rs}(\lambda_A)} - \frac{R_{rs}(\lambda_C)}{R_{rs}(\lambda_B)}$$

Figure 7. Algorithm band locations for operationally deployed ocean chlorophyll algorithms (Table 5, L-N). The A band (443 nm), B band (489 nm) and C band (510 nm) were chosen to measure the intensity of chlorophyll absorption in the blue region. The algorithm uses whichever of these three bands has the highest reflectance value. The D band (550 nm, 555 nm or 560 nm depending on sensor) is used as an anchor point against which to measure the changes in the other bands. The light gray spectrum is typical of low chlorophyll lakes ($5.7 \mu\text{g L}^{-1}$). The dark gray spectrum is typical of high chlorophyll lakes ($36.6 \mu\text{g L}^{-1}$).



$$ratio = \frac{\max[R_{rs}(\lambda_A), R_{rs}(\lambda_B), R_{rs}(\lambda_C)]}{R_{rs}(\lambda_D)}$$

Figure 8. Relationship between MERIS bands at 754 nm and 709 nm. Data set includes spectra from this current work (Great Salt Lake, New England lakes), as well as, data obtained from Spanish Lakes (personal communication, Ruiz-Verdu, 2012). This 3rd order relationship was applied to the 748 nm MODIS band generated from each spectrum to create a simulated 709 nm band which could be used in algorithm development for that sensor.



$$\log R_{rs}(\lambda_A) =$$

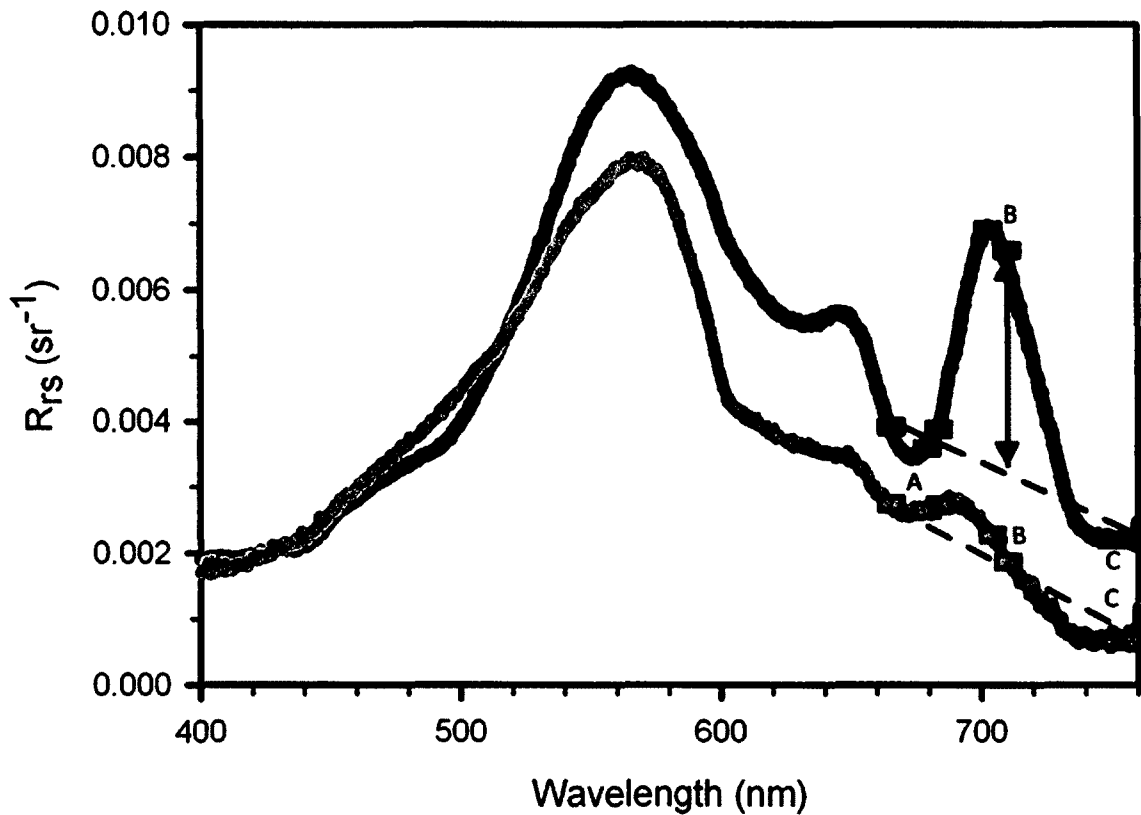
$$-0.2003[\log[R_{rs}(\lambda_B)]^3]$$

$$-1.9001[\log[R_{rs}(\lambda_B)]^2]$$

$$-4.8280[\log[R_{rs}(\lambda_B)] - 5.3044]$$

where, $A = 709\text{nm}$, $B = 754\text{nm}$

Figure 9. Algorithm band locations for the Maximum Chlorophyll Index (MCI) algorithms (Table 5, O-S). The A band (665 nm, 667 nm, 677 nm, 678 nm, 681 nm), was chosen to measure the intensity of chlorophyll absorption in the red region. The B band (703 nm, 709 nm) was chosen as to characterize peak which appears between 690 nm and 710 nm with increasing phytoplankton density. The C band (748 nm, 754 nm) is used as an anchor point against which to measure the changes in the other bands. The light gray spectrum is typical of low chlorophyll lakes ($5.7 \mu\text{g L}^{-1}$). The dark gray spectrum is typical of high chlorophyll lakes ($36.6 \mu\text{g L}^{-1}$).



$$MCI = R_{rs}(\lambda_B) - [R_{rs}(\lambda_A) - f[R_{rs}(\lambda_C) - R_{rs}(\lambda_A)]]$$

where, $f = (\lambda_B - \lambda_A) / (\lambda_C - \lambda_A)$

CHAPTER III

CHLOROPHYLL ALGORITHMS FOR NEW ENGLAND LAKES

Introduction

General description

New England lakes were formed during the retreat of the glaciers approximately 10,000 years ago, a process that littered the region with thousands of lakes with soils consisting largely of glacial till. Three EPA nutrient ecoregions span New England - glaciated dairy, glaciated northeast and eastern coastal plain. Based on chlorophyll concentration, nearly 75% of the lakes in New England are classified as oligo-mesotrophic, compared to 50% on the national scale, and the region is second only to the Pacific Northwest in the percentage of oligotrophic lakes (USEPA 2010). When considering an evaluation of stressors on lakes, 79% (for phosphorus) and 88% (for nitrogen) of New England lakes are ranked as good, compared to 58% and 54% of lakes nationally (USEPA 2010).

Although the lakes in New England are nutrient poor compared to most lakes in much of the rest of the United States, the lakes are at high risk for degradation. Lakes in the region possess little buffering capacity due to the non-calcareous

bedrock or high silicate soils upon which they sit, and as such, lack the ability to effectively mediate increases of nutrient concentrations without effecting the lake ecosystem. Little to no information is available on suitable remote sensing methods for monitoring lakes in this area of the country, and most research on the development of lake algorithms in other regions around the world has not included lakes with these characteristics in their datasets.

Methodology

Sampling

Measurements of hyperspectral reflectance were made at 125 lake sites from 2002 to 2009, representing 78 different lakes from seven states (Figure 10). Of these sampling sites, 31 lake sites (on 17 lakes) were measured with the single-radiometer system and 94 sites (on 64 lakes) with the dual-radiometer system. The range of geographic and temporal variation ensured good representation of the range of lake conditions found throughout New England.

Chlorophyll a

At each sampling site, lake water was collected throughout the epilimnion using an integrated sampling tube (Table 2). Chlorophyll analysis differed based on the project under which the sampling was conducted (Table 3). All of the lake sites

sampled from 2002 to 2005 and in 2008, (n=69), were conducted during University of New Hampshire (UNH) class field trips or research trips. Chlorophyll analyses for these samples were performed at UNH, except for a single lake visit, which was analyzed at the University of Maine. Lake sites sampled in 2007 (n=14) were part of the US EPA National Lakes Assessment Project, and lakes sampled in 2009 (n=3) were part of continuing collaboration with the EPA Region I Laboratory in Chelmsford, MA. Chlorophyll analyses for these 17 lake sites were conducted at the US EPA Region I Laboratory.

Data collected from lakes in 2006 were part of the US EPA New England Lakes Project (NELP) sampling program. This project involved a comparison of analytical methods from seven laboratories: Connecticut Department of Energy and Environmental Protection (CT), Massachusetts Department of Environmental Protection (MA), Maine Department of Environmental Protection (ME), New Hampshire Department of Environmental Services (NH), UNH, University of Rhode Island (URI), and Vermont Department of Environmental Conservation (VT). Following a round-robin protocol, all water samples were to be analyzed by each of the seven laboratories, and results compared.

A total of 39 lakes were sampled by the NELP project during the summer and fall of 2006. The majority of the lakes had chlorophyll data for each of the seven analytical methods used, but occasionally missing field equipment (filters) or mishandling of samples led to missing chlorophyll data for a given method for a

particular lake (Table 6). To assess which of the methods produced results most similar to the UNH method (upon which much of the other New England chlorophyll data were based), the sum of squared differences was calculated for each method as compared to the chlorophyll values produced by UNH (Table 7). A total of 34 lakes from six different methods (including UNH) were included in the comparison. The method from MA was excluded due to insufficient chlorophyll data.

Based on the comparison of the relative sum of squares, the VT method was chosen as the alternate chlorophyll method with values most similar to those produced with the UNH method. As such, chlorophyll concentrations from the VT method were used when no chlorophyll data were available from the UNH method for a given lake (n=4) or when the average chlorophyll concentration of all seven methods for a lake was greater than $10 \mu\text{g L}^{-1}$ (n=8) to reduce potential issues related to suspected degradation effects (Figure 11).

Dual-radiometer data collection/processing

At 94 lake sites, spectral measurements were made using the dual-radiometer technique described in Chapter II. Raw spectral measurements were processed and converted to remote sensing reflectance (R_{rs} , sr^{-1}) using equations (6) to (17). For two of the spectra, no chlorophyll measurements were available, and two other spectra were determined to be of poor quality due to adverse weather

conditions during collection (high waves). As a result, a total of 90 spectra were used to test the algorithms described in Tables 4 and 5.

As shown in Table 8, all algorithms were examined in a log-log relationship to relate the spectral measurements to the chlorophyll concentration. All of the 2-band and 3-band ratio algorithms were also examined as linear relationships. The best algorithms for each sensor type and chlorophyll range were identified based on the RMS, relative error, and r^2 values, as well as a visual evaluation of the goodness of fit.

To examine the effects of very low and very high chlorophyll concentrations on linear regression analyses, all algorithms were run with four different datasets: all chlorophyll data (n=90), chlorophyll $> 5 \mu\text{g L}^{-1}$ (n=40), chlorophyll $< 50 \mu\text{g L}^{-1}$ (n=89), and chlorophyll between 5 and $50 \mu\text{g L}^{-1}$ (Appendix C).

Single-radiometer data collection/processing

At 31 lake sites, spectral measurements were made using the single-radiometer technique described in Chapter II. Raw spectral measurements were processed and converted to remote sensing reflectance (R_{rs} , sr^{-1}) using equations (1) to (5). Six of the spectra were far outside the norm for water spectra based on intensity, spectral characteristics, or both, probably due to poor collection technique (i.e. not holding the radiometer at the correct angles, changing light conditions

between measurements) and/or adverse optical conditions (i.e., high CDOM). An additional seven spectra were determined to be outliers compared to the dual-radiometer spectra (Figure 12). This was based on the fact that they varied > 1.5 standard deviations from the predicted value and thus, were excluded from further analysis. After removing sub-optimal spectra, a final batch of 18 single-radiometer spectra remained and were combined with dual-radiometer spectra to evaluate selected algorithms (Tables 4, 5) as described in Table 8. Finally, the RMS and relative errors produced by the dual-radiometer spectra were compared to the combined single- and dual-radiometer collected dataset.

Results

Spectral measurements

Description of dual-radiometer spectra. The 90 dual-radiometer spectra remaining after quality control exhibited a great deal of variability in green/yellow (540 nm to 600 nm), red (600nm to 700 nm) and near-infrared (700 nm to 710 nm) portions of the spectrum (Figures 13, 14). Relatively little variability was observed in the blue end of the spectrum, especially at wavelengths less than 450 nm. Unlike the open ocean, where there is high variability in the blue, in CDOM-rich lakes, spectra were noticeably influenced by the strong absorption of CDOM in the blue and green wavelengths (Figure 15).

Description of single-radiometer spectra. The 18 spectra remaining after quality control exhibited a great deal of variability in green/yellow (530nm to 600 nm), red (600nm to 700 nm) and near-infrared (700 nm to 735 nm) portions of the spectra (Figures 16, 17). A higher level of variability than expected was observed in the blue end of the spectrum, especially at wavelengths less than 450 nm, which was likely due to poor measurement technique, the insufficient removal of reflected skylight, and/or insufficient sensor sensitivity in that wavelength range.

Chlorophyll a

For the spectra collected with the dual-radiometer system, chlorophyll ranged from 0.8 $\mu\text{g L}^{-1}$ to 126 $\mu\text{g L}^{-1}$ (Figures 18, 19). The mean concentration of all sites was 9.9 $\mu\text{g L}^{-1}$, and the median chlorophyll value was 4.4 $\mu\text{g L}^{-1}$. A total of 8 lakes could be classified as hypereutrophic (9%), 20 as eutrophic (22%), 45 as mesotrophic (52%) and 17 as oligotrophic (18%). This distribution is similar to lakes across the Northern Appalachian region found in 2009 (EPA 2009), although shifted slightly more toward eutrophic lakes due to targeted sampling of this lake type. For the spectra collected with the single-radiometer system, chlorophyll ranged from 0.7 $\mu\text{g L}^{-1}$ to 61.9 $\mu\text{g L}^{-1}$ with a median of 2.9 $\mu\text{g L}^{-1}$, and mean of 7.3 $\mu\text{g L}^{-1}$.

Evaluation of algorithms

Results on the evaluation of algorithms presented in this chapter are all based on the log-log regression analyses. Results for linear regressions are presented in Appendix C, as well as the coefficients for the best log-log algorithms. For simplicity of notation in the figures and tables, reflectance ratios and other predictor variables are denoted by the wavelengths involved (e.g., $R_{rs}(\lambda_A)/R_{rs}(\lambda_B)$ is denoted λ_A/λ_B).

Dual radiometer - hyperspectral band algorithms. A variety of algorithms using hyperspectral data proved effective for estimating chlorophyll concentration, with 11 exhibiting an RMS < 0.250 (Table 9). The most effective algorithm was a modified MCI using 677 nm (wavelength optimized for this dataset), followed by two 3-band algorithms, and a 2- band algorithm also using an optimized chlorophyll absorption minimum band (677 nm) (Figure 20, Figure 21). Out of the three MCI algorithms examined (using 677 nm, 665 nm, or the standard 681 nm), the standard algorithm had the highest RMS (13% higher than 677 nm version).

Dual radiometer - MERIS algorithms. All algorithms based on MERIS bands proved effective for estimating chlorophyll concentration (highest RMS was 0.252) (Table 9; Figures 20, 22). The most effective algorithm was a modified MCI using an alternate band (665 nm), followed by a 3-band algorithm, and the

standard MCI (681 nm). The most effective blue band for the OC algorithm was 489 nm, which offered a 4% improvement over the band chosen by the OC4 algorithm (510 nm). Out of the two MCI algorithms examined (665 nm and the standard 681 nm), the standard algorithm had the higher RMS (5% higher than with 665 nm).

Dual radiometer - MODIS algorithms. The OC algorithms based on MODIS bands proved most effective for estimating chlorophyll concentration (highest RMS was 0.252), while MCI algorithms relying on the simulated 709 nm band were slightly less effective (Table 9; Figures 22, 23). The most effective approach was an OC algorithm using the band chosen by OC3 (489 nm). The standard MCI (678 nm) proved barely better (2%) than the alternate version (668 nm). All approaches using the simulated 709 band in 2- and 3-band algorithms were much less effective than other options.

Dual radiometer - SeaWiFS algorithms. All algorithms based on SeaWiFS bands proved effective for estimating chlorophyll concentration (highest RMS was 0.252) (Table 9; Figures 22, 23). The most effective blue band for the OC algorithm was 489 nm, which offered a 3% improvement over the band chosen by the standard OC4 algorithm (510 nm).

Comparison of single- and dual-radiometer algorithms

The 18 spectra from the single-radiometer setup were combined with the 90 valid spectra from the dual-radiometer method into one dataset. This combined grouping of spectra were used to examine a subset of the chlorophyll algorithms that were run using the dual-radiometer dataset (Table 8). Not all algorithms could be analyzed due to the lack of spectral data above 725 nm in the spectra collected with the single radiometer.

The majority (19) of algorithms produced higher RMS (1% to 35%) values for the combined datasets than when using the dual-radiometer spectra alone. However, four of the algorithms exhibited a reduced RMS with the combined data set (1% to 5%), and three of the algorithms demonstrated no change in RMS between the two datasets (Table 10). The algorithms most altered when using the combined dataset were the MERIS algorithms relying on the scattering peak band (709 nm). The algorithms least affected by the addition of the single-radiometer spectra were the ocean color algorithms for satellite sensors, for which the RMS increased a maximum of 2%, and decreased up to 5%.

Discussion

General observations

Round robin chlorophyll methods. While the lack of UNH-analyzed chlorophyll concentrations for some of the lakes sampled in 2006, and the possible mishandling of some UNH filters for other lakes that summer, might have led to the exclusion of some lake spectra, the availability of additional chlorophyll data from the round robin experiment ultimately allowed all spectra collected to be used in algorithm development. The chlorophyll analytical method used by the state of Vermont produced results quite comparable to those from UNH, in spite of the fact that the two techniques used different filter preservation techniques (dried vs. frozen) and different analytical methods (spectrophotometric vs. fluorometric). The Vermont data proved to be an adequate replacement for missing or potentially compromised UNH chlorophyll concentration data. Overall, the substituted data represented a minority of the lakes sampled that year (31%) and made up an even smaller proportion of all dual-radiometer spectra in this study (13%).

Single- vs. dual-radiometer spectra. The comparison of spectra collected with the different methods (single- vs. dual-radiometer) revealed several insights. First, it was more difficult to collect valid spectral data using the single radiometer. This difficulty was due to a combination of technical capabilities of the equipment, as

well as the different methods in which measurements were taken. In the case of the single-radiometer method, data capture was less automated and required a series of four measurements to be taken in succession (dark, water, sky, gray) to capture all of the necessary data. A fundamental assumption in the single-radiometer technique is a constant ambient light field across the duration of all four measurements. While the four measurements were usually completed within 1 minute, it is probable that ambient light changes occurred during most of the measurement periods. The dual-radiometer system relied on CDAP to collect data, which was much more automated, used averaging, and automatically adjusted integration times based on ambient light conditions at the beginning of the measurement. In addition, the dual-radiometer system measured upwelling and downwelling light simultaneously, removing much of the error introduced by changing light conditions during the measurement period. Finally, the directionality of the sensor was more difficult to maintain accurately with the single radiometer (45° and 135°) than with the dual-radiometer equipment (180°).

In spite of the inherent limitations of the single-radiometer measurement technique, 80% of the measurements produced usable spectra (58% of spectra met the standards of this study). This number could potentially have been increased by the collection of more replicates at each lake, which would have provided a greater chance to overcome the limitations of the device and the method. When compared to the typical scatter of data around the best algorithms developed using dual-radiometer spectra alone, less than 1/3 of the valid single-

radiometer spectra were determined to be outliers. In general, it is clear that the single-radiometer spectra were mostly comparable to data produced with the dual-radiometer method, although technical and logistical difficulties resulted in less measurement accuracy, and as such, more scatter introduced in the regression analysis between spectral bands and chlorophyll concentration.

As a result of the additional scatter, and the related increase in RMS introduced by the inclusion of single-radiometer collected spectra (Table 10), these data were not included in the final evaluation of New England lake spectra. The increased RMS values introduced by these spectra artificially changed the ranking of algorithms, since not all of the algorithms could be evaluated with the single-radiometer spectra due to lack of spectral data above 725 nm. While these data were ultimately not used in the final analyses presented here, the single-radiometer collection technique still provided potentially useful, although less accurate data, and this method could stand as a relatively inexpensive and less technically demanding method for spectral data collection on lakes.

Algorithms

Hyperspectral algorithms. Many algorithms for estimating chlorophyll concentration in New England Lakes using hyperspectral bands were quite effective, making it difficult to definitively choose the best algorithm to use for this sensor. Based on RMS values, the top choices were a combination of MCI, 3-

band, and 2-band algorithms with RMS values from 0.206 to 0.211. Perhaps not surprisingly, three of these top choices utilized bands optimized for this spectral data set (677 nm for chlorophyll absorption, 703 nm for scattering peak).

Interestingly, the top three algorithms (and five of the top six) could only be included in the log-log analyses after the addition of a constant to prevent the predictor variable (spectral difference) from being negative. While this may not be a standard practice, it produced some of the most effective options for estimating chlorophyll in New England lakes, and as such, should be investigated further. A key question that remains to be answered is how results might differ if a different constant is added.

Several of the hyperspectral algorithms used in this study were identified as useful for Nebraska lakes, although the algorithms found to be most effective differed from the ordering described here (Dall'Olmo and Gitelson 2005). The RMS values demonstrated by these algorithms were far below those shown by Dall'Olmo, and were not subject to the same difficulty under $10 \mu\text{g L}^{-1}$ as exhibited in the Nebraska lakes.

Satellite sensor algorithms. The best satellite-based algorithms were those based on the MERIS sensor bands, with RMS values as low as 0.218 for an alternate version of the MCI (using 665 nm). Several of the MERIS algorithms found to be most useful for New England lakes were also highly effective at estimating chlorophyll in Nebraska lakes, Lake Kinneret, and the Azov Sea (Gitelson et al.

2011b; Yacobi et al. 2011a; Gitelson et al. 2011a; Yacobi et al. 2011b), although in these studies the 2-band algorithm was found to be more effective than the 3-band (which was the opposite in the current study). Six of the algorithms for the MERIS sensor were better than the best MODIS algorithm, but the OC algorithm using 489 nm for MODIS and 489 nm for SeaWiFS exhibited low RMS values (0.242 and 0.231, respectively). These algorithms are re-parameterized versions of the OC3 and OC4 algorithms which are currently employed to produce the chlorophyll a product by the NASA ocean team for these satellite sensors. While there is no specific reason to expect that these Case I algorithms would work well in a Case II system (O'Reilly et al. 1998), the parameterized version of this algorithm is surprisingly effective at estimating chlorophyll in New England Lakes.

Table 6. Chlorophyll values for each lake site from different laboratories in the New England Lakes and Ponds project. Data labeled with * were excluded from the comparison analysis due to lack of UNH data for those points. MA data (labeled ^) were excluded from the analysis due to excessive data gaps. CT - Connecticut Department of Energy and Environmental Protection, ME - Maine Department of Environmental Protection, NH - New Hampshire Department of Environmental Services, UNH - University of New Hampshire, URI - University of Rhode Island, VT - Vermont Department of Environmental Conservation. Chlorophyll values in $\mu\text{g L}^{-1}$.

Lake		Analytical Chlorophyll Method						
Name	State	VT	CT	NH	ME	URI	UNH	MA
Shelbourne Pond	VT	126	47.8	176	140	95.1	73.3	161 [^]
Chauncey Lake	MA	36.0	36.3	39.8	37.0	5.1	33.2	36.2 [^]
Showell Pond	NH	69.6	40.7	24.4	34.0	35.4	23.8	46.5 [^]
Love Joy Pond	ME	24.0	9.0	27.9	23.0	15.7	13.4	22.0 [^]
French Pond	NH	30.6	17.0	40.7	30.0	22.7	11.7	37.3 [^]
Hundred Acre Pond	RI	14.2	17.2	16.9	19.0	14.0	8.8	---
Amos Lake	CT	21.6	23.5	20.6	18.0	16.8	5.8	---
Watchaug Lake	RI	4.8	7.0	5.2	5.1	2.6	4.4	---
Upper Statesville Res.	RI	7.5	5.5	9.0	8.1	5.2	5.8	---
Sennebec Pond	ME	6.7	26.5	8.7	6.7	5.7	5.8	7.0 [^]
Long Pond	MA	6.3	6.0	3.3	2.4	4.0	4.4	5.2 [^]
Gorton Pond	RI	12.2	9.3	11.7	11.0	4.9	4.6	---
Silver Lake	VT	5.4	3.7	5.8	4.9	3.5	5.4	5.5 [^]
Sunset Lake	MA	7.5	8.5	6.7	9.2	8.0	4.0	10.0 [^]
Five Mile Pond	MA	4.6	4.6	4.5	5.8	2.8	3.6	4.9 [^]
Ewell Pond	VT	4.4	1.2	5.4	5.0	1.2	5.6	5.0 [^]
Winncheck Pond	RI	3.4	3.6	3.5	3.0	2.0	1.7	---
Hayward Lake	CT	4.5	4.4	8.2	5.4	2.7	3.0	---
Quacumquasit lake	MA	3.2	3.2	1.7	3.0	1.5	3.2	3.6 [^]
Perch Pond	NH	7.0	4.2	7.3	3.1	4.3	2.9	5.4 [^]
Figure Eight Pond	ME	4.2	3.4	16.9	3.4	3.7	4.1	3.0 [^]
Mashapaug Lake	CT	2.5	2.6	0.5	3.0	1.3	3.2	---
Diamond Pond	NH	3.5	1.8	4.0	2.7	2.0	3.4	2.7 [^]
Goose Pond	MA	2.7	2.2	1.8	2.4	1.9	2.8	2.2 [^]
Lake Mattawa	MA	1.9	2.2	2.4	2.0	1.4	3.2	1.4 [^]
Stearus Pond	ME	3.5	3.4	4.6	2.7	2.1	2.6	3.1 [^]
Lowell Lake	VT	2.5	1.5	2.7	4.1	1.5	2.5	2.6 [^]
Quinnebaug Lake	CT	2.6	3.6	3.2	3.1	1.9	2.0	---
Keola Lake	ME	3.2	2.7	3.6	2.3	2.0	2.1	2.2 [^]
Granite Lake	NH	1.3	0.6	1.8	1.1	0.3	2.3	1.1 [^]
Forest Lake	VT	1.0	0.3	0.8	1.0	0.8	2.3	1.0 [^]
Whalom Lake	MA	1.4	1.9	0.9	1.3	0.9	2.4	1.1 [^]
Wallum Lake	RI	2.0	2.0	1.7	2.4	0.8	2.1	1.9 [^]
Shadow Lake	VT	1.8	1.5	1.3	1.6	1.0	1.7	1.6 [^]
Batterson Park Pond	CT	22.9*	22.3*	25.3*	25.0*	18.2*	---	---
East Twin Lake	CT	0.8*	2.0*	4.6*	4.7*	0.4*	---	---
Pleasant Lake	ME	4.1*	3.4*	4.1*	3.0*	2.8*	---	3.2 [^]
Partridge Lake	NH	3.0*	3.4*	4.1*	---	2.0*	2.9*	3.1 [^]
Lake Attitash	MA	23.8*	25.8*	19.6*	21.0*	---	12.4*	23.6 [^]

Table 7. Comparison of chlorophyll values from different laboratories in the New England Lakes and Ponds project. The sum of squares were calculated in reference to values from the University of New Hampshire chlorophyll concentrations. CT - Connecticut Department of Energy and Environmental Protection, ME - Maine Department of Environmental Protection, NH - New Hampshire Department of Environmental Services, URI - University of Rhode Island, VT - Vermont Department of Environmental Conservation.

Chlorophyll Range	Analytical Chlorophyll Method				
	CT	ME	NH	URI	VT
Sum of squares					
All data	130.3	127.2	200.4	112.3	142.6
<11 $\mu\text{g L}^{-1}$	53.2	34.1	54.6	51.9	28.4
Average relative sum of squares					
All data	40.7	32.0	51.9	43.0	31.5
<11 $\mu\text{g L}^{-1}$	40.9	28.8	48.4	45.8	23.9
Median relative sum of squares					
All data	30.9	31.2	35.1	44.6	25.4
<11 $\mu\text{g L}^{-1}$	30.5	21.3	33.2	44.7	16.0

Table 8. Algorithms run with spectra from New England lakes. Black dots indicate dual radiometer spectra, white dots indicate both dual radiometer spectra, as well as, a dataset using spectra from both collection techniques. The number of spectra used: black dots - all chlorophyll (n=90), chlorophyll > 5 $\mu\text{g L}^{-1}$ (n=40), chlorophyll < 50 $\mu\text{g L}^{-1}$ (n=89), chlorophyll between 5 $\mu\text{g L}^{-1}$ and 50 $\mu\text{g L}^{-1}$ (n=39), white dots - all chlorophyll (n=108), chlorophyll > 5 $\mu\text{g L}^{-1}$ (n=47), chlorophyll < 50 $\mu\text{g L}^{-1}$ (n=106), chlorophyll between 5 $\mu\text{g L}^{-1}$ and 50 $\mu\text{g L}^{-1}$ (n=45).

Type	Algorithm	log-log				linear			
		1st	2nd	3rd	4th	all	>5	<50	5-50
Hyper	703/677	○	○	○	○	○	○	○	○
	705/675	○	○	○	○	○	○	○	○
	710/665	○	○	○	○	○	○	○	○
	710/673	○	○	○	○	○	○	○	○
	720/670	○	○	○	○	○	○	○	○
	725/665	●	●	●	●	●	●	●	●
	735/673	●	●	●	●	●	●	●	●
	730/[675-695]	●	●	●	●	●	●	●	●
	740/[671-710]	●	●	●	●	●	●	●	●
	754/[665-709]	●	●	●	●	●	●	●	●
	754/[677-703]	●	●	●	●	●	●	●	●
	MCI (665)	●	●	●	●				
	MCI (677)	●	●	●	●				
	MCI (681)	●	●	●	●				
MERIS	709/665	○	○	○	○	○	○	○	○
	709/681	●	●	●	●	●	●	●	●
	709/(665:681)	○	○	○	○	○	○	○	○
	754/[665-709]	●	●	●	●	●	●	●	●
	MCI (665)	●	●	●	●				
	MCI (681)	●	●	●	●				
	OC (443)	○	○	○	○				
	OC (489)	○	○	○	○				
MODIS	709s/667	○	○	○	○	○	○	○	○
	709s/678	●	●	●	●	●	●	●	●
	709s/(667:678)	○	○	○	○	○	○	○	○
	748/[667-709s]	○	○	○	○	○	○	○	○
	MCI (667)	●	●	●	●				
	MCI (678)	●	●	●	●				
	OC3 (443)	○	○	○	○				
	OC3 (488)	○	○	○	○				
SeaWiFS	OC4 (489)	○	○	○	○				
	OC4 (510)	○	○	○	○				
	OC4 (443)	○	○	○	○				
	OC4 (443)	○	○	○	○				

Table 9. Log-log regression models (n=90) for predicting chlorophyll concentrations in the New England lakes sorted by RMS. The order column indicates the power of the polynomial equation which resulted in the best fit.

Type	Algorithm	RMS	Rel Error	r ²	Order
Hyper	MCI (677)	0.206	42%	0.78	3rd
	754/[677-703]	0.211	38%	0.77	2nd
	730/[675-695]	0.212	42%	0.76	2nd
	703/677	0.219	48%	0.75	2nd
	MCI (665)	0.221	51%	0.74	3rd
	754/[665-709]	0.225	41%	0.73	3rd
	705/675	0.226	45%	0.73	2nd
	710/673	0.229	47%	0.72	2nd
	MCI (681)	0.232	53%	0.72	3rd
	740/[671-710]	0.236	44%	0.71	3rd
	710/665	0.249	53%	0.67	2nd
	720/670	0.315	71%	0.48	2nd
	725/665	0.329	73%	0.43	2nd
	735/673	0.403	86%	0.14	3rd
	MERIS	MCI (665)	0.218	50%	0.75
754/[665-709]		0.223	40%	0.74	3rd
MCI (681)		0.229	51%	0.72	4th
OC (489)		0.233	42%	0.71	2nd
709/681		0.240	50%	0.70	2nd
709/(665:681)		0.241	51%	0.69	2nd
OC (510)		0.242	42%	0.69	2nd
OC (443)		0.252	47%	0.67	2nd
709/665		0.252	54%	0.67	2nd
MODIS		OC (488)	0.242	42%	0.69
	OC (443)	0.252	48%	0.67	2nd
	MCI (678)	0.281	67%	0.58	3rd
	MCI (667)	0.286	67%	0.58	3rd
	709s/678	0.367	84%	0.29	2nd
	709s/(667:678)	0.375	85%	0.26	2nd
	748/[667-709s]	0.382	85%	0.23	2nd
	709s/667	0.383	86%	0.23	2nd
SeaWiFS	OC (489)	0.231	42%	0.72	2nd
	OC (510)	0.238	42%	0.70	2nd
	OC (443)	0.253	47%	0.66	2nd

Table 10. Comparison of log-log algorithms for determining chlorophyll concentrations in New England lakes analyzed with only dual-radiometer spectra (DRS) and a combined data set of single- and dual-radiometer spectra (DRS+RS). Δ RMS indicates the difference between RMS values between the two datasets. Chlorophyll values are $\mu\text{g L}^{-1}$.

Type	Algorithm	Δ RMS	RMS		Rel Error	
			DRS	DRS+RS	DRS	DRS+RS
Hyper	703/677	+1%	0.219	0.221	48%	48%
	705/675	0%	0.226	0.226	45%	48%
	710/673	+8%	0.229	0.247	47%	55%
	710/665	+9%	0.249	0.272	53%	61%
	720/670	+8%	0.315	0.340	71%	81%
MERIS	709/(665:681)	+34%	0.241	0.323	51%	77%
	709/665	+35%	0.252	0.339	54%	80%
	OC (489)	0%	0.233	0.233	42%	50%
	OC (510)	-1%	0.242	0.240	42%	51%
	OC (443)	+2%	0.252	0.256	47%	57%
MODIS	OC (488)	-5%	0.242	0.229	42%	50%
	OC (443)	+2%	0.252	0.258	48%	57%
SeaWiFS	OC (489)	0%	0.231	0.230	42%	50%
	OC (510)	-1%	0.238	0.236	42%	51%
	OC (443)	+2%	0.253	0.258	47%	57%

Figure 10. Sampling sites for New England Lakes from 2002 to 2009. Measurements made at lakes with pink points were used in analysis, while data from lakes with orange points were discarded due to poor quality.

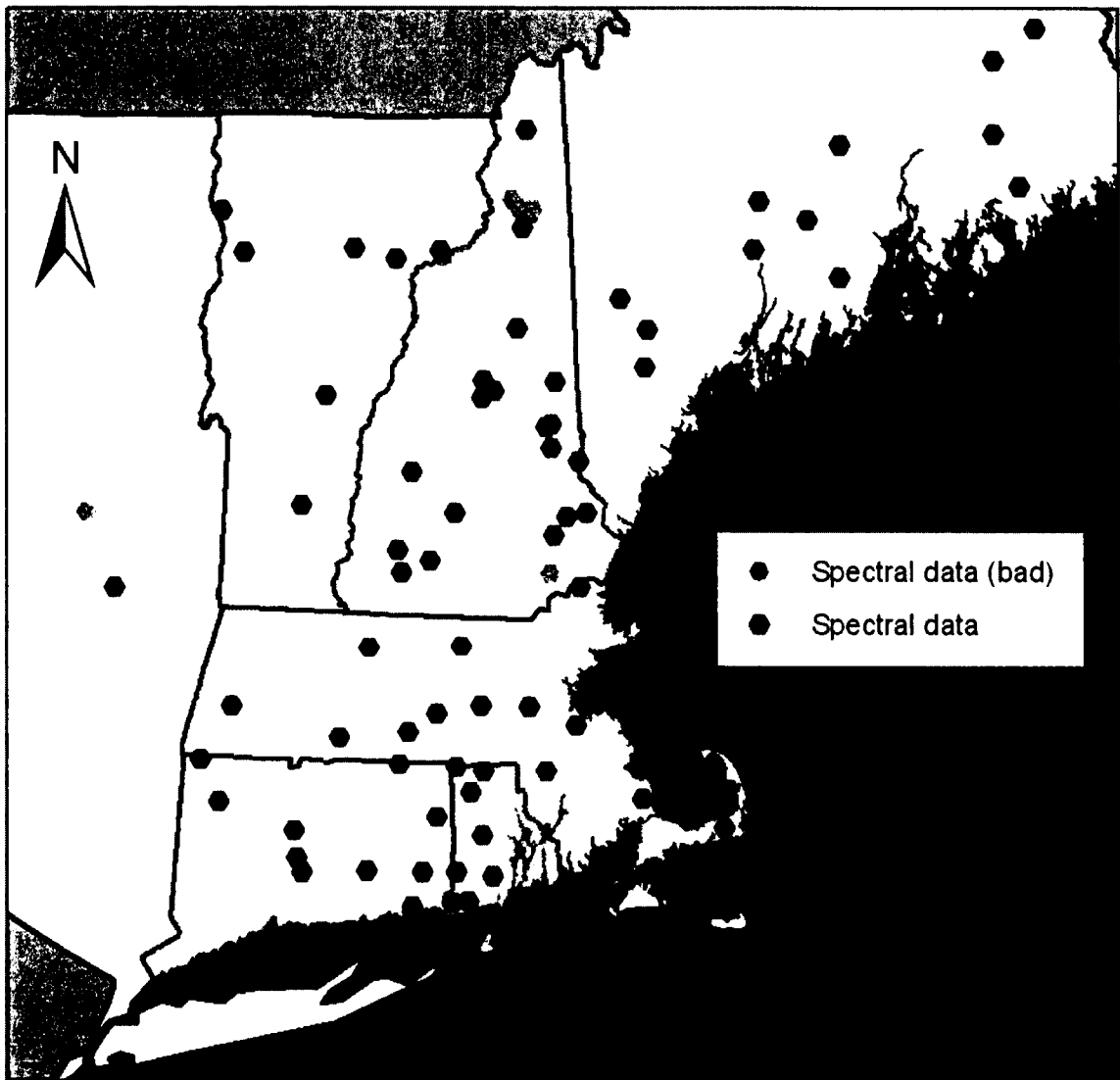


Figure 11. Comparison of chlorophyll concentrations determined by the Vermont Department of Environmental Conservation (VT) and the University of New Hampshire (UNH). The gray dotted line at $10 \mu\text{g L}^{-1}$ indicates the chlorophyll concentration above which the two methods are less comparable, providing potential evidence of chlorophyll degradation (green points) on some UNH filters at higher chlorophyll concentrations.

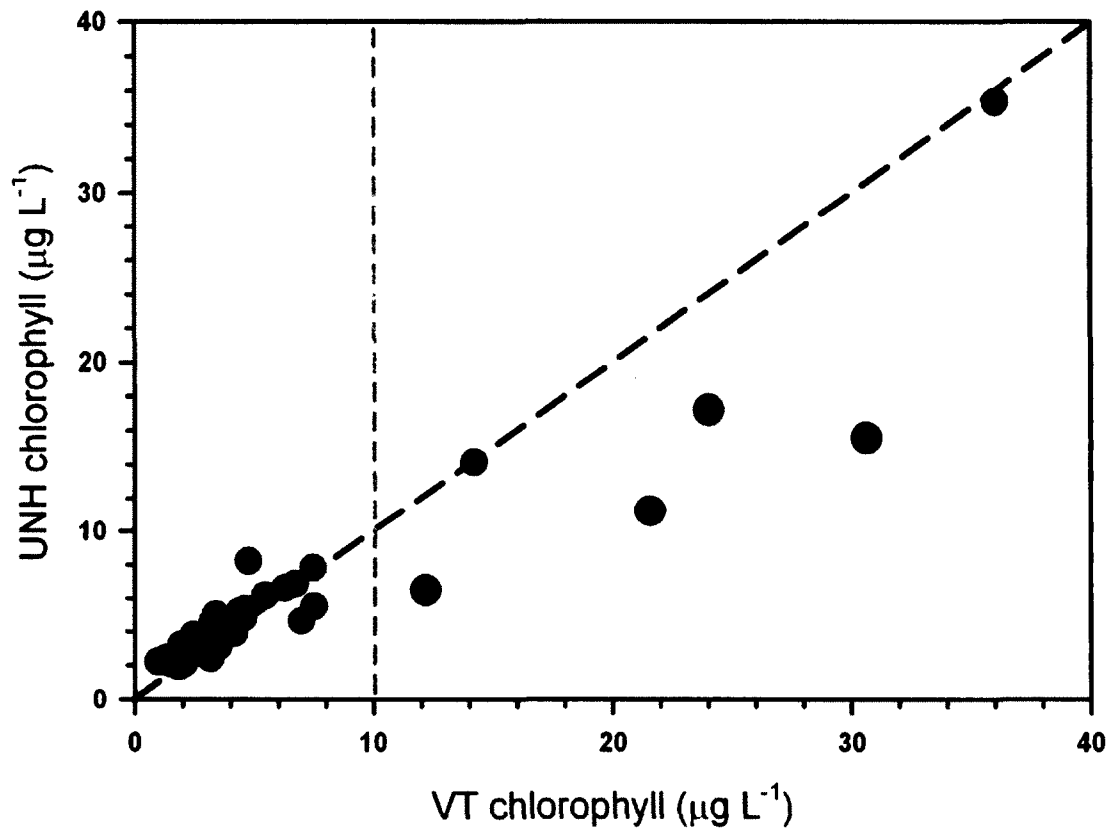


Figure 12. Comparison of single-radiometer and dual-radiometer spectra using three chlorophyll algorithms. Dual-radiometer points are blue, single-radiometer points are magenta. Red line represents best-fit algorithm developed with dual-radiometer points. Green boxes highlight single-radiometer points which fall outside the typical scatter of the dual-radiometer data.

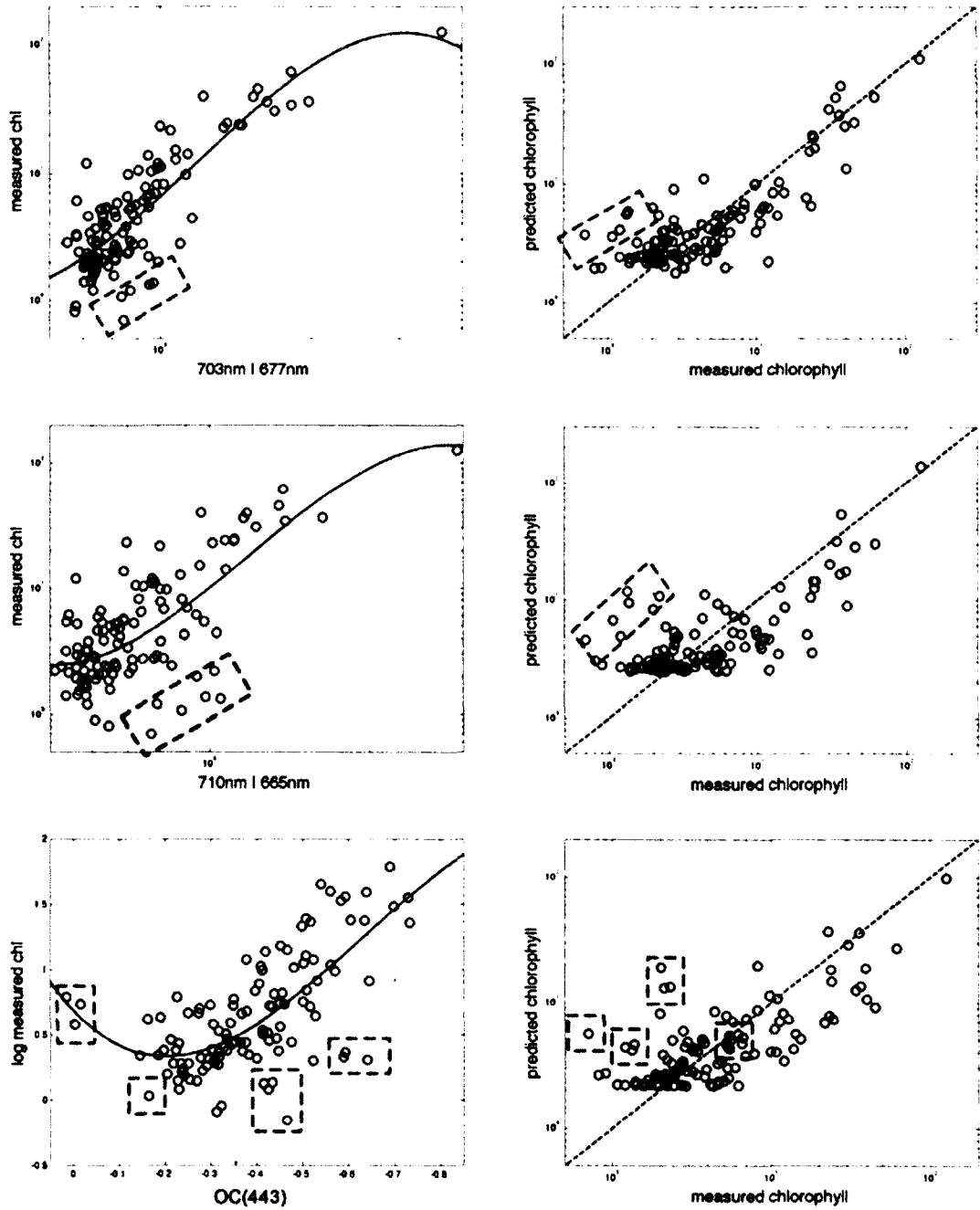


Figure 13. Hyperspectral reflectance spectra taken in New England lakes with the dual-radiometer system from 2005 to 2009. The spectra shown below (n=90) were used in algorithm development.

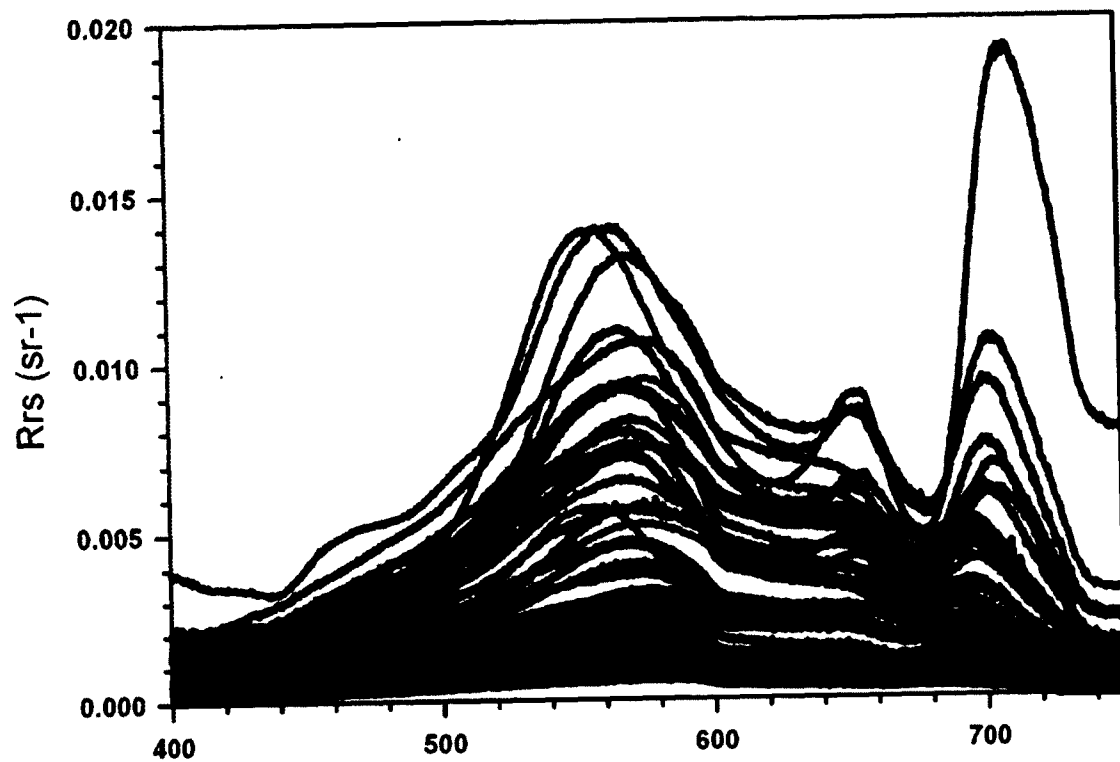


Figure 14. Average value and standard deviation for hyperspectral reflectance spectra taken of New England Lakes with the dual-radiometer system from 2005 to 2009 (n=90).

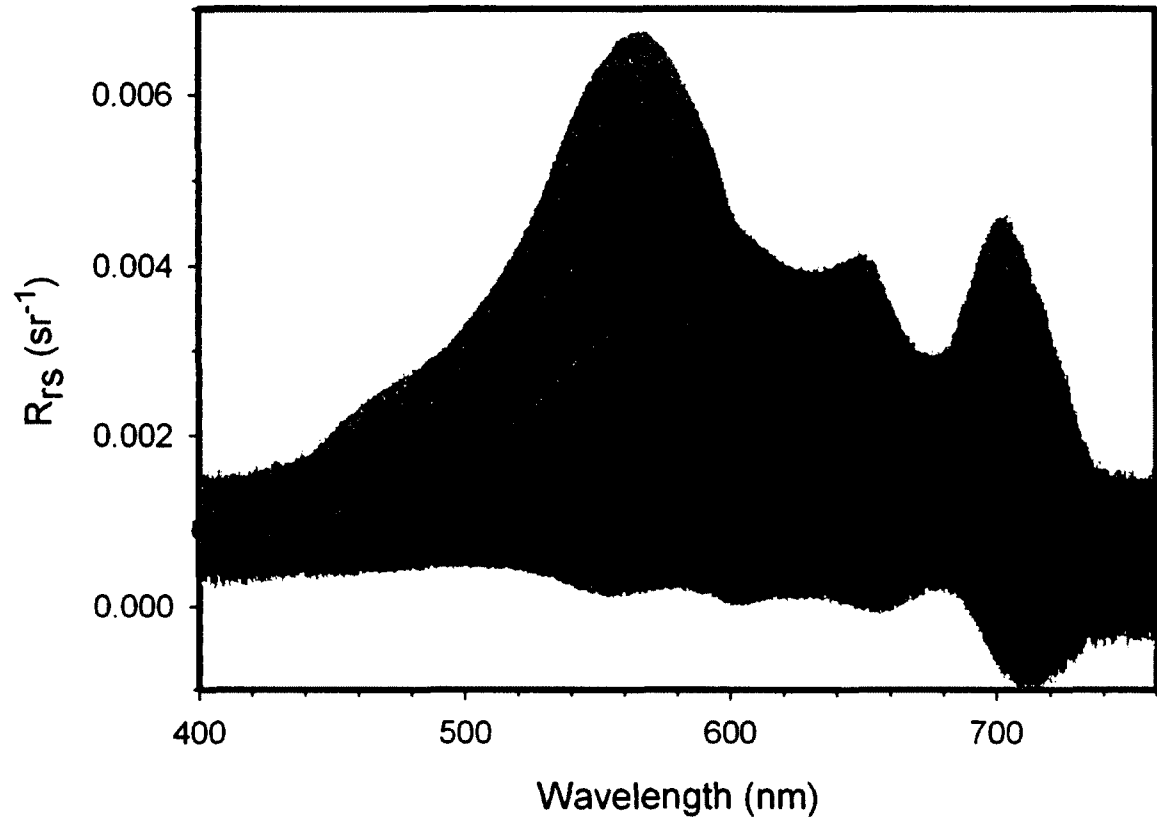


Figure 15. Examples of spectra collected from CDOM-rich New England lakes. R_{rs} intensity is lower than in most of the other lakes sampled. As is characteristic of spectra from such lakes, much of the signal in the blue and green areas each spectrum has been absorbed, causing the spectra to appear tilted toward higher wavelengths.

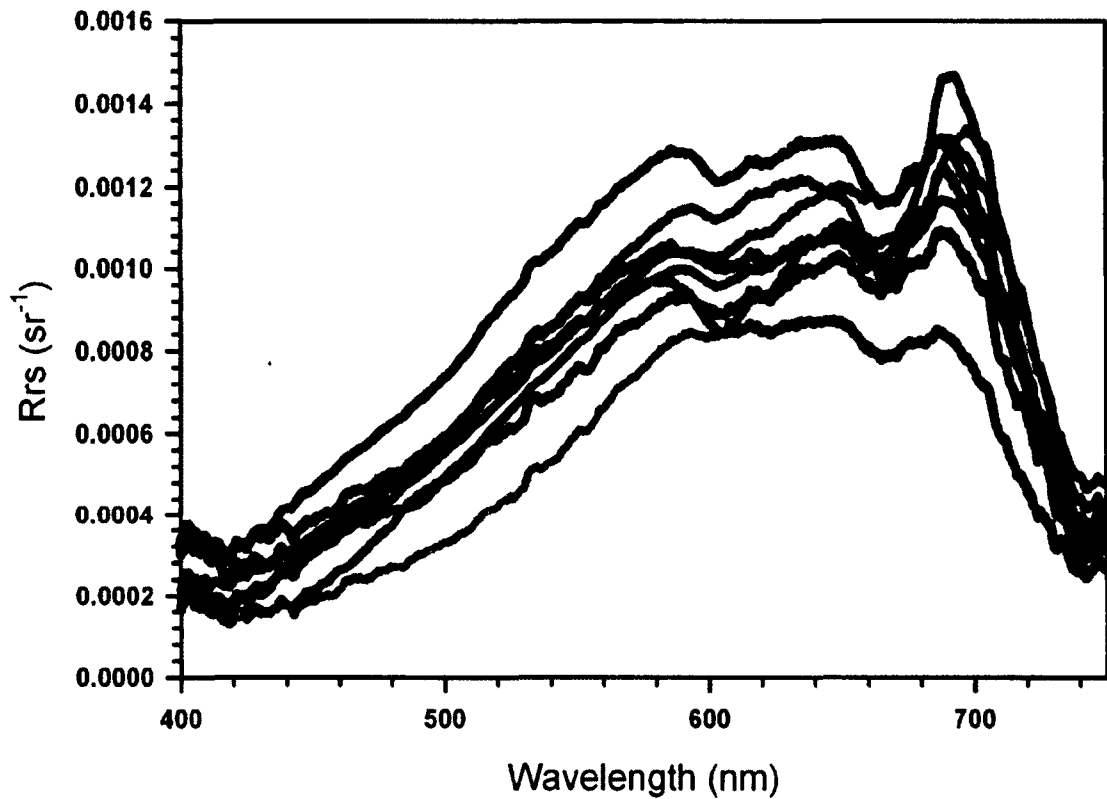


Figure 16. Hyperspectral reflectance spectra taken in New England lakes with the single-radiometer system from 2002 to 2004. The spectra shown below (n=18) were used in algorithm development.

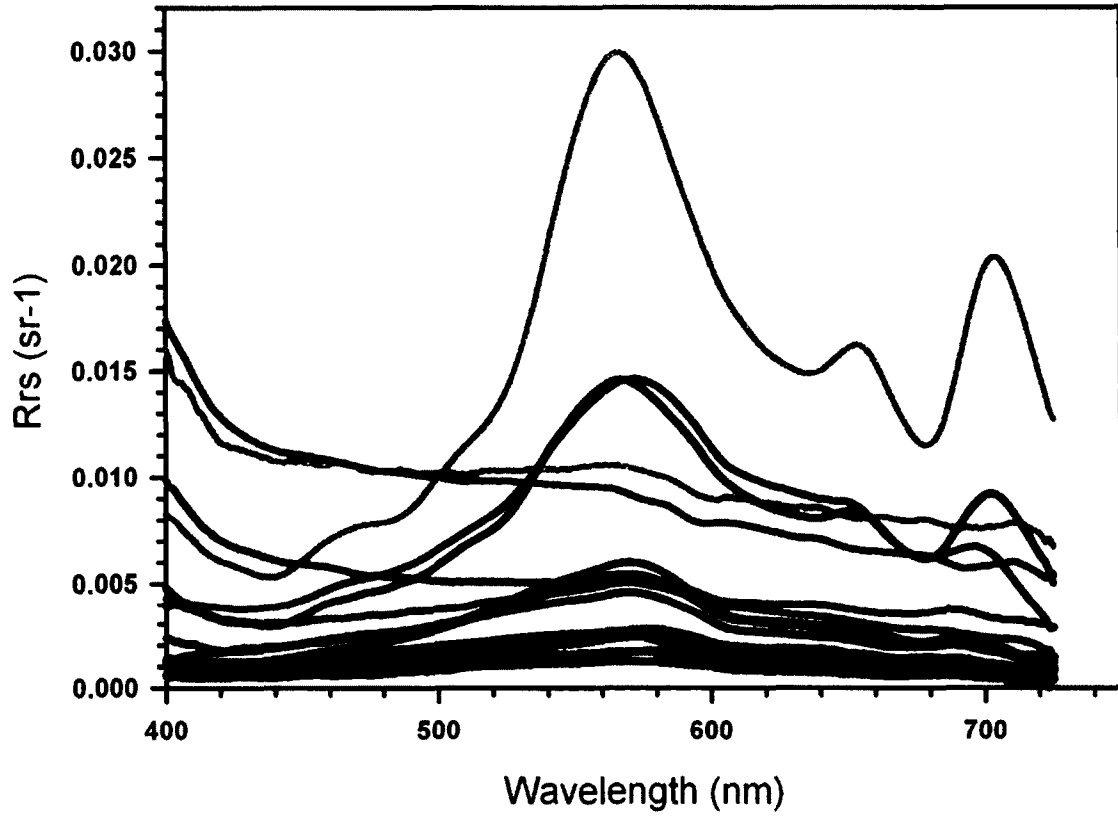


Figure 17. Average value and standard deviation for hyperspectral reflectance spectra taken of New England Lakes with the single-radiometer system from 2002 to 2004 (n=18).

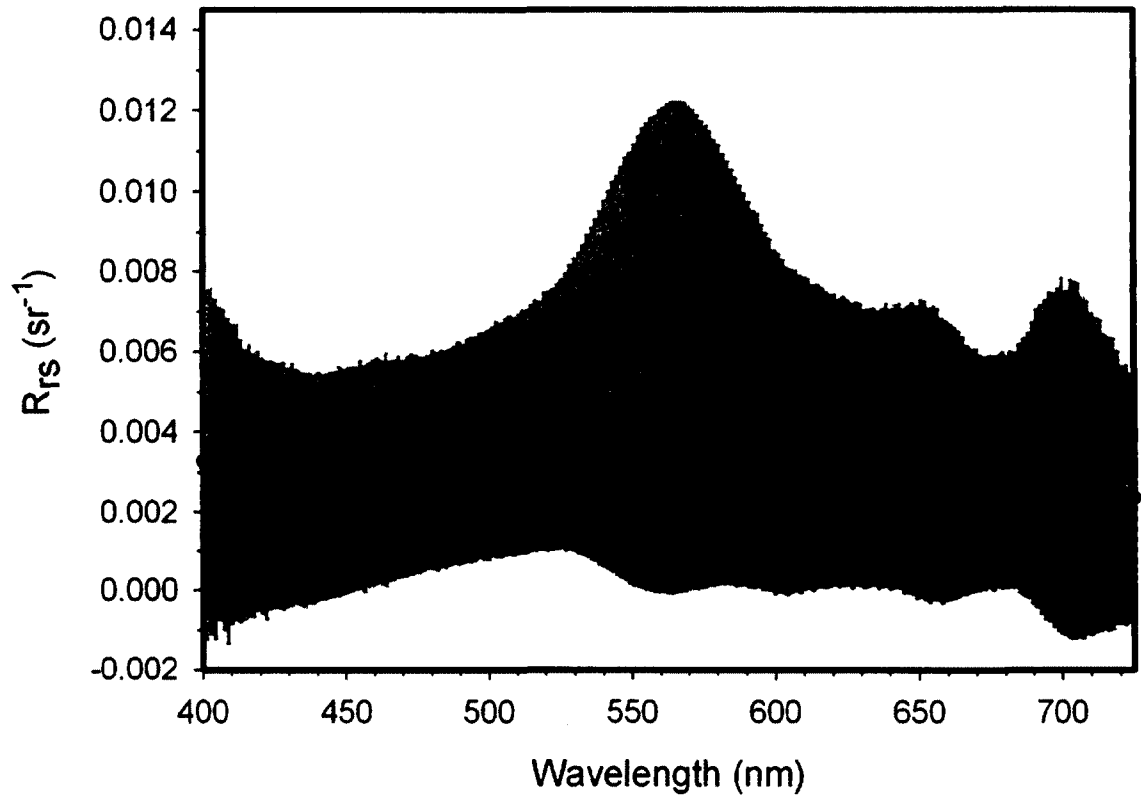


Figure 18. Sampling sites for New England Lakes from 2002 to 2009. Chlorophyll concentrations for each lake site visit shown in $\mu\text{g L}^{-1}$.

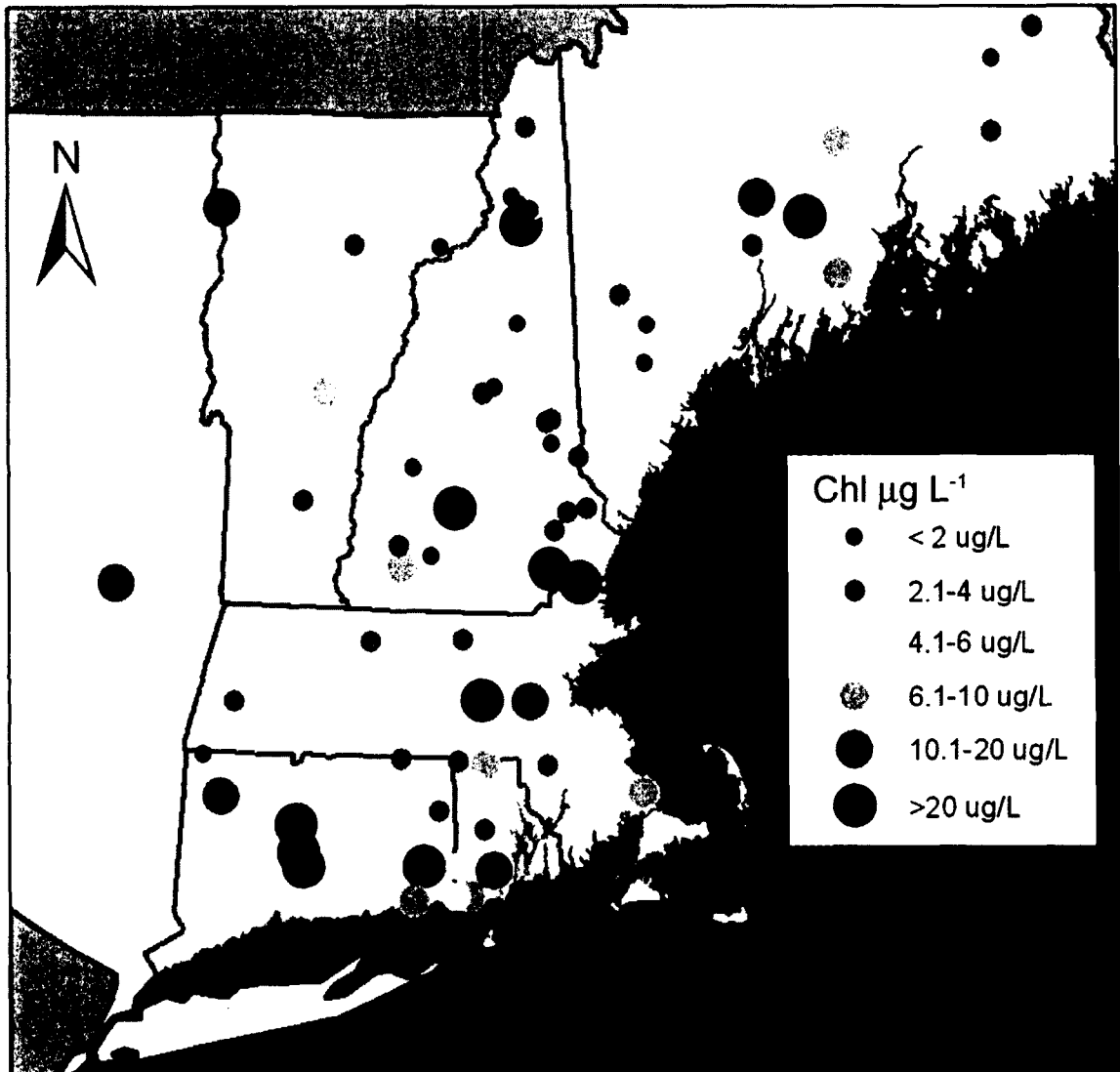


Figure 19. Histogram of extracted chlorophyll concentrations ($\mu\text{g L}^{-1}$) for lake sites on New England Lakes ($n=90$). One lake site with a high concentration ($126 \mu\text{g L}^{-1}$) not shown on graph. Dashed blue line represents median chlorophyll concentration ($4.4 \mu\text{g L}^{-1}$), dotted blue line represents mean chlorophyll concentration ($9.9 \mu\text{g L}^{-1}$).

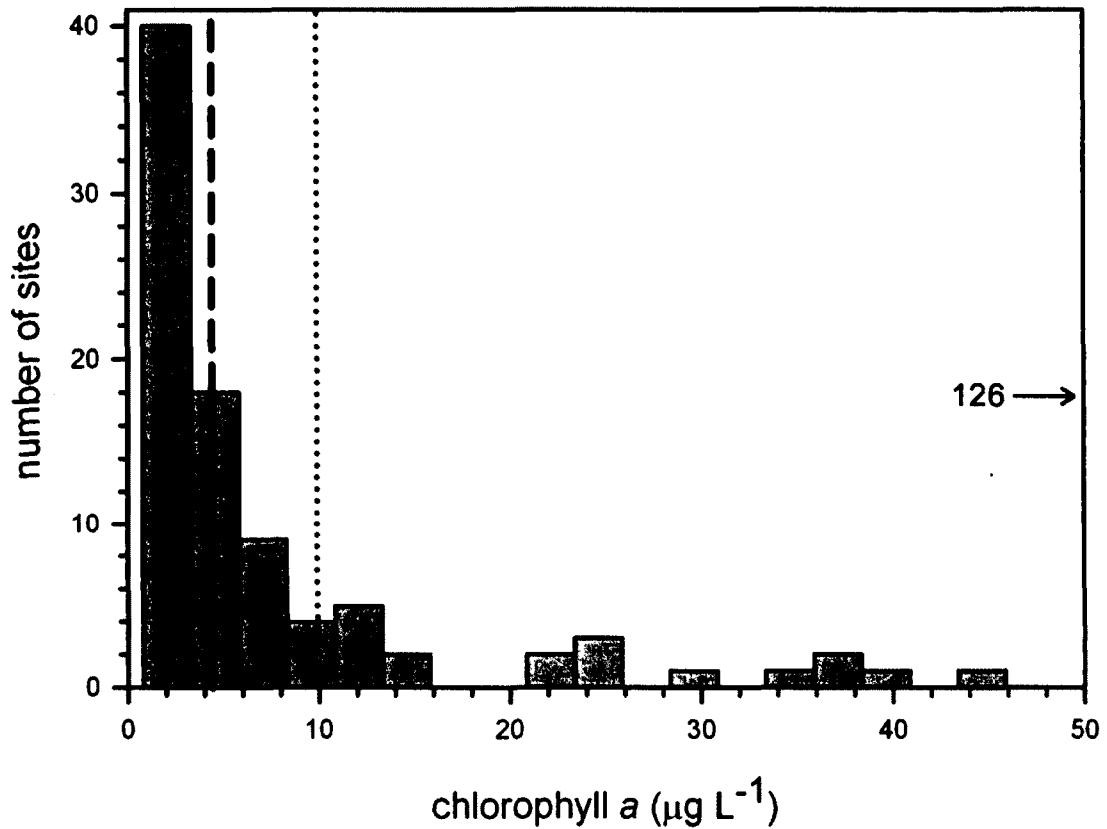


Figure 20. RMS values for chlorophyll estimation algorithms for New England lakes using (A) hyperspectral bands and (B) MERIS bands. MCI - maximum chlorophyll index, OC - ocean color.

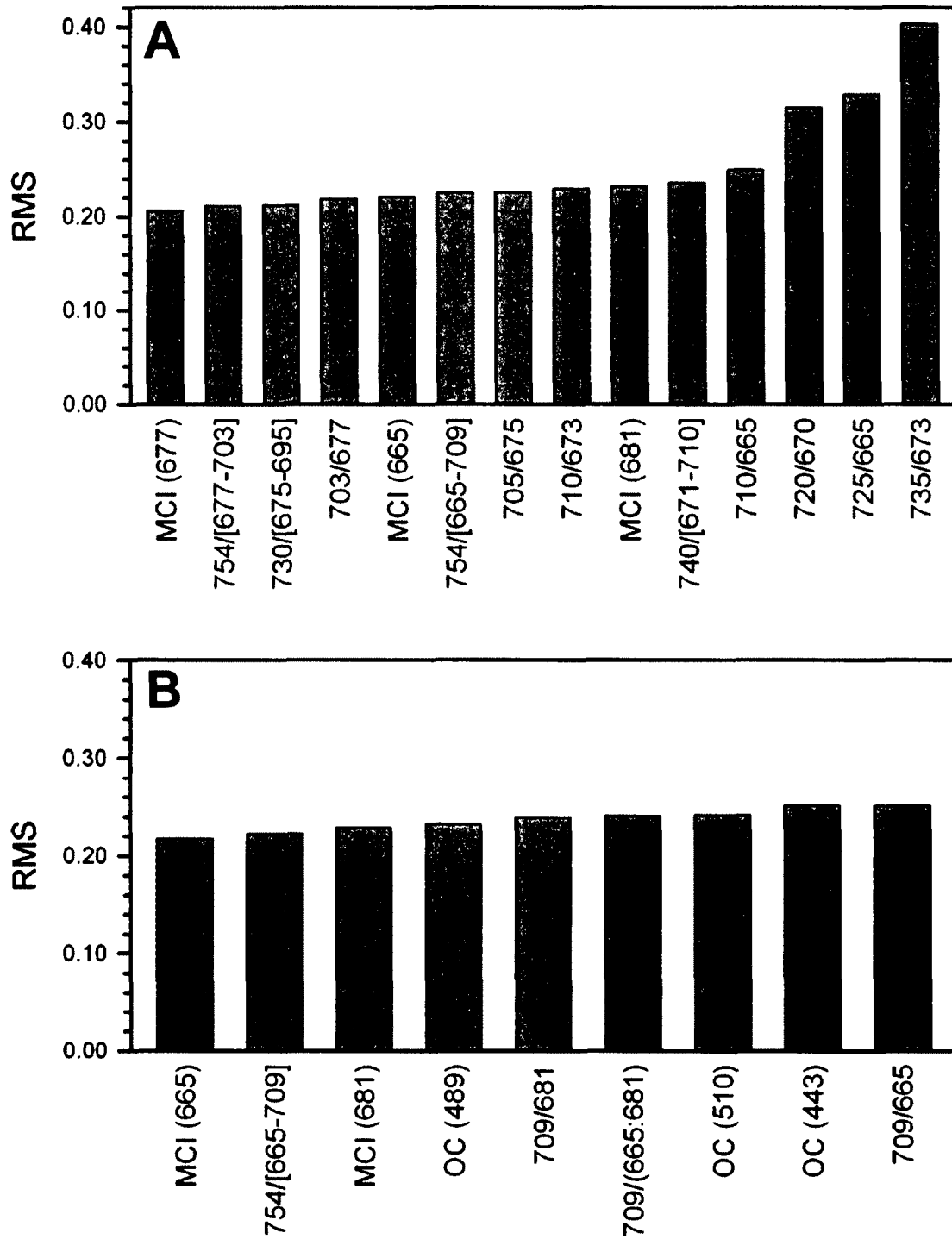


Figure 21. Best log-log regression models using hyperspectral bands for predicting chlorophyll concentrations in the New England lakes (n=90). Graphs on left demonstrate the relationship between the band ratio and chlorophyll concentration. Graphs on the right indicate the measured vs. predicted relationship for chlorophyll concentration based on the algorithm immediately to its left.

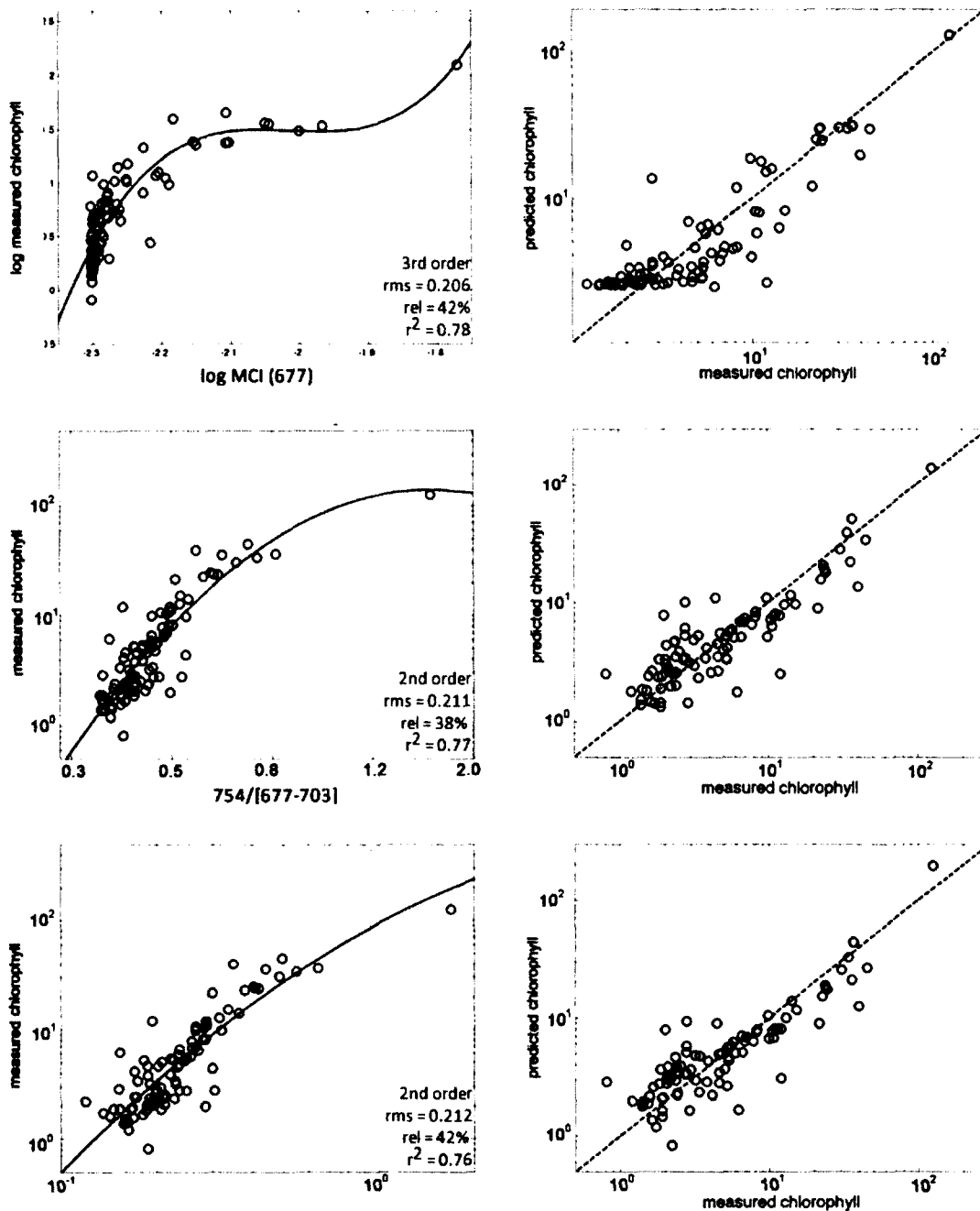


Figure 22. Best log-log regression models using satellite sensor bands for predicting chlorophyll in New England lakes (n=90). Graphs on left demonstrate the relationship between the band ratio and chlorophyll concentration. Graphs on the right indicate the measured vs. predicted relationship for chlorophyll concentration based on the algorithm immediately to its left. Satellite sensors band used are (A) MERIS, (B) MODIS and (C) SeaWiFS.

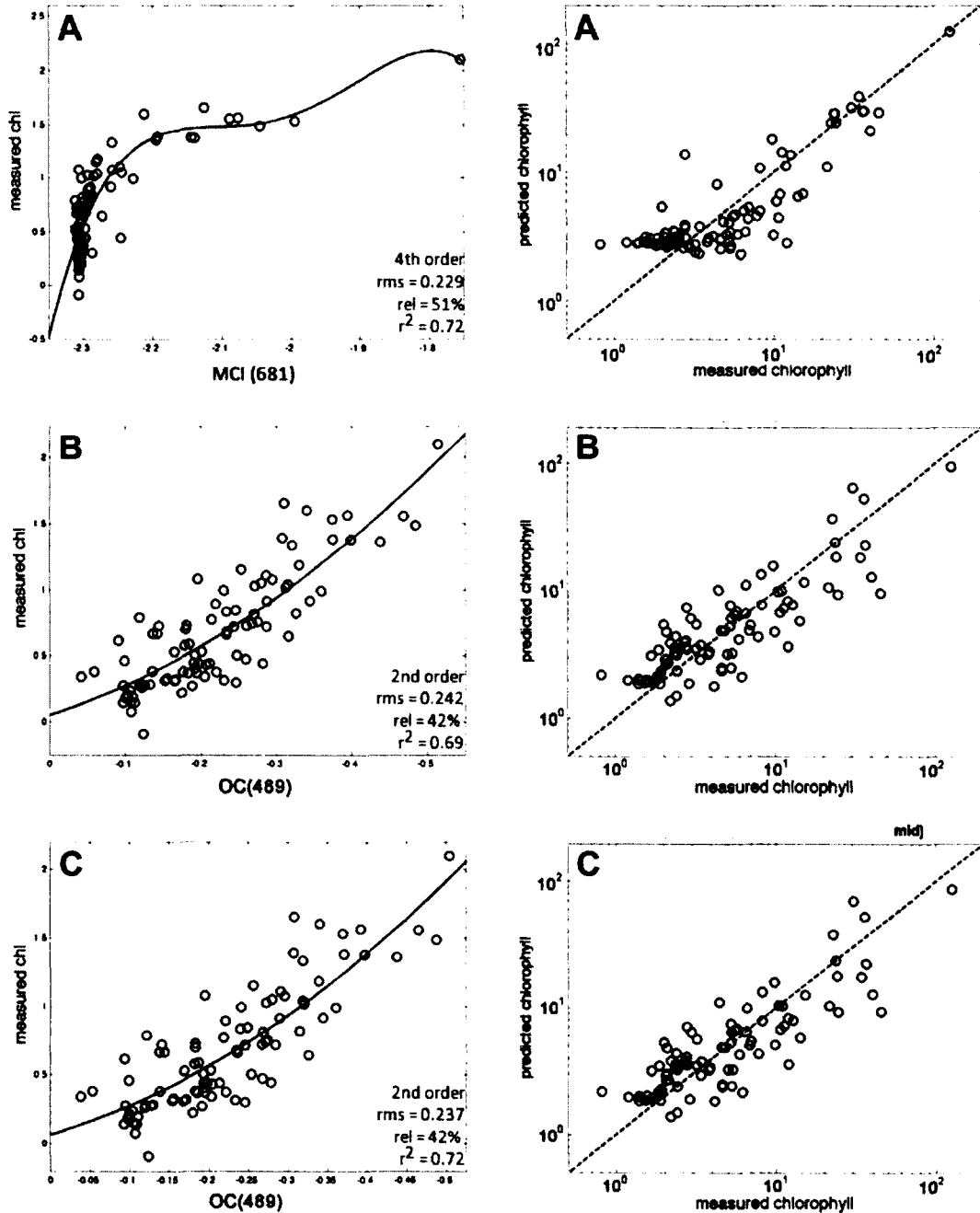
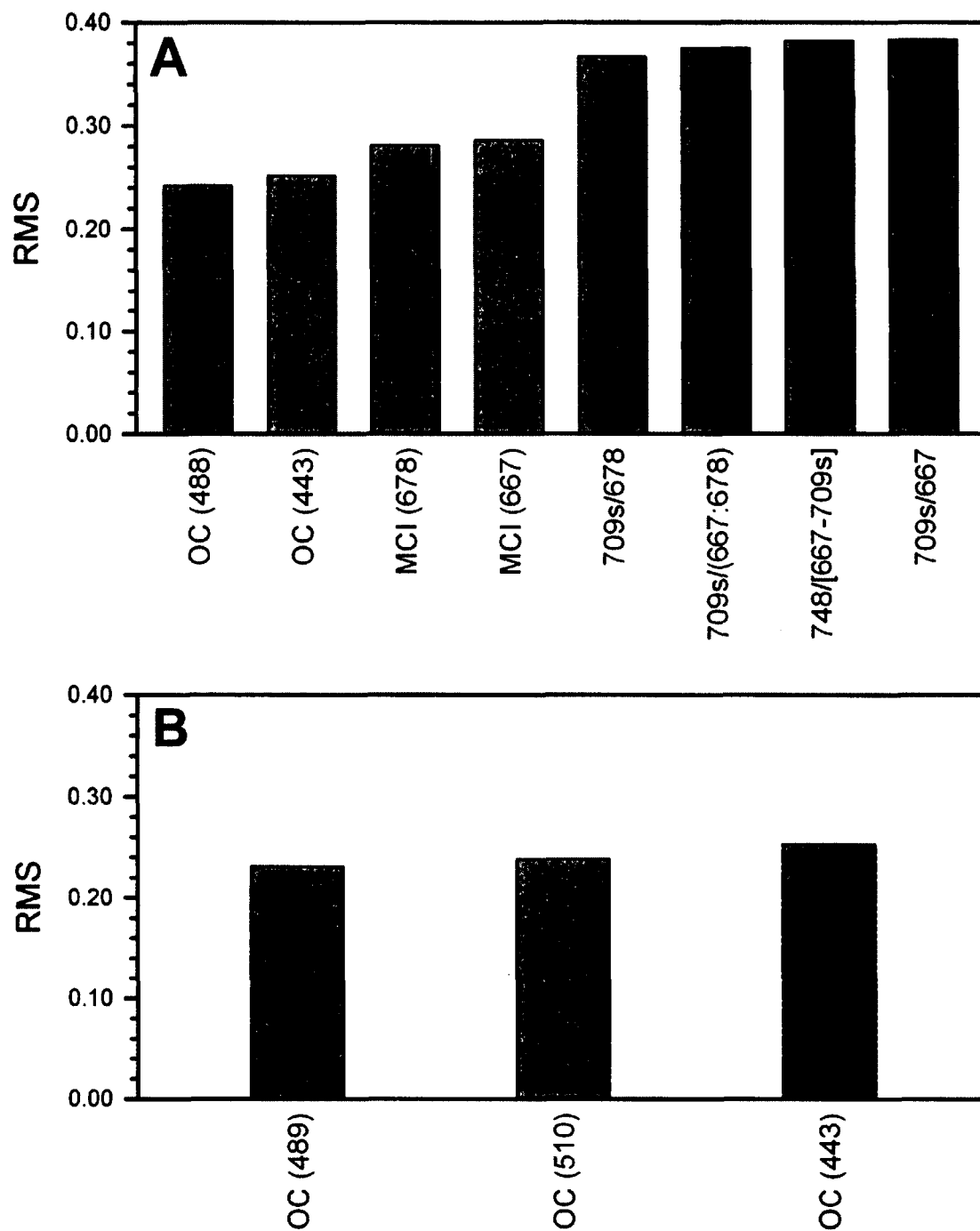


Figure 23. RMS values for chlorophyll estimation algorithms for New England lakes using (A) MODIS bands and (B) SeaWiFS bands. MCI - maximum chlorophyll index, OC - ocean color.



CHAPTER IV

CHLOROPHYLL ALGORITHMS FOR THE GREAT SALT LAKE

Introduction

The Great Salt Lake is a large, terminal water body located near Salt Lake City in Utah, USA. Causeways separate the lake into four main sections, Bear River Bay, Gilbert Bay, Gunnison Bay, and Farmington Bay (Figure 24). The railroad causeway built in 1959 that separated Gunnison Bay from Gilbert Bay created two ecologically distinct lakes (Stephens 1990). As a result, salinity concentrations are consistently higher in Gunnison Bay (160-290 ppt) than Gilbert Bay (~60-150 ppt). Gilbert, Farmington and Bear River Bays are fed largely from freshwater inputs arriving from outside the lake (Bear River to the North, Jordan River to the South), while Gunnison Bay gets most of its inflow from a brine layer moving through culverts in the railroad causeway from Gilbert Bay. While generally driven by freshwater input, both the Bear River (up to 200 ppt) and Farmington Bay (up to 90 ppt) can have high salinity levels. In addition to surface water inputs, the Great Salt Lake is fed by a small amount of rainfall each year (~15 inches, 38 cm). Rain and snowfall patterns in the region have a large influence on the physical properties of the Great Salt Lake. Salinity can

vary greatly in a given bay from year to year, as can the area covered by the lake (Stephens 1990). The lake area has been as low as 2500 km², but has been as high as 6500 km², and is driven by inter-annual variations in precipitation and water withdrawals (Stephens 1990).

Major nutrient loading enters the Great Salt Lake from the Jordan River through Farmington Bay, both from watershed drainage and discharge from sewage treatment plants. The vast majority of Utah's population lives within the lake watershed, and the majority of the treated sewage from these people enters Farmington Bay. Due to the terminal nature of the Great Salt Lake, there are few means for the nutrients to exit the lake once they have entered. Farmington Bay is consistently ranked one of the most polluted surface waters in the state of Utah, but due to its status as a saline water body, it has only recently gained attention from regulating agencies. As such, little to no attention has been paid to remediation and mitigation planning of this highly eutrophic water body. Water outflow from Farmington Bay enters Gilbert Bay through a small breach in the causeway, transporting the nutrients and phytoplankton into the rest of the system.

As is typical in hypersaline lakes, the food web of the Great Salt Lake is fairly simple (Wurtsbaugh 1992; Williams 1998). The brine shrimp, *Artemia*, plays a central role in the lake ecosystem, acting as the dominant grazer of phytoplankton in Gilbert Bay (White et al. 1992; Wurtsbaugh 1992). During the

spring, a pulse of nutrient input from snowmelt leads to phytoplankton blooms, which are followed shortly by dramatic population booms of brine shrimp and their predators. Such food web dynamics can cause chlorophyll concentrations to spike and crash in Gilbert Bay over the course of a few weeks.

In addition to the importance of brine shrimp to the internal food web of the Great Salt Lake, *Artemia* are also food sources for migratory birds and waterfowl (Cooper et al. 1984), up to 5 million of which visit the lake each year. The harvest of brine shrimp cysts, used in aquaculture and biomedical industry, began on the Great Salt Lake in the 1950's (Stephens 1990), and continues on the lake to this day. The harvesting brings millions of dollars a year into the local economy, providing a direct economic reason for good lake management.

In spite of its importance in the region, relatively limited information is available on the water quality of the Great Salt Lake. Sampling on the lake is time consuming due to its large size, and difficult due its sizable wind fetch (often leading to high waves), extreme salinity and severe winter weather. Routine water quality sampling occurs on a monthly basis, although not all year round, and on only a few lake sites. Little is understood about the true temporal and spatial variation in lake water quality and phytoplankton populations on the Great Salt Lake, let alone how these conditions might vary with increases in nutrient loading from Farmington Bay or changes in brine shrimp populations. Remote sensing algorithms to accurately estimate chlorophyll in the Great Salt Lake will

allow a much greater understanding of the lake ecosystem dynamics, something which will prove invaluable in protecting and managing this important ecological and economic resource.

Methodology

Sampling

A total of 51 measurements of hyperspectral reflectance were collected during three synoptic surveys in 2005 and 2006. Between May 31 and June 3, 2005, spectral measurements were collected at 17 of the 42 survey sampling sites (Figure 25). From May 17 to 20, 2006, spectral measurements were collected at 26 of the 29 survey sampling sites (Figure 26). Between November 30 and December 2, 2006, spectral measurements were collected at 8 of the 19 survey sampling sites (Figure 27). These three trips took place during different lake conditions, at two different times of the year and in two different years, ensuring that spectral data were not overly biased by potentially rare conditions present during a single collection trip.

Chlorophyll a

At each sampling site, lake water was collected from the top 1 meter of the water column using a peristaltic pump (Table 2). A total of 20 ml of lake water was

filtered through a GF/C filter, and filters were subsequently kept frozen until fluorometric analysis to determine chlorophyll concentration (Table 3).

Dual-radiometer data collection/processing

All spectral measurements were made using the dual-radiometer technique described in Chapter II. Raw spectral measurements were processed and converted to remote sensing reflectance (R_{rs} , sr^{-1}) using equations (6) to (17). After processing, three spectral measurements were determined to be invalid during quality control inspection due either to intensity or spectral deviations outside of the expected characteristics of water spectra. The sub-optimal state of these spectra was likely due to difficult conditions during data collection (in two cases high winds, in the third, proximity to shore and shallow water). As a result, a total of 48 spectra (Figures 28, 29) were used to test the algorithms listed in Tables 4 and 5. As shown in Table 11, all algorithms were examined in a log-log relationship to relate the spectral measurements to the chlorophyll concentration. In addition, several 2-band and 3-band ratio algorithms were also examined as linear relationships. For graphing and additional statistical analysis, the best algorithms for each sensor type and chlorophyll range were identified based on the RMS, relative error, and r^2 values, as well as a visual evaluation of the goodness of fit.

To examine the effects of very low and very high chlorophyll concentrations on linear regression analysis, all algorithms were run with four different datasets: all chlorophyll data (n=48), chlorophyll > 1.5 $\mu\text{g L}^{-1}$ (n=22), chlorophyll < 80 $\mu\text{g L}^{-1}$ (n=45), and chlorophyll between 1.5 and 80 $\mu\text{g L}^{-1}$ (n=18) (Appendix D).

Examination of the linear relationships revealed a great deal of scatter at chlorophyll concentrations less than 1.5 $\mu\text{g L}^{-1}$. Upon further examination, it became clear that the scatter was due to spectral measurements collected in Gilbert Bay during a two-day period (May 19 and 20, 2006) under difficult weather conditions. The synergistic effect of substantial waves present on the lake during these sampling cruises, making it difficult to accurately hold the upwelling radiometer cable at the prescribed depth, and low chlorophyll concentrations, leading to longer integration times and less dramatic variation in spectra between depths, apparently resulted in the collection of inaccurate spectral data.

To evaluate the effects of these potentially inaccurate spectral measurements on algorithm development, regression analyses were conducted with two datasets: all data (n=48) and restricted data (n=31) in which data collected on May 19 and 20, 2006 were excluded.

Results

Spectral measurements

Description of dual-radiometer spectra. The 48 spectra in the full dataset exhibited a great deal of variability in green/yellow (530 nm to 600 nm), red (600 nm to 700 nm) and near-infrared (700 nm to 735 nm) portions of the spectrum (Figures 28, 29). Relatively less variability was observed in the blue end of the spectrum, especially at wavelengths less than 450 nm. Relative minima were observed in numerous spectra around (510 nm and 543 nm), especially in those taken in Gilbert Bay (the open water section of the lake). These features are likely due to carotenoid absorption by the dominant phytoplankton in this area of the lake, *Dunaliella salina*.

Spectral data collected under adverse conditions. The effect of the data collected on May 19-20, 2006, on the linear regression is shown in Figure 30. The spectral ratios derived using these spectra were $\ll 1$, indicating absence of both the scattering peak near 710 nm and the strong chlorophyll absorption around 675 nm. Such spectral characteristics would be associated with chlorophyll levels in the open ocean, well below even the lowest levels measured in the Great Salt Lake. The general effect of removing these spectra was the reduction of RMS values an average of 14% to 26%, depending on the sensor that was being simulated (Figure 31).

Chlorophyll a

At sites where spectra were measured, the chlorophyll concentration ranged from $0.1 \mu\text{g L}^{-1}$ to $303 \mu\text{g L}^{-1}$, indicating a skewed distribution with a predominance of low chlorophyll concentrations (Figure 32). The mean concentration of all sites was $29.0 \mu\text{g L}^{-1}$, and the median chlorophyll value was $1.5 \mu\text{g L}^{-1}$. Twelve lakes sites could be classified as hypereutrophic (25%), 7 as eutrophic (15%), 3 as mesotrophic (6%), and 26 as oligotrophic (54%). For the restricted dataset (when sites visited on May 19 and 20, 2006, were eliminated), the number of oligotrophic sites dropped to 9, moving the mean concentration to $45.5 \mu\text{g L}^{-1}$, and the median to $24.2 \mu\text{g L}^{-1}$. The trophic composition of sites also changed markedly, shifting the composition to 39% hypereutrophic, 22% eutrophic, 10% mesotrophic, and 29% oligotrophic.

Evaluation of algorithms

Results on the evaluation of algorithms presented in this chapter are all based on the log-log regression analyses. Results for linear regressions are presented in Appendix D, as well as the coefficients for the best log-log algorithms. For simplicity of notation in the figures and tables, reflectance ratios and other predictor variables are denoted by the wavelengths involved (e.g., $R_{rs}(\lambda_A)/R_{rs}(\lambda_B)$ is denoted λ_A/λ_B).

Hyperspectral band algorithms

Several 2-band hyperspectral algorithms proved effective for estimating chlorophyll concentration (RMS < 0.250 when using the restricted dataset) (Tables 12, 13; Figures 33, 34). The most effective algorithm was a 2-band algorithm using 673 nm and 710 nm. Out of the three MCI algorithms examined (using 677 nm, 665 nm, or the standard 681 nm), the optimized band algorithm (677 nm) had the highest RMS, but the model using 665 nm was better than the standard approach (681 nm) by < 0.5%.

MERIS algorithms

When using the restricted dataset, only one algorithm based on MERIS bands had an RMS < 0.250 (Tables 12, 13; Figures 33, 35). However, a total of 6 additional algorithms had RMS values between 0.250 and 0.270. The most effective algorithms utilized a single 2- or 3-band ratio, closely followed by two MCI and an OC algorithm. The most effective blue band for the OC algorithm was 489 nm, which offered a 40% improvement in RMS over the band chosen by the OC4 algorithm (510 nm). Out of the two MCI algorithms examined (665 nm and the standard 681 nm), the standard algorithm had a higher RMS (1% higher than with 665 nm).

MODIS algorithms

Only one algorithm based on MODIS had an RMS < 0.250 when using the restricted dataset (Tables 12, 13; Figures 35, 36). The most effective approach was an OC algorithm using the blue band chosen by OC3 (488 nm). Out of the two MCI algorithms examined (667 nm and the standard 678 nm), the standard algorithm had a lower RMS (5% lower than with 667 nm). All approaches using the simulated 709 band in 2- and 3-band algorithms were much less effective than other options.

SeaWiFS algorithms

All algorithms based on SeaWiFS bands proved effective for estimating chlorophyll concentration (highest RMS was 0.255 using the restricted dataset) (Tables 12, 13; Figures 35, 36). The most effective blue band for the OC algorithm was 489 nm, which offered a 18% improvement over the band chosen by the standard OC4 algorithm (510 nm).

Discussion

General observations

Spectral data collected under adverse conditions. The exclusion of spectral measurements from May 19 and 20, 2006, in algorithm development was a critical decision. These potentially suspect data, collected under difficult conditions, likely had an undue influence on algorithm performance (Figure 30) far outweighing their actual importance. The RMS of the algorithms produced with the restricted dataset were markedly lower than those produced using all data (Figure 31), which is likely a better indication of the potential usefulness of these algorithms in real-world situations over the range of conditions experienced in the Great Salt Lake over the course of the year. Additional work may be necessary to address the fit of the models when chlorophyll values are extremely low due to phytoplankton grazing by *Artemia*.

Algorithms

Hyperspectral algorithms. In the case of the Great Salt Lake, five hyperspectral algorithms stood out from others based on RMS values. The four most effective algorithms were 2-band ratios, with RMS values ranging from 0.236 to 0.250. MCI was found to be reasonably effective in the Great Salt Lake using both a

standard and alternate band, and the version using the alternate band was virtually equal to the standard algorithm.

Satellite sensor algorithms. The best satellite-based algorithms across all platforms exhibited similar effectiveness based on RMS. While band ratios focusing on chlorophyll absorption around 675 nm and the scattering peak around 709 nm worked best in the case of MERIS (RMS 0.249 to 0.259), versions of the OC algorithm using the blue band at 489 nm for SeaWiFS and MODIS were found to be equally effective (0.246, 0.255) and had low relative error (30%). Several of the MERIS algorithms found to be most useful for Great Salt Lake were found to be highly effective at estimating chlorophyll in Nebraska lakes, Lake Kinneret, and the Azov Sea (Gitelson et al. 2011b; Yacobi et al. 2011a; Gitelson et al. 2011a; Yacobi et al. 2011b). In contrast to New England lakes, and in agreement with the studies published in 2011, the 2-band algorithm (709 nm / 665 nm) was found to be more effective than the 3-band approach (754 nm / [665 nm–709 nm]). As in the case with New England lakes, OC algorithms were effective although there is no specific reason to expect that these Case I algorithms would work well in a Case II system (O'Reilly et al. 1998). In spite of this, the re-parameterized versions of these algorithms are surprisingly good at estimating chlorophyll in this lake across a wide range of chlorophyll concentrations.

Table 11. Algorithms run with Great Salt Lake spectra. Black dots indicates the algorithm approaches included in analysis. The number of spectra used for each type of regression analysis: all chlorophyll (n=48), restricted dataset (n=30), chlorophyll > 1.5 $\mu\text{g L}^{-1}$ (n=22), chlorophyll < 80 $\mu\text{g L}^{-1}$ (n=45), chlorophyll between 1.5 $\mu\text{g L}^{-1}$ and 80 $\mu\text{g L}^{-1}$ (n=18).

Type	Algorithm	log-log								linear			
		1st		2nd		3rd		4th		all	>1.5	<80	1.5-80
Hyper	703/677	•	•	•	•	•	•	•	•	•	•	•	•
	705/675	•	•	•	•	•	•	•	•	•	•	•	•
	710/665	•	•	•	•	•	•	•	•	•	•	•	•
	710/673	•	•	•	•	•	•	•	•	•	•	•	•
	720/670	•	•	•	•	•	•	•	•	•	•	•	•
	725/665	•	•	•	•	•	•	•	•	•	•	•	•
	735/673	•	•	•	•	•	•	•	•	•	•	•	•
	730/[675-695]	•	•	•	•	•	•	•	•	•	•	•	•
	740/[671-710]	•	•	•	•	•	•	•	•	•	•	•	•
	754/[665-709]	•	•	•	•	•	•	•	•	•	•	•	•
	754/[677-703]	•	•	•	•	•	•	•	•	•	•	•	•
	MCI (665)	•	•	•	•	•	•	•	•				
	MCI (677)	•	•	•	•	•	•	•	•				
	MCI (681)	•	•	•	•	•	•	•	•				
MERIS	709/665	•	•	•	•	•	•	•	•	•	•	•	•
	709/681	•	•	•	•	•	•	•	•	•	•	•	•
	709/(665:681)	•	•	•	•	•	•	•	•	•	•	•	•
	754/[665-709]	•	•	•	•	•	•	•	•	•	•	•	•
	MCI (665)	•	•	•	•	•	•	•	•				
	MCI (681)	•	•	•	•	•	•	•	•				
	OC (443)	•	•	•	•	•	•	•	•				
	OC (489)	•	•	•	•	•	•	•	•				
MODIS	OC (510)	•	•	•	•	•	•	•	•				
	709s/667	•	•	•	•	•	•	•	•	•	•	•	•
	709s/(667:678)	•	•	•	•	•	•	•	•	•	•	•	•
	748/[667-709s]	•	•	•	•	•	•	•	•	•	•	•	•
	MCI (667)	•	•	•	•	•	•	•	•				
	MCI (678)	•	•	•	•	•	•	•	•				
	OC (443)	•	•	•	•	•	•	•	•				
	OC (488)	•	•	•	•	•	•	•	•				
SeaWiFS	OC (489)	•	•	•	•	•	•	•	•				
	OC (510)	•	•	•	•	•	•	•	•				
	OC (443)	•	•	•	•	•	•	•	•				

Table 12. Log-log regression models using all spectra (n=48) for predicting chlorophyll concentrations in the Great Salt Lake sorted by RMS. The order column indicates the power of the polynomial equation which resulted in the best fit.

Type	Algorithm	RMS	Rel Error	r^2	Order
Hyper	703/677	0.298	97%	0.91	4th
	710/673	0.299	87%	0.91	4th
	705/675	0.300	95%	0.91	4th
	730/[675-695]	0.302	105%	0.91	3rd
	710/665	0.305	84%	0.91	4th
	MCI (681)	0.327	100%	0.89	3rd
	MCI (677)	0.327	101%	0.89	3rd
	754/[677-703]	0.327	106%	0.89	4th
	MCI (665)	0.342	98%	0.88	3rd
	720/670	0.357	65%	0.87	4th
	740/[671-710]	0.363	114%	0.87	2nd
	754/[665-709]	0.370	120%	0.86	2nd
	725/665	0.429	71%	0.81	2nd
	735/673	0.592	95%	0.64	2nd
	MERIS	709/(665:681)	0.305	86%	0.91
709/665		0.307	88%	0.90	3rd
709/681		0.309	87%	0.90	3rd
MCI (681)		0.310	95%	0.90	3rd
MCI (665)		0.329	96%	0.89	3rd
OC (489)		0.340	89%	0.88	3rd
OC (443)		0.360	93%	0.87	3rd
754/[665-709]		0.365	120%	0.86	2nd
OC (510)		0.448	106%	0.80	3rd
MODIS		OC (488)	0.308	81%	0.91
	OC (443)	0.347	90%	0.88	3rd
	MCI (678)	0.422	109%	0.82	3rd
	MCI (667)	0.451	116%	0.80	3rd
	709s/678	0.491	102%	0.76	3rd
	748/[667-709s]	0.541	109%	0.71	2nd
	709s/667	0.565	114%	0.68	2nd
SeaWiFS	OC (489)	0.322	84%	0.90	3rd
	OC (443)	0.352	91%	0.88	3rd
	OC (510)	0.389	97%	0.85	3rd

Table 13. Log-log regression models using a dataset without spectra collected in the open water of Gilbert Bay on May 19-20, 2006 (n=31) for predicting chlorophyll concentrations in the Great Salt Lake sorted by RMS. The order column indicates the power of the polynomial equation which resulted in the best fit.

Type	Algorithm	RMS	Rel Error	r^2	Order
Hyper	710/673	0.236	70%	0.93	4th
	705/675	0.249	80%	0.92	4th
	703/677	0.250	83%	0.92	4th
	710/665	0.250	62%	0.92	4th
	MCI (665)	0.268	92%	0.91	3rd
	MCI (681)	0.269	86%	0.91	3rd
	730/[675-695]	0.291	92%	0.89	3rd
	MCI (677)	0.304	80%	0.88	3rd
	754/[677-703]	0.310	101%	0.88	4th
	720/670	0.314	66%	0.87	4th
	740/[671-710]	0.329	89%	0.86	2nd
	754/[665-709]	0.336	95%	0.86	2nd
	725/665	0.386	82%	0.81	2nd
	735/673	0.487	112%	0.70	2nd
	MERIS	709/(665:681)	0.249	66%	0.92
709/665		0.255	61%	0.92	3rd
709/681		0.259	60%	0.91	3rd
MCI (665)		0.267	92%	0.91	3rd
OC (489)		0.269	29%	0.90	3rd
MCI (681)		0.270	83%	0.91	3rd
OC (443)		0.321	35%	0.86	3rd
754/[665-709]		0.334	94%	0.86	2nd
OC (510)		0.378	45%	0.81	3rd
MODIS		OC (488)	0.246	30%	0.92
	OC (443)	0.296	36%	0.88	3rd
	MCI (678)	0.337	78%	0.87	3rd
	MCI (667)	0.353	80%	0.85	3rd
	709s/678	0.363	73%	0.85	3rd
	748/[667-709s]	0.403	75%	0.81	2nd
	709s/667	0.420	86%	0.79	2nd
SeaWiFS	OC (489)	0.255	30%	0.91	3rd
	OC (510)	0.302	31%	0.88	3rd
	OC (443)	0.306	35%	0.88	3rd

Figure 24. National Agriculture Imagery Program real color image of the Great Salt Lake captured in summer 2006 by aircraft and displayed at a resolution of 30 m. Red lines indicate causeways which restrict water movement between adjacent areas of the lake. Labeled features: A - Salt Lake City, B - Jordan River, C - Bear River, 1 - Farmington Bay, 2 - Gilbert Bay, 3 - Gunnison Bay, 4 - Bear River Bay.



Figure 25. Sampling sites on the Great Salt Lake in Farmington and Gilbert Bays from May 31 to June 3, 2005. Chlorophyll concentrations shown in $\mu\text{g L}^{-1}$.

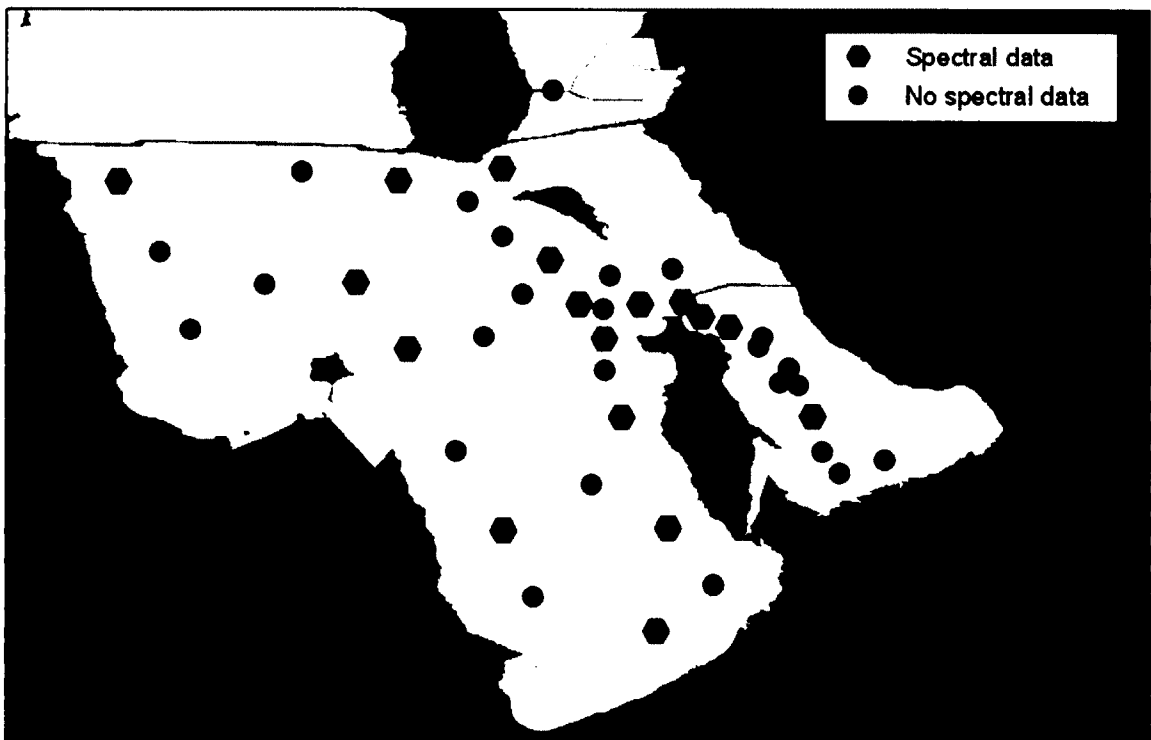
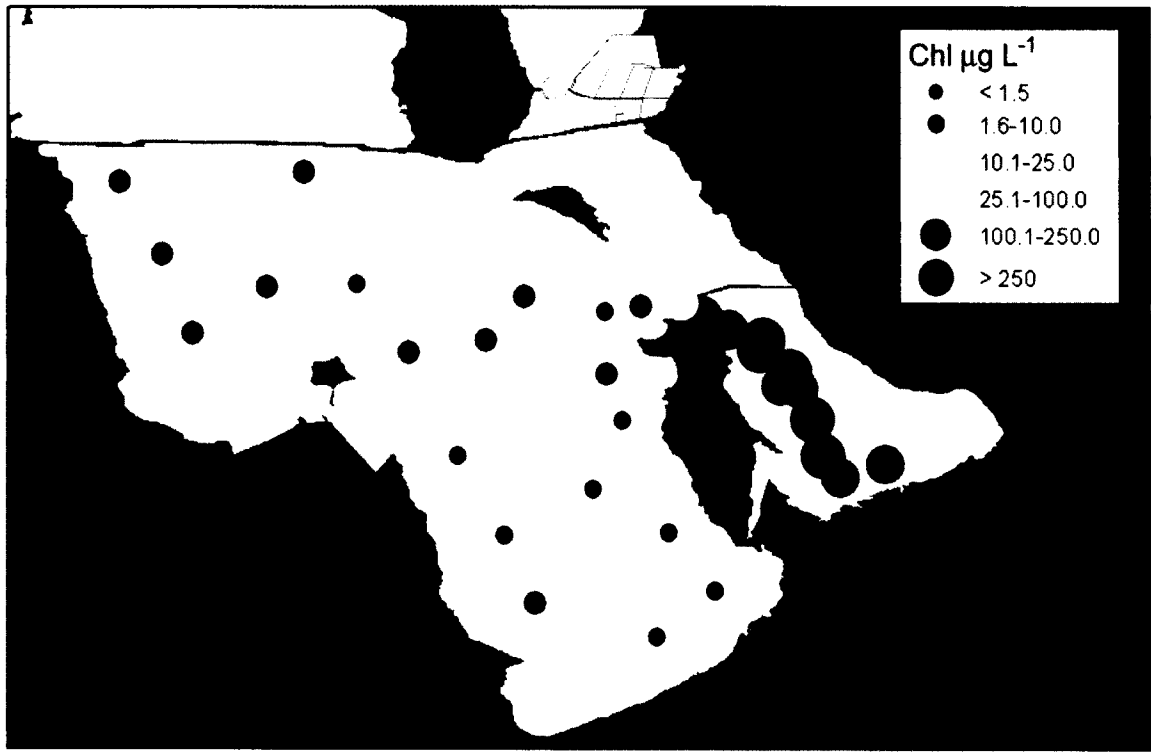


Figure 26. Sampling sites on the Great Salt Lake in Farmington and Gilbert Bays from May 17 to May 20, 2006. Chlorophyll concentrations shown in $\mu\text{g L}^{-1}$.

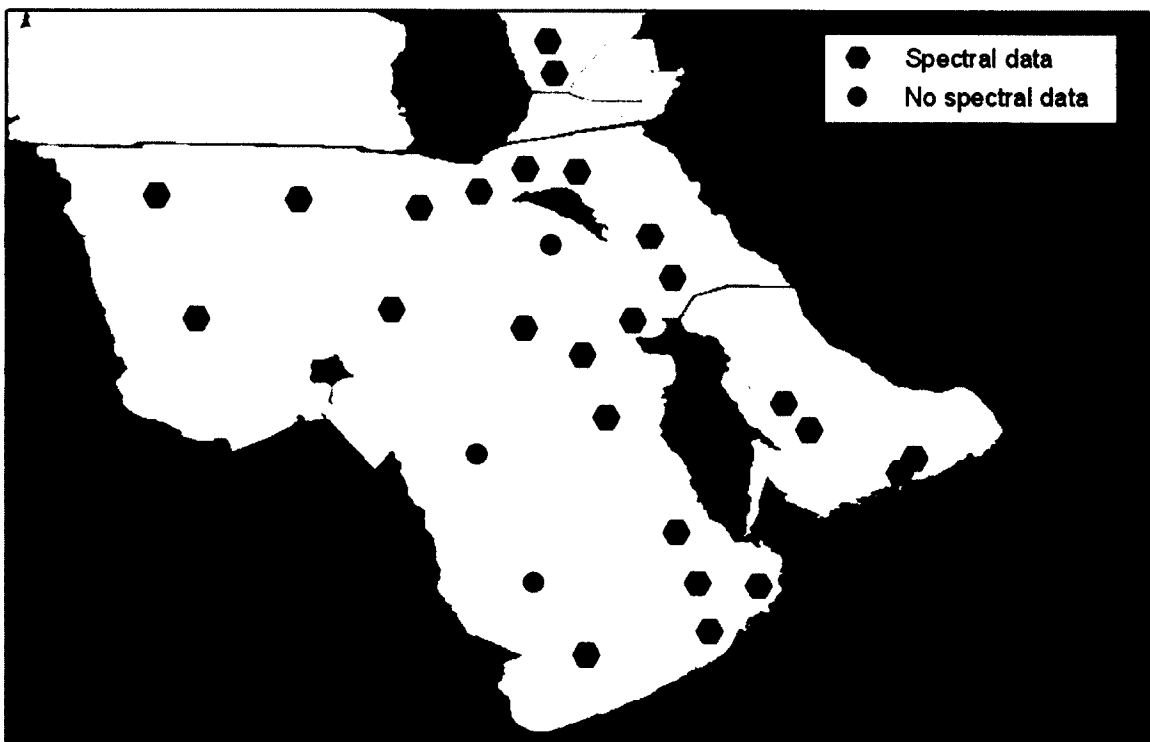
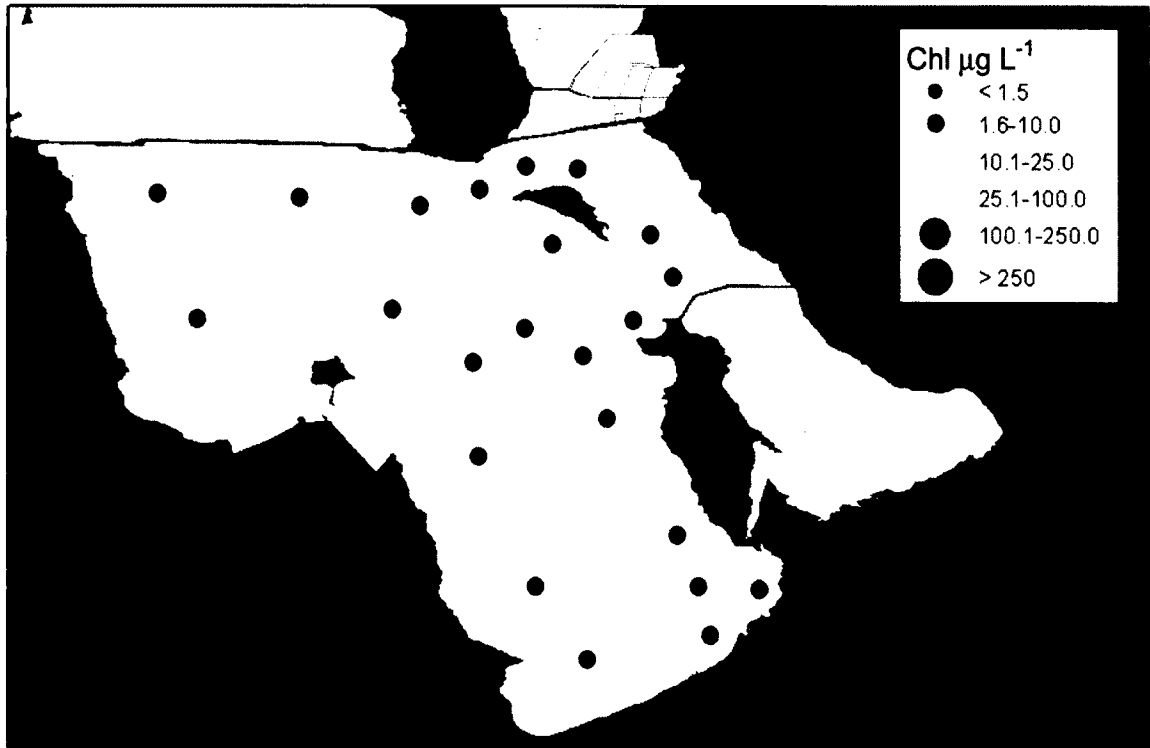


Figure 27. Sampling sites on the Great Salt Lake in Farmington and Gilbert Bays from November 30 to December 2, 2006. Chlorophyll concentrations shown in $\mu\text{g L}^{-1}$.

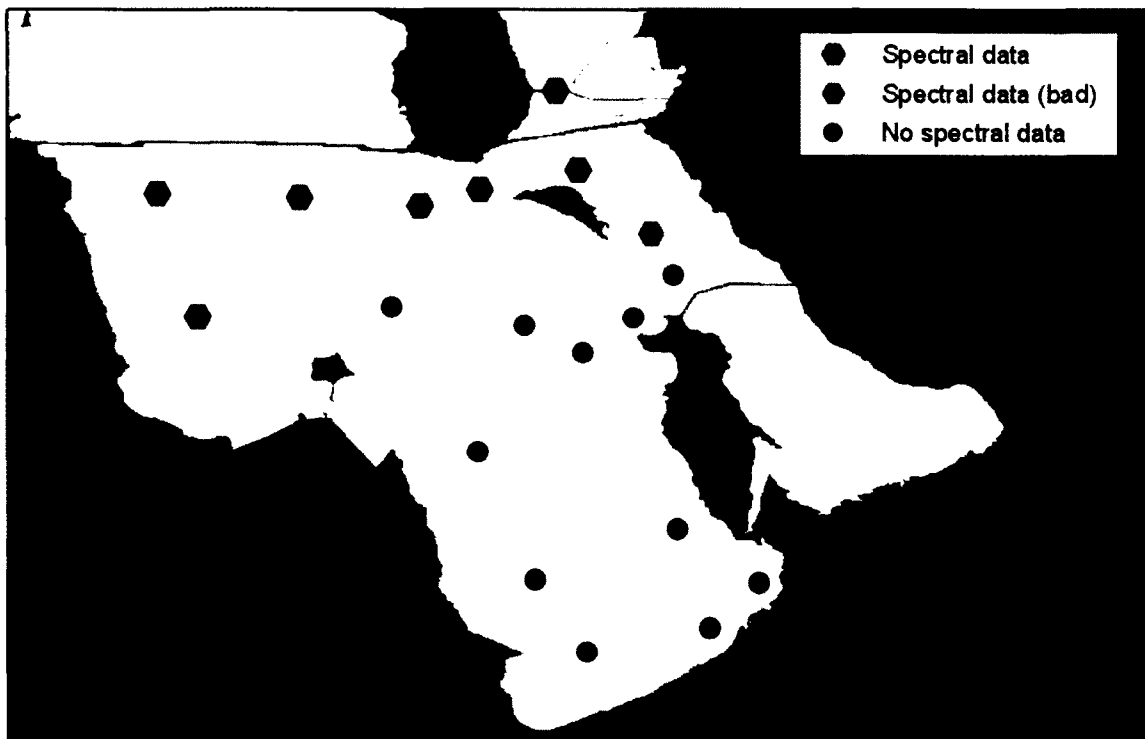
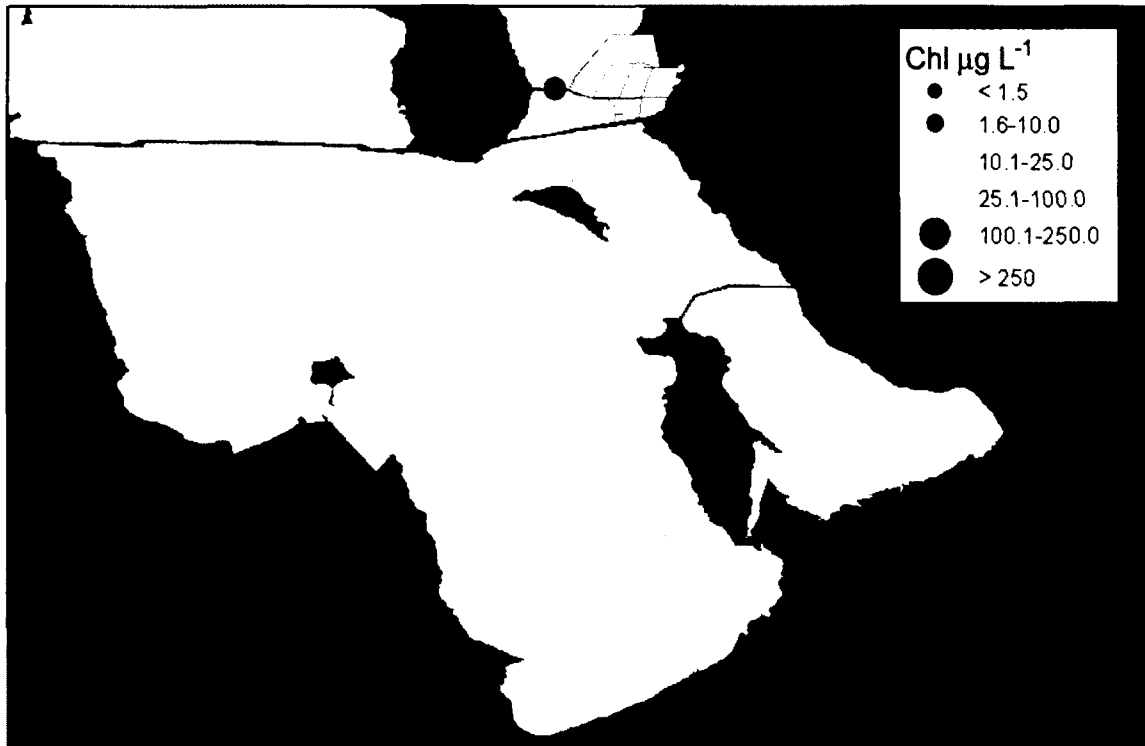


Figure 28. Hyperspectral reflectance spectra taken with the dual-radiometer system on the Great Salt Lake in 2005 and 2006. The spectra shown below (n=48) were used in algorithm development.

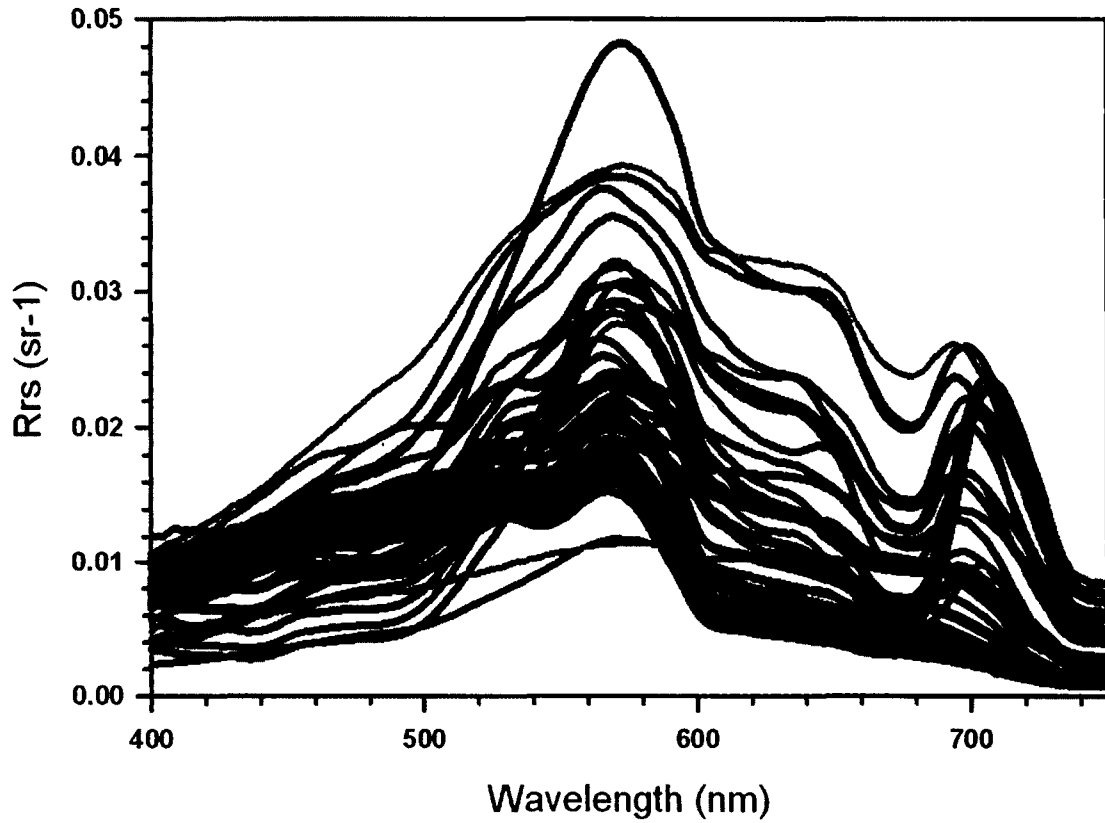


Figure 29. Average value and standard deviation for hyperspectral reflectance spectra taken on the Great Salt Lake with the dual-radiometer system in 2005 and 2006 (n=48).

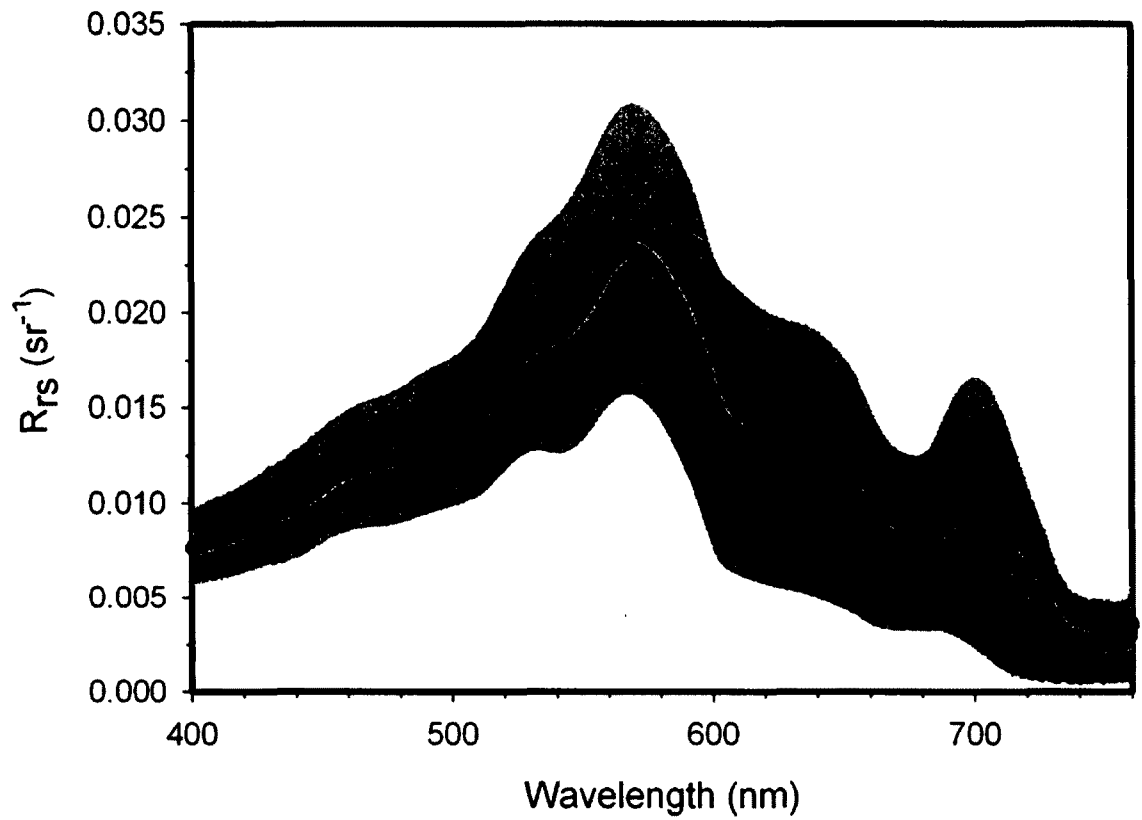


Figure 30. Demonstration of the effect of excluding from algorithm development the open water Gilbert Bay spectra collected in May 2006. Magenta line represents the algorithm with all spectra (red and blue points, n=48), cyan line represents the algorithm excluding Gilbert Bay spectra from May 19-20, 2006 (blue points, n=31). A - full data range shown, B - data range cropped to $20 \mu\text{g L}^{-1}$.

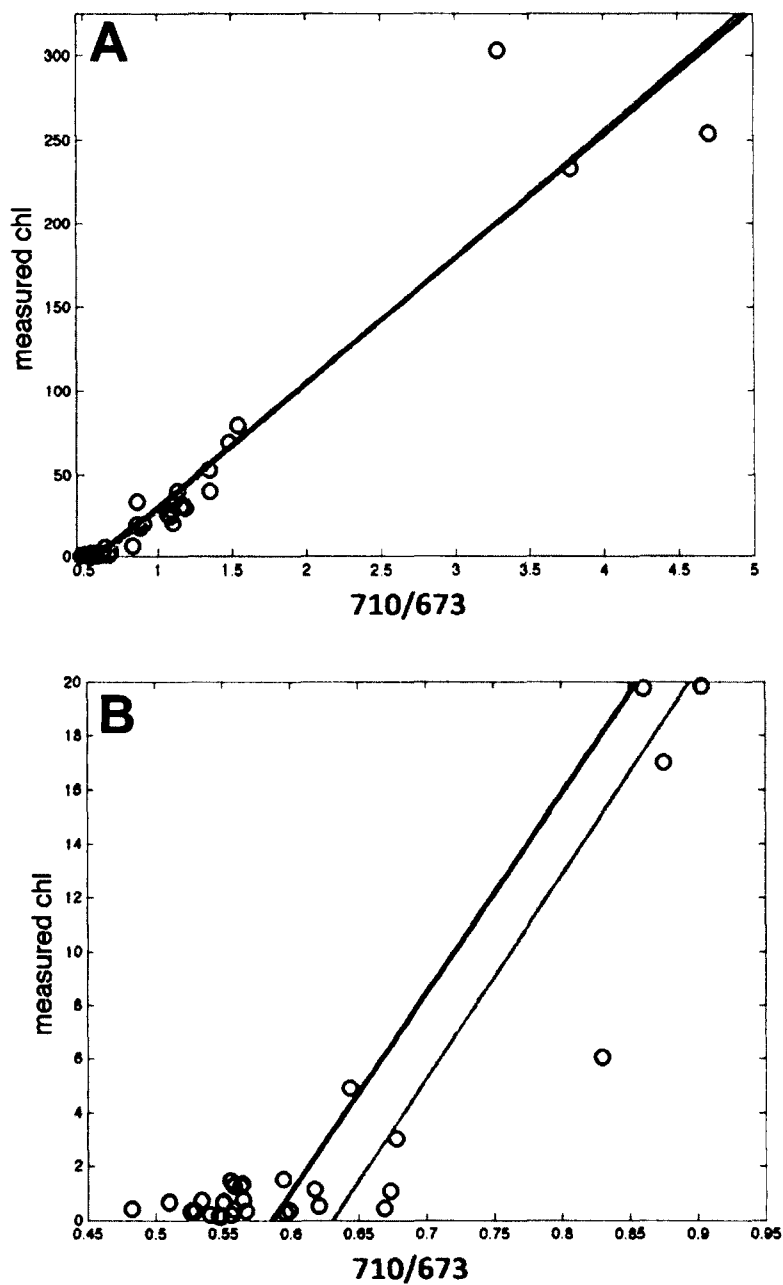


Figure 31. Plot of RMS reduction produced when using restricted dataset (n=31) compared to the same algorithms using all data (n=48) for chlorophyll concentration estimation algorithms for Great Salt Lake for each sensor type.

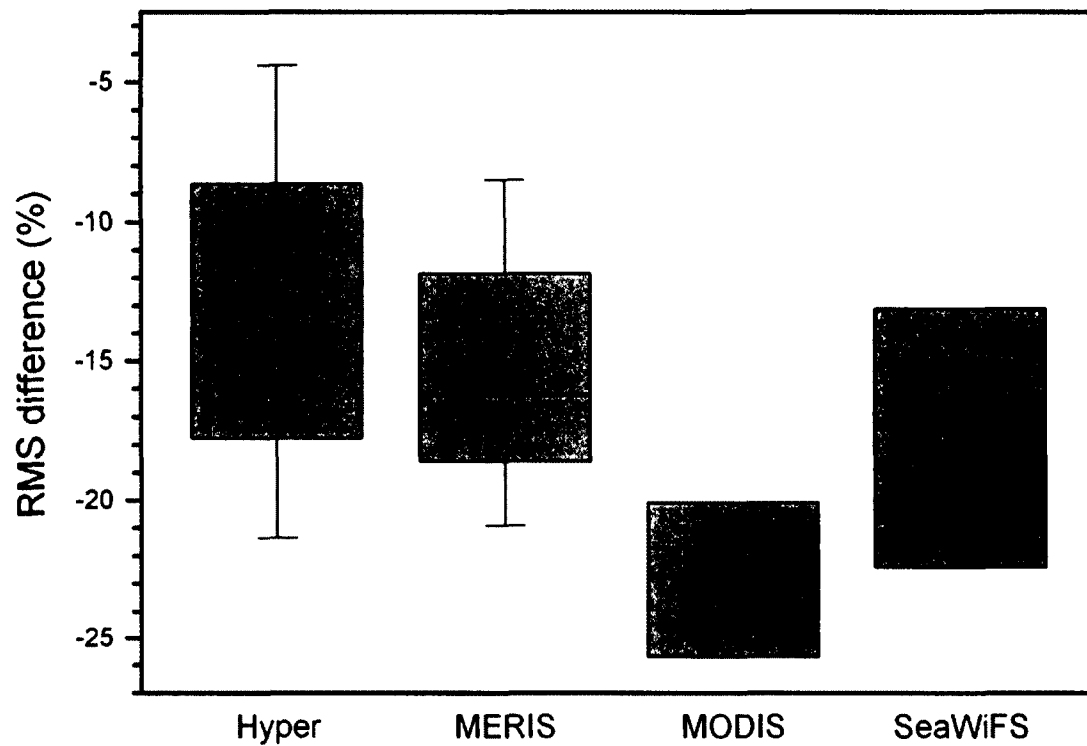


Figure 32. Histogram of extracted chlorophyll concentrations ($\mu\text{g L}^{-1}$) for lake sites on the Great Salt Lake. Three sites with high concentrations (233, 254, 303 $\mu\text{g L}^{-1}$) not shown on graph. For all spectra ($n=48$), dashed red line represents median chlorophyll concentration ($1.5 \mu\text{g L}^{-1}$), dotted red line represents mean chlorophyll concentration ($29.0 \mu\text{g L}^{-1}$). For dataset excluding Gilbert Bay May 2006 sites ($n=31$), dashed blue line represents median chlorophyll concentration ($24.2 \mu\text{g L}^{-1}$), dotted blue line represents mean chlorophyll concentration ($45.5 \mu\text{g L}^{-1}$). Hatched bar illustrates the low-chlorophyll value spectra lost in the restricted dataset.

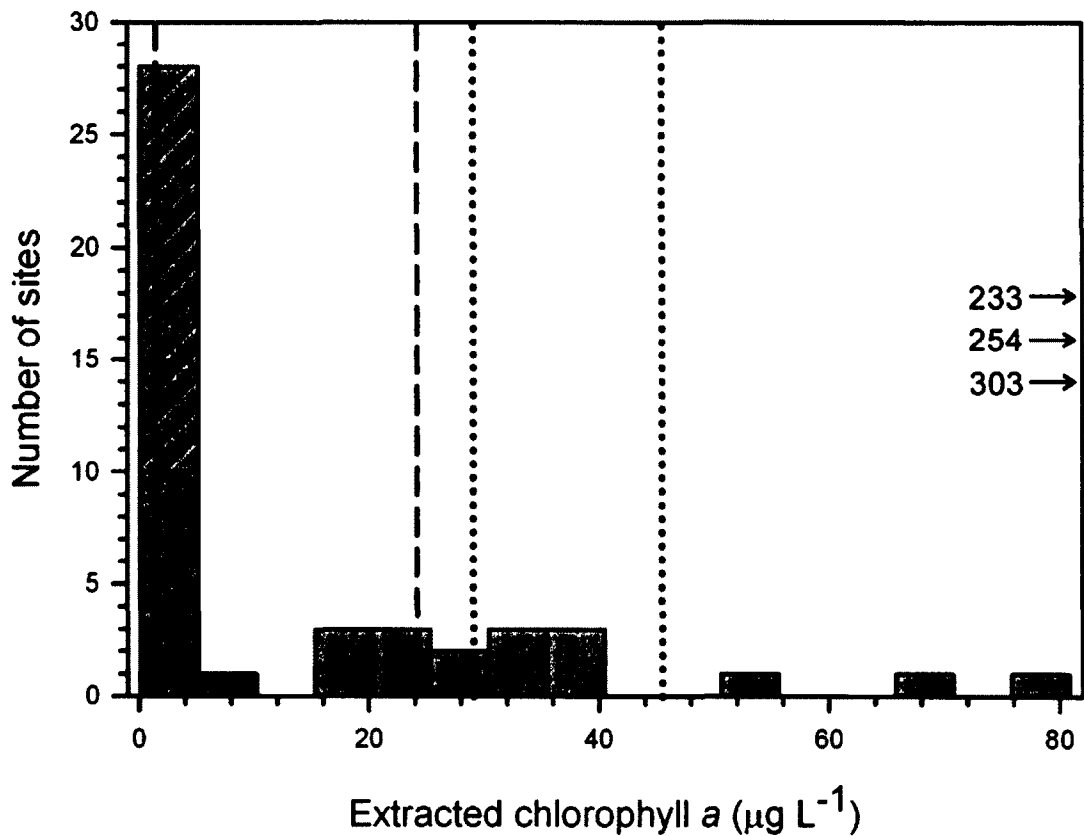


Figure 33. RMS values for chlorophyll estimation algorithms for The Great Salt Lake using (A) hyperspectral bands and (B) MERIS bands. Blue bars represent algorithms developed with the restricted dataset (n=31), gray bars represent algorithms developed with all data (n=48). MCI - maximum chlorophyll index, OC - ocean color.

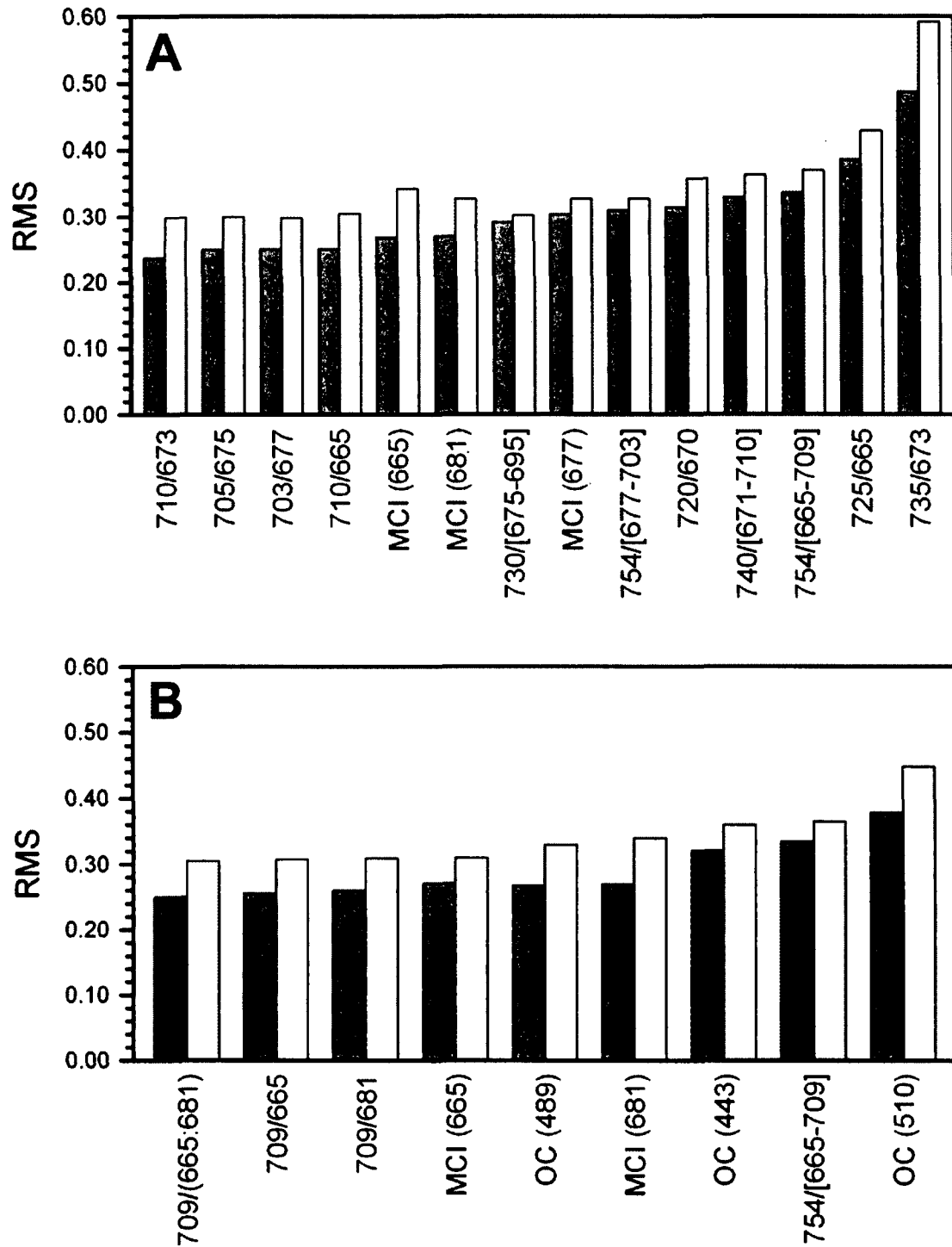


Figure 34. Best log-log regression models using hyperspectral bands for predicting chlorophyll concentrations in the Great Salt Lake based on the restricted dataset (n=31). Graphs on left demonstrate the relationship between the band ratio and chlorophyll concentration. Graphs on the right indicate the measured vs. predicted relationship for chlorophyll concentration based on the algorithm immediately to its left.

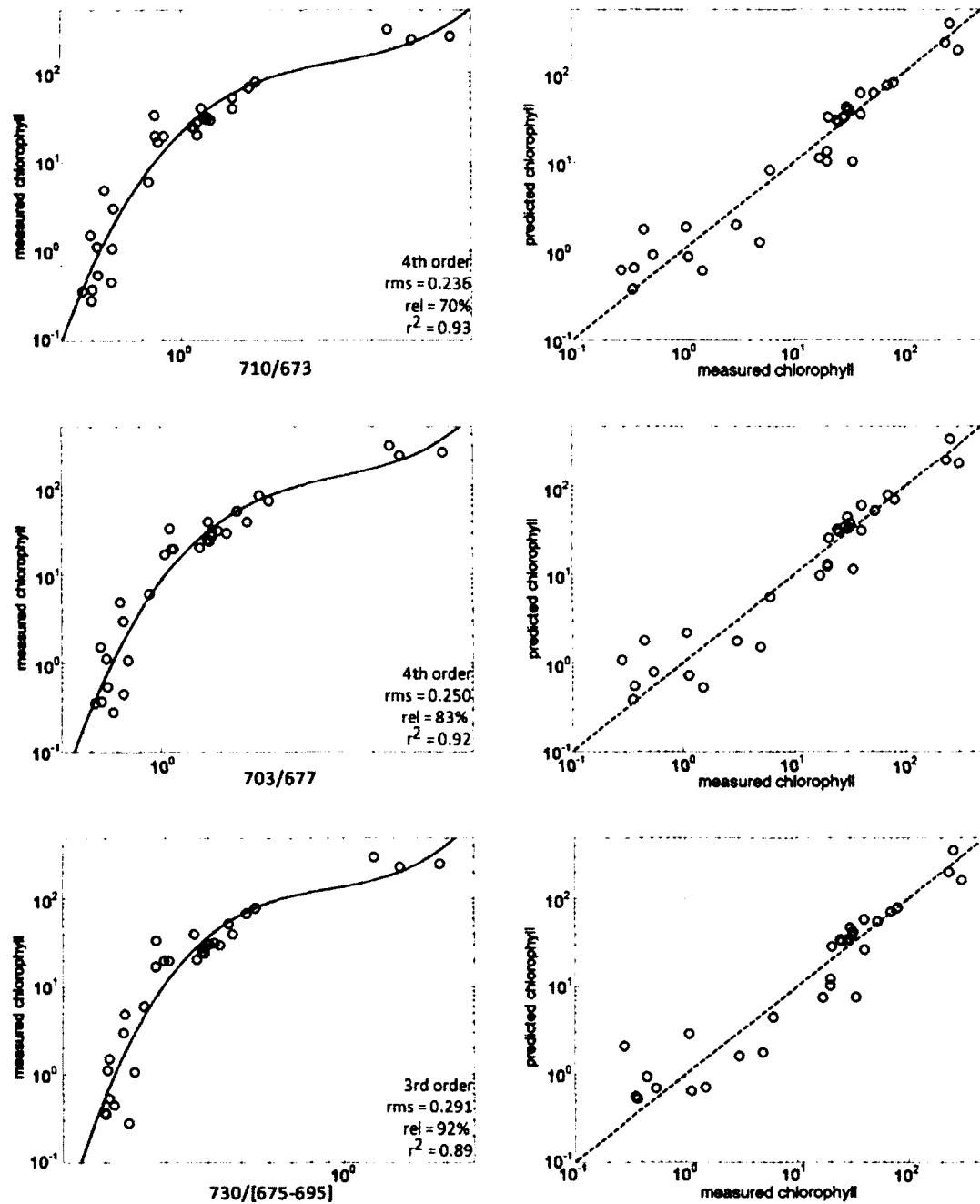


Figure 35. Best log-log regression models using satellite sensor bands for predicting chlorophyll concentrations in the Great Salt Lake based on the restricted dataset (n=31). Graphs on left demonstrate the relationship between the band ratio and chlorophyll concentration. Graphs on the right indicate the measured vs. predicted relationship for chlorophyll concentration based on the algorithm immediately to its left. Satellite sensors bands used are (A) MERIS, (B) MODIS and (C) SeaWiFS.

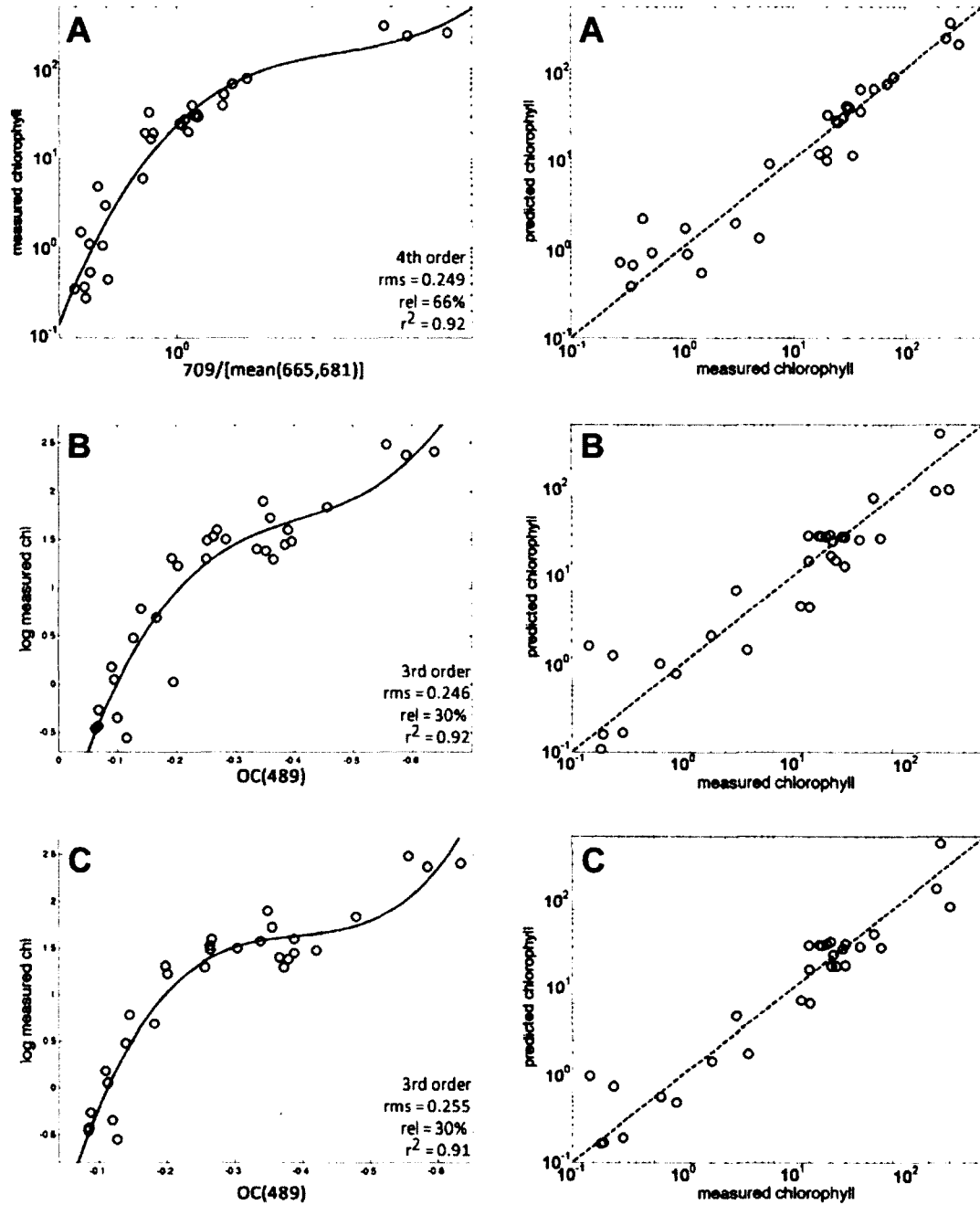
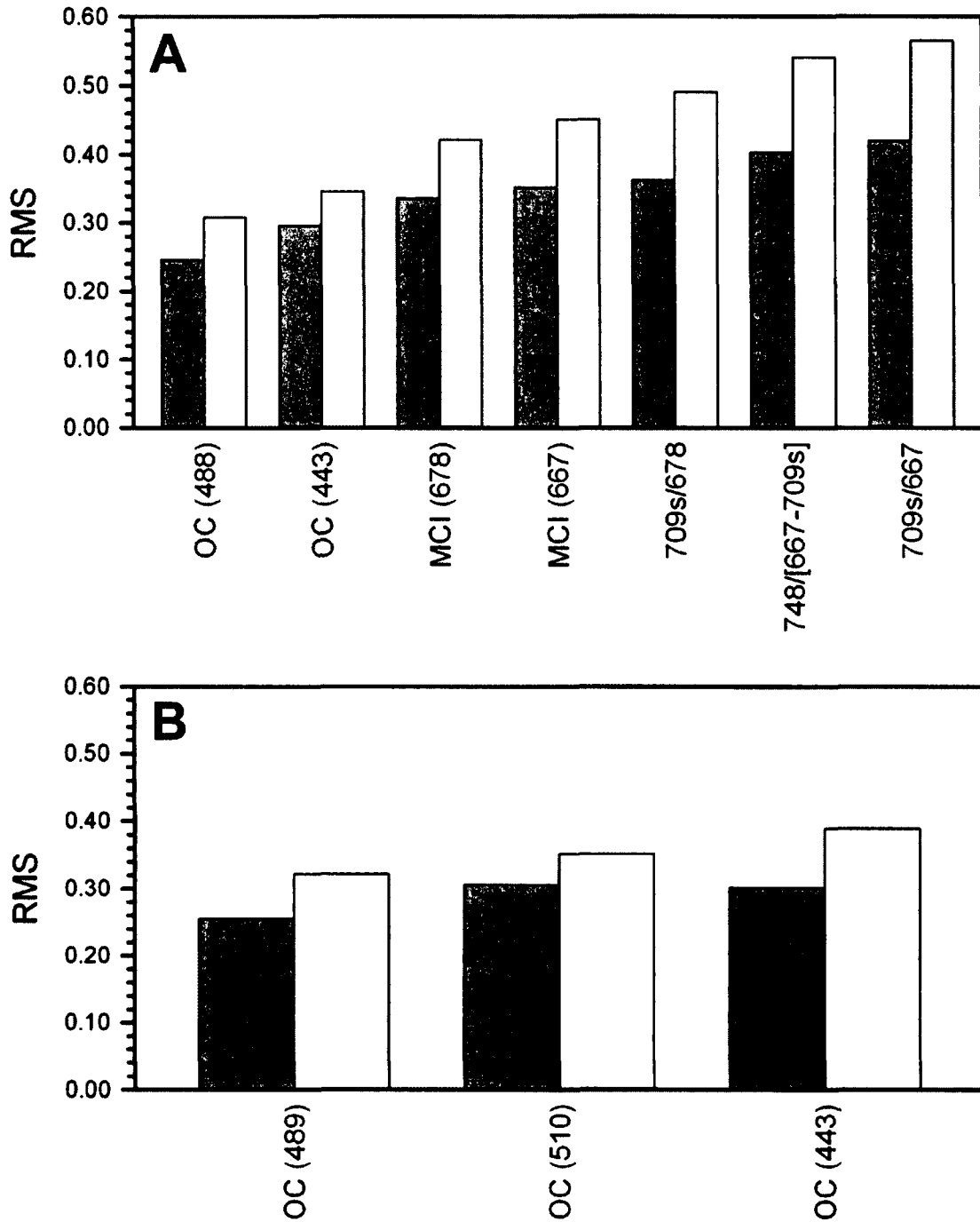


Figure 36. RMS values for chlorophyll estimation algorithms for The Great Salt Lake using (A) MODIS bands and (B) SeaWiFS bands. Blue bars represent algorithms developed with the restricted dataset (n=31), gray bars represent algorithms developed with all data (n=48). MCI - maximum chlorophyll index, OC - ocean color.



CHAPTER V

SUMMARY AND CONCLUSIONS

Ocean color algorithm band selection

This work explored the usefulness of the ocean color algorithms for MODIS, MERIS, and SeaWiFS to estimate chlorophyll in the New England lakes and the Great Salt Lake. Early in algorithm evaluation, it became clear that the standard band-switching ocean color algorithms (OC3, OC4) were not switching between the blue bands as chlorophyll concentrations increased (as happens in the ocean). For every spectrum in New England Lakes and the Great Salt Lake, the highest wavelength blue band included in the algorithm was always selected. This pattern can be understood by observing the general patterns of the spectra (Figures 13, 14, 28, 29), which are characterized by low, fairly constant R_{rs} values at 440 nm, moderately higher R_{rs} values near 489 nm, and higher still R_{rs} values near 510 nm. As such, the spectral characteristics of the study lakes turned the band switching algorithms into simple, predictable band ratios (as would be true for the vast majority of lakes in the world). In this study, OC3 when applied to MODIS always chose 489 nm for the blue band, and OC4 applied to MERIS and SeaWiFS always chose 510 nm.

Early analytical results revealed another interesting trend - the optimized switching algorithm for MODIS modeled on OC3 (blue band selected: 489 nm) produced lower RMS values than either MERIS or SeaWiFS optimized algorithms modeled on OC4 (blue band selected: 510 nm). While having three bands to choose from would seem to be an advantage for the OC4 approach, the additional band turned out to be a disadvantage. In reality, the advantage of the OC3 approach was not related directly to the number of bands employed by the algorithm, but instead that the highest wavelength blue band selected for use (489 nm) by OC3 happened to be a better choice than the band selected by OC4 (510 nm).

In order to determine which of the blue bands provided best results for OC algorithms for each sensor, OC algorithms were evaluated for each of the individual blue bands used in the algorithms. Instead of allowing the "switching" to occur, and therefore, always choosing the highest wavelength blue band, I evaluated all possible blue to green band combinations used in OC3 for MODIS (443 nm / 550 nm, 489 nm / 550 nm), OC4E for MERIS (443 nm / 560 nm, 489 nm / 560 nm, 510 nm / 560 nm), and OC4 for SeaWiFS (443 nm / 555 nm, 489 nm / 555 nm, 510 nm / 555 nm). It is important to note that the OC algorithms developed in this study do not represent the actual OC3 and OC4 algorithms (and thus, do not use the standard coefficients), but instead are algorithms that rely on the same band combinations with coefficients optimized for both study areas.

For all three satellite sensors in both study areas (Tables 9, 13), the OC algorithm using the 489 nm band resulted in the lowest RMS value. In the case of OC4-styled algorithms for New England Lakes, the use of the 489 nm band provided a 3.8% (MERIS) and 2.9% (SeaWiFS) reduction in RMS compared to the band selected by the switching algorithm (510 nm). In the case of the Great Salt Lake, RMS reduction was much greater, 16.2% (MERIS) and 15.6% (SeaWiFS) when using 489 nm instead of 510 nm. Considering the effectiveness displayed by the algorithms using the 489 nm band for all sensors and in both study areas, I suggest the use of a single 489 nm / green band ratio instead of the standard OC4 algorithms. The fact that the OC algorithms worked so well in this study was quite surprising, and may have been due to having an algorithm developed for a single lake (the Great Salt Lake) and another algorithm developed for a region with low variability in total suspended sediments (New England). However, even if these patterns do not hold up in other lake systems, the OC algorithms detailed here can still be very useful to estimate chlorophyll in the regions included in this study.

Simulated 709 nm band for MODIS

The usefulness of MODIS for lake remote sensing has been limited due to the lack of a band to capture the scattering peak that rises between 700 nm and 710 nm with increasing phytoplankton densities. This peak is a key feature of many inland-water chlorophyll algorithms (Gitelson 1992; Gitelson et al. 1999;

Dall'Olmo and Gitelson 2005; 2006; Gitelson et al. 2009), but is rarely used for remote sensing in the open ocean. While it may not be surprising that MODIS, a sensor designed for ocean remote sensing, is missing a band in this wavelength range, it is clear that MODIS could have much greater potential for use in near-shore and inland water systems if it possessed a band at 709 nm.

While it is not possible to alter the position of bands on the currently deployed MODIS sensors, I considered the possibility that a 709 nm band could be simulated based on spectral data from a MODIS band in another wavelength range. In order to select an appropriate MODIS band to use for simulation of R_{rs} at 709 nm, the exact nature of the peak must be considered. The majority of the signal in this wavelength range is likely due to increased backscatter from higher densities of phytoplankton particles as chlorophyll concentrations increase, although there may be some contribution from chlorophyll fluorescence from photosystem I and/or photosystem II (Letelier and Abbott 1996; Harbinson and Rosenqvist 2003; Gitelson et al. 2007). The amount of contribution from chlorophyll fluorescence to R_{rs} can be difficult to quantify, and is likely overwhelmed by scattering in this wavelength range under high chlorophyll conditions. As such, the band best suited to simulate a band at 709 nm would be the MODIS band least influenced by in-water constituents (i.e., CDOM, chlorophyll), but most influenced by backscattering in the visible/NIR wavelength range. Out of the available bands, the MERIS band centered at 754 nm best

complied with these criteria and proved to be the source of data to create the simulated 709 nm band.

To develop the method with which the simulated 709 nm bands for MODIS would be created, a relationship between the R_{rs} at 754 nm and 709 nm (Figure 8) was established using a dataset containing all valid spectra from this study (New England lakes and the Great Salt Lake) together with 179 spectral from lakes throughout Spain (personal communication, Ruiz-Verdú, 2012). The relationship was applied to the MODIS 748 nm band to create a simulated 709 nm band for use in MODIS algorithm development. The simulated MODIS 709 nm band was used in combination with other MODIS bands to evaluate two 2-band algorithms, two 3-band algorithms, and two versions of MCI in both study areas.

In New England, the MCI algorithms exhibited the lowest RMS values (678 nm - 0.281, 667 nm - 0.286) of the algorithms using the simulated 709 nm band, while all the 2-band and 3-band algorithms had RMS values higher than 0.365 (Table 9; Figure 23). However, the best New England MODIS MCI algorithm (using 678 nm) had an RMS value 14% higher than the best algorithms for that study area (OC using 488 nm), and were 22% higher than the RMS values of the best MCI algorithm using MERIS bands (using 665 nm).

In the Great Salt Lake, the MCI algorithms exhibited the lowest RMS values (678 nm - 0.337, 667 nm - 0.354) of the algorithms using the simulated 709 nm band,

while all the 2-band and 3-band algorithms had RMS values higher than 0.360 (Table 13; Figure 36). Again, however, the best Great Salt Lake MODIS MCI algorithm (using 678 nm) had an RMS value 27% higher than the best algorithms for that study area (OC using 488 nm), and were 21% higher than the RMS values of the best MCI algorithm using MERIS bands (using 665 nm).

Maximum Chlorophyll Index

This work explored the use of the standard MCI algorithm to estimate chlorophyll in the study areas, and also investigated the use of alternate bands to serve as the chlorophyll absorption anchor point. Originally developed for the MERIS sensor, the traditional MCI approach relies on the band at 681 nm (band "A" in Figure 9) for the red wavelength with which it forms a baseline connection to the near infrared band at 754 nm (band "C" in Figure 9) (Gower et al. 2005a; b). MCI is normally used solely as an index to describe the relative variability in chlorophyll; this study represents one of the first attempts to relate MCI to chlorophyll concentration in lakes. In an attempt to avoid interference from sun-stimulated fluorescence at 681 nm, alternate choices for band "A" were examined. In the case of the satellite algorithms, alternate bands were fixed (MERIS - 665 nm, MODIS - 667 nm). For the hyperspectral algorithms, 677 nm was chosen based on the wavelength in that region of the spectrum that showed the highest variability in this study (Figures 14, 29).

In New England, the hyperspectral MCI using 677 nm provided the lowest RMS (0.218) of all algorithms evaluated (Table 9; Figures 20, 23). Both the optimized MCI using 677 nm, and the additional alternative MCI using 665 nm (RMS = 0.221) had lower RMS values compared to the standard MCI using 681 nm (0.232). The MERIS MCI using 665 nm had the lowest RMS (0.218) of all MERIS algorithms, offering a moderate improvement over the RMS of the standard MCI (0.229). When using the simulated 709 nm band for MODIS, the standard MCI approach using 678 nm provided an RMS (0.281) nearly identical to the MCI using 667 nm (0.281). In the case of MODIS, the MCI algorithms had lower RMS values than all of the other algorithms using the simulated 709 nm bands.

In the Great Salt Lake, the hyperspectral MCI algorithms using the alternate band at 665 nm (RMS=0.268) and standard band at 681 nm (RMS=0.269) proved useful, but fell short of the four best algorithms (Table 13; Figures 33, 36). The RMS of the MERIS MCI options using 665 nm (0.267) and 681 nm (0.270) were among the lowest, but these algorithms also fell slightly short of the best MERIS algorithms for this lake. When using the simulated 709 nm band for MODIS, the RMS of the standard MCI using 678 nm (0.337) was better than the alternate MCI approach using 667 nm (0.353). In the case of MODIS, and as in the case of New England lakes, the MCI algorithms had lower RMS values than all of the other algorithms using the simulated 709 nm band.

This study confirms the usefulness of the MCI algorithm for estimating chlorophyll concentration in both study areas. In the New England lakes, the MCI algorithms had the lowest RMS values in both the hyperspectral algorithms and the MERIS algorithms, but were not as effective as by the OC algorithms in the case of MODIS. In the Great Salt Lake, the MCI algorithms were among the top algorithms (although not the best) for both hyperspectral and MERIS bands, but were again less accurate than the OC algorithms for MODIS. Especially considering the recent cessation of the Envisat mission (MERIS), the application of MCI to MODIS data could be invaluable for remote sensing of lakes, coastal and ocean system for the next decade.

Improved estimation of chlorophyll in study regions

This study represents the first comprehensive effort to develop remote sensing algorithms for the estimation of chlorophyll in the Great Salt Lake and New England lakes. The collection of hyperspectral data has provided a wonderful opportunity to explore algorithms for a wide variety of sensor types, and these data could be used with any future sensor to predict the optimal way in which to use the data it would capture. Without such research, the use of remote sensing to estimate lake water quality in the study areas would not be as quantitatively useful, since algorithms developed for other lakes and in different regions of the world may not be applicable. For example, in the case of the Great Salt Lake, the standard OC3 algorithm for MODIS has a tendency to over-estimate chlorophyll

concentrations below $2 \mu\text{g L}^{-1}$, and at times underestimate chlorophyll between 10 and $100 \mu\text{g L}^{-1}$ (Figure 37). As a result, an image of estimated chlorophyll using the standard OC3 method could provide misleading concentrations (Figure 38) potentially leading to misinterpretation of trophic state in that area of the lake. When validated lake-specific algorithms are used, however, the amount of data on chlorophyll concentration for a given lake would increase dramatically, revealing patterns nearly impossible to capture with traditional sampling approaches (Figure 39) (Bradt et al. 2008). With the wealth of information now available on the suitability of a variety of chlorophyll estimation algorithms for the study locations, researchers and managers can move forward to embrace the use of remote sensing to help monitor and manage lakes in their regions.

The hyperspectral algorithms developed in this study could be used in a variety of methods with radiometric equipment, including:

1. On a boat to provide real-time in-the-field estimates of chlorophyll concentration;
2. Paired with GPS on a boat to provide a platform for detailed spatial mapping of chlorophyll;
3. Deployed on a buoy system to continually estimate chlorophyll concentration at a given lake site;
4. Deployed on a tower pointed at a lake to continually estimate chlorophyll concentration at a given lake site;

5. Deployed on an airplane to provide estimates of chlorophyll across a given lake and/or in many lakes over a short period of time.

The satellite sensor algorithms developed in this study could be used in a variety of methods with radiometric equipment, including:

1. Applied to data from currently deployed satellite sensors to provide near-real time estimates of chlorophyll concentration across the surface of a lake and/or on one or many lakes (depending on lake size);
2. Applied to archived satellite data to analyze past patterns of chlorophyll concentration and distribution, linking environmental factors of interest (nutrient loading, rainfall, water cycle patterns, internal lake circulation) to phytoplankton community dynamics, and to document trends over time that might have occurred.

Figure 37. A comparison of the standard MODIS OC3 algorithm with a MODIS OC algorithm optimized for the Great Salt Lake using the restricted dataset (n=31). A. Comparison of MODIS OC3 algorithm (dotted pink line) with optimized MODIS OC algorithm for the Great Salt Lake (dotted black line). B. Plot of measured vs. predicted chlorophyll concentrations for MODIS OC3 algorithm. D. Plot of measured vs. predicted chlorophyll concentrations for Great Salt Lake optimized MODIS OC algorithm.

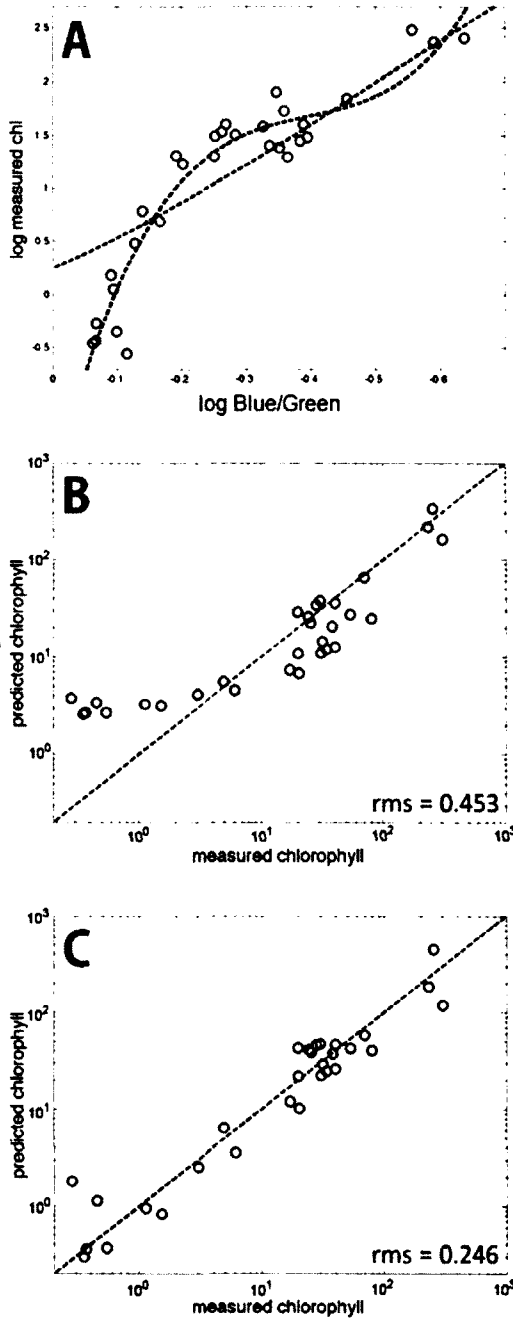


Figure 38. A comparison of chlorophyll maps derived from a MODIS Aqua image of the Great Salt Lake from September 28, 2006 using (A) standard MODIS OC3 algorithm and (B) MODIS OC algorithm optimized for the Great Salt Lake. The differences in the two algorithms shown in Figure 37 are visible below (a few examples are indicated with pink arrows). Chlorophyll concentration shown in $\mu\text{g L}^{-1}$.

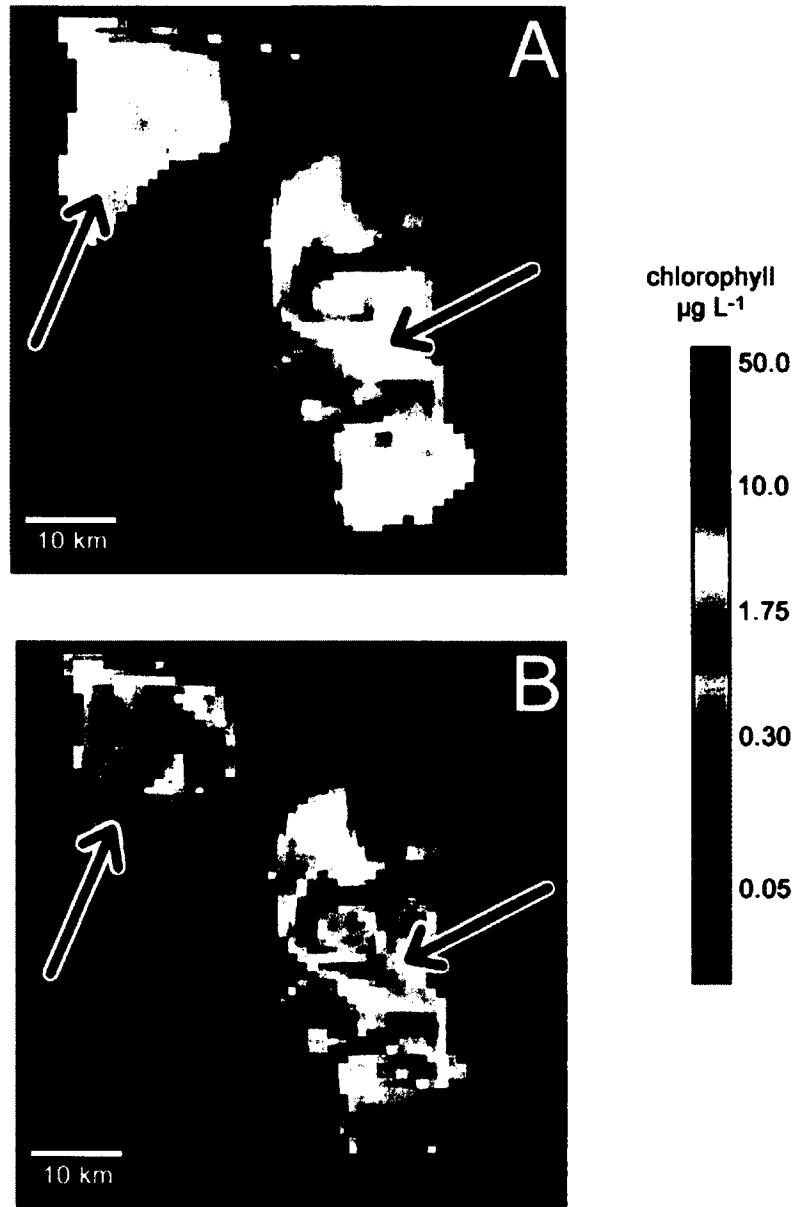
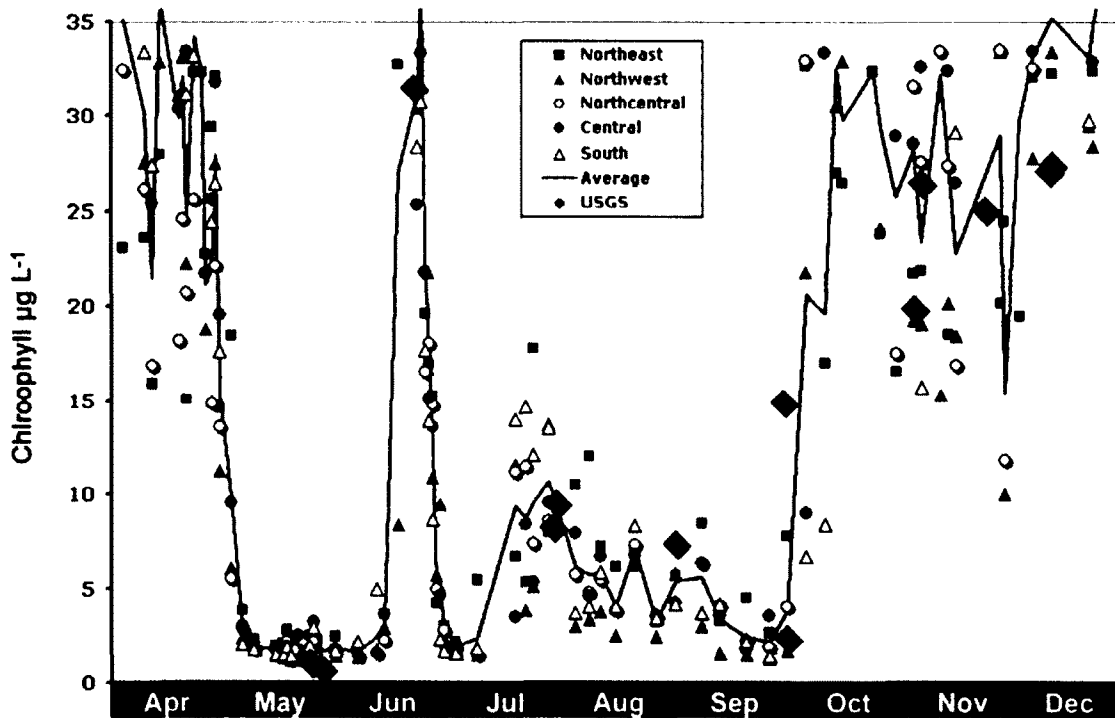
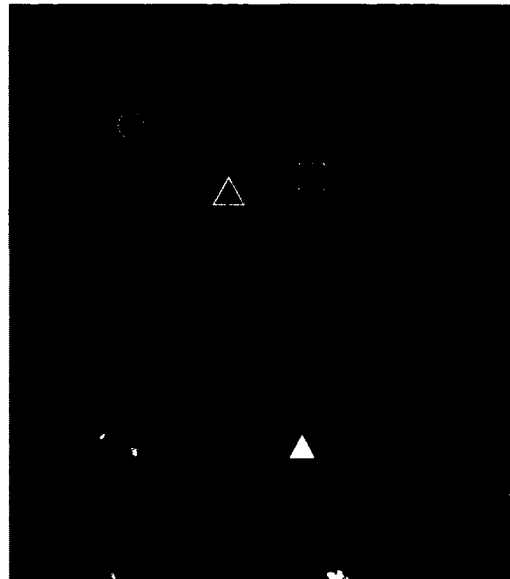


Figure 39. Satellite-derived chlorophyll concentration estimates over time for five locations in the Great Salt Lake in 2006. Chlorophyll estimates were derived from analysis of Aqua MODIS satellite imagery using an OC algorithm optimized for the Great Salt Lake developed with image-based spectral analysis (Bradt et al., 2008). Orange line represents average satellite-derived chlorophyll estimate for the five pixels most closely aligned with the five stations every day when clear satellite imagery available. The blue diamonds represents average extracted chlorophyll concentration from all five lake stations during USGS on-lake sampling cruises.



$$\text{Chl} = -0.0021x^2 + 0.5314x - 0.5984$$

where, $x = \text{MODIS OC3 Chl}$



APPENDICES

APPENDIX A

REMOTE SENSING BASICS

Remote sensing as a concept

Remote sensing devices are used throughout the world to measure an incredibly diverse set of environmental features, including wave heights, bathymetry, topography, water quality, land cover and surface temperature. Remote sensors accomplish these varied tasks by recording the intensity of light, or other types of electromagnetic radiation, which are emitted or reflected from the objects which the sensor is designed to measure (lakes, oceans, forests, etc.). While the entire spectrum of electromagnetic radiation covers energies ranging from gamma rays to radio waves, most water-focused remote sensors rely on the visible and near infrared wavelengths (400 nm to 775 nm). These wavelengths represent the portion of the spectrum that interacts in a measurable and predictable manner with optically active constituents of oceans and lakes, including sediments, colored dissolved organic matter (CDOM) and phytoplankton. By monitoring the variations in intensity and spatial patterns at these wavelengths, remote sensors

provide a mechanism for quantifying in-water constituents of interest, and tracking change in water bodies both spatially and temporally.

All remote sensors measure radiation reflected off of or emitted from an object of interest. Remote sensors fall into two broad categories based on the way in which they interact with the features they are measuring. The majority of sensors, known as passive sensors, rely on the sun to provide the electromagnetic radiation which illuminates the object of interest. For sensors focused on visible and near-infrared wavelengths, the signal measured from the object is portion of incoming solar radiation reflected from that object. For other types of sensors (thermal), the measurement is based on the amount of radiation reemitted from the object at those wavelengths . While thermal sensors are often best used during the nighttime, sensors measuring visible and near-infrared wavelengths can only make measurements during daylight hours. On the other hand, active sensors produce their own radiation with which objects can be measured. These sensors can be used with equal effectiveness regardless of the time of day, and due to the types of wavelengths on which they rely (SONAR, LIDAR, RADAR), are less hampered by environmental conditions. Active sensors have the advantage of measuring wavelengths of electromagnetic energy not typically provided in high quantities in sunlight, providing for advanced measurements not possible with passive sensors.

When deciding which sensor to use for a particular application, key characteristics should be considered, including spatial resolution, foot print, temporal resolution, spectral resolution and radiometric resolution.

Spatial resolution

Description. The spatial resolution of a sensor describes the size of a pixel in the imagery produced by that sensor. The size of an image pixel produced by a sensor is the result of a range of design factors, including the type of lens, the number of sensor elements on the sensor electronics, the elevation above the ground from which the sensor captures images, the angle of view of the sensor, etc. The size of pixels on publicly accessible satellite remote sensors range from as large as a 1.1 km to less than 1 meter.

Importance. Pixel size is a very important factor in determining the size and types of features visible in an image. Images with large pixels can reveal large-scale patterns in the ocean or a large lake, but will not have enough fine detail to document smaller features. In the case of small lakes or lakes with a convoluted shoreline, large pixels can leave out many of the most interesting sections of the water body. On the other hand, while images with small pixels allow for the observation of small water body features, these images are often data dense and cover a relatively narrow area on the ground with each sensor overpass (swath width). Images with smaller pixels could result in a data density requiring

intensive data manipulation, or might not cover the entire water body when working with a larger lake system.

Temporal resolution

Description. Temporal resolution describes how often a remote sensor has the chance to capture an image of the same place on the Earth, a length of time often referred to as revisit time. Some satellite sensors record data from an swath centered directly below the sensor, or at nadir. In the case of nadir-looking sensors, the swath width determines the repeat time. The wider the swath width, the less time it takes for the swath width to “repaint” the same spot on the earth. Some satellites have the ability to tilt or point the sensor, providing the ability to capture images of the same spot on the Earth more often than would be possible with a fixed sensor. The off-center views produced when the satellites are tilted to capture imagery from locations not directly beneath the satellite are known as off-nadir. While the ability to capture off-nadir imagery can be seen as an advantage, measurements at non-nadir view angles can cause the sensor to miss measurements of some portions of the nadir swath. As such, off-nadir sensors can lead to data gaps compared to strict nadir-viewing sensors.

Aircraft-borne sensors are in a completely different category when it comes to temporal resolution. Unlike satellites, airplanes are not constantly in flight and can not provide global coverage. The temporal resolution of an individual aircraft

sensor is difficult to predict, since a wide variety of factors need to be considered (distance from aircraft origin of the study site, local weather conditions, competing aircraft usage, etc.). In general, aircraft-borne sensors have good temporal resolution in the short term, and poor temporal resolution in the long term.

Importance. The frequency with which the images of an area can be obtained, and the number of images of a water body that can be captured over time, has an enormous impact on the potential applications of a particular sensor. Satellite sensors with revisit times from one to several days can be used for tracking environmental changes (i.e., water quality) on a weekly basis, allowing detailed observation of ecosystem dynamics over time. Sensors with revisit times closer to two weeks provide information on system dynamics over a broader times scale, such as monthly or seasonally. Aircraft-borne sensors are difficult to use for long term studies, due to the difficulty in obtaining repeated images of the same area over time. However, one benefit of aircraft sensors lies in the ability to vary the time of day at which images are captured, while satellite-borne sensors are normally tuned to collect data at a precisely chosen, but fixed time each day.

Spectral resolution

Description. Spectral resolution describes the width, number and position of the “bands” a remote sensor uses to measure incoming radiation. Unlike laboratory spectrophotometers that capture spectral information at increments of ~1 nm, most remote sensors measure radiation at broader, discrete areas of the spectrum based on the spectral characteristics of the features which the sensor is designed to measure. Some multispectral sensors (e.g. Landsat ETM) have fewer than 10 bands or segments of the spectrum over which data are collected, while others measure radiation at over 30 wavelength ranges. Hyperspectral sensors provide a vastly increased number of spectral measurements (often 200+ bands), and provide continuous spectral data approximating laboratory equipment.

Importance. The number, position and width of bands present in a sensor have an enormous influence on the applications for which a sensor can be used. While a few sensors have the ability to adjust bands on the fly, the vast majority of remote sensors have unmovable bands which are chosen based on the application for which the sensor was designed. For the measurement of land features (as in the case of Landsat ETM), wide bands in the visible and near-infrared range provide sufficient information for many applications. For the observation of in-water features (as in the case of MODIS), sensors with narrow bands strategically placed in the visible portion of the spectrum are best suited.

While hyperspectral sensors are rare in satellites, their continuous spectral measurements allow for ultimate application versatility. Due to the detailed spectral data they provide, and resultant ability to match the bands of any other sensor, hyperspectral sensors are often deployed on boats or in aircraft during algorithm development using *in situ* data.

Radiometric resolution

Description. Radiometric resolution refers to sensitivity with which a sensor can measure changes in the intensity of radiation. This type of resolution is measured in “bits”, which refers to the range of numbers by which radiation intensity is measured by the sensor. For example, an 8-bit sensor has a minimum value of 0 and a maximum value of 255 ($2^8 = 256$). Without considering the gain setting on the sensor, a 8-bit sensor would measure the darkest pixel in the world as 0, and the brightest as 255, leaving 256 possible levels of intensity for each individual measurement. A 12-bit sensor would have a maximum value of 4,095 ($2^{12} = 4,096$), allowing for over 16 times as many levels of intensity as an 8 bit sensor. In reality, gain settings on sensors can be adjusted to provide the maximum measurement sensitivity of a given spectral feature in a particular environment. A few sensors, such as SeaWiFS, have multiple gain settings for select bands to ensure the signal in that channel is captured appropriately, regardless of the light conditions they encounter. However, most sensors have a single gain setting used for each band at one

time, and while that setting can be adjusted over time, it can not be applied differently to individual pixels in one image.

Importance. The higher radiometric resolution a sensor possesses, the finer detail with which it can measure changes in radiation intensity. Higher radiometric resolution is most important when measuring features characterized by low reflectance, such as areas in shadow on the land and water bodies such as lakes and oceans. In the case of surface water, typically less than 10% of incoming light from the sun at a given band would be reflected toward the sensor. When sensors designed for remote sensing of water are capturing data over the ocean, the gain setting can be adjusted to more accurately measure the lower signal coming from the water. However, in the case of lakes, many sensors are making measurements over land using the gain setting for appropriate for the higher light intensities typical of terrestrial remote sensing. If data were captured over land using the gain setting tailored for ocean remote sensing, much of the data would be completely saturated, and thus largely useless. On the other hand, the gain setting for land does not take into account the low reflectance characteristics of lakes, resulting in only a portion of the potential dynamic range of the sensor to be used for signal coming from lakes (except in a few special cases, i.e., SeaWiFS). As a result, the sensor would have a much lower dynamic range with which to measure variations in signal from water bodies.

A good analogy for different levels of radiometric resolution in remote sensors is the task of making measurements of the height of a tomato plant with three different meter sticks (assuming the gain of the meter sticks can not be adjusted). Meter stick number 1 would be marked with decimeters only, stick number 2 would be marked only with centimeters, and the final meter stick would have millimeter markings. The ability to accurately measure small changes in size would be much greater with the stick number 3, because the increased "radiometric resolution" would allow for the measurement of smaller increments of variation than either stick 1 or stick 2. In the case of these meter sticks, a crude estimate would have to be made between the decimeter and centimeter markings, resulting in a lack of sensitivity to small increments of growth, and a likely under or overestimation of plant size.

APPENDIX B

HYDROLIGHT SETTINGS

Hydrolight 4.2 was used to produce modeled spectra for each lake measured with the single-radiometer technique. Two modeled spectra were produced for each lake, one using the epilimnetic extracted chlorophyll concentration and another using the chlorophyll profile measured with the YSI probe. The ABCASE2 routine was run with the settings shown below:

Pure water absorption: Pope and Fry's (1997) "pure water" absorption values

Chlorophyll concentration: run 1 - extracted chlorophyll as a constant

run 2 - YSI chlorophyll profile with data binned 0.5 m

Chlorophyll phase function: avgpart.dpf

CDOM concentration: measured CDOM concentration

Mineral concentration: a constant of 0

Chlorophyll fluorescence: enabled

Wavelengths: every 5 nm from 395 nm to 755 nm

Wind speed: 5 meters per second

Sky model: semi-empirical sky model (based on RADTRAN)

Solar zenith angle: 30 degrees

Cloud cover: 0%

Sky radiance: RADTRAN

Angular pattern: hcnrad

Bottom boundary condition: infinitely deep

Output depths: every 0.1 m from surface to 1 m, every 0.5 m from 1 m to 10 m

APPENDIX C

CHLOROPHYLL ALGORITHMS FOR NEW ENGLAND LAKES

Hyperspectral linear

For algorithms using all chlorophyll values, the four best techniques were a combination of a 2-band ratios and 3-band ratios (Table 14; Figures 40, 41). Among all four methods, three chlorophyll absorption bands (673 nm, 675 nm, 677 nm) and four scattering peak bands (695 nm, 703 nm, 705 nm, 710 nm) were used. The average values of the four best algorithms using all chlorophyll values were characterized by high r^2 (0.92) and low RMS ($4.5 \mu\text{g L}^{-1}$), and a relative error of 63% (Table 15). When chlorophyll concentrations above $5 \mu\text{g L}^{-1}$ were used, the best four algorithms showed an RMS increase of 24% ($5.6 \mu\text{g L}^{-1}$), with virtually identical r^2 values (0.93), and half the relative error (30%) compared to the algorithms using all chlorophyll concentrations.

Nearly the same set of algorithms were best suited when chlorophyll concentrations above $50 \mu\text{g L}^{-1}$ were excluded from the analysis (Table 16; Figures 40, 41). With this chlorophyll range the RMS dropped 2% ($4.4 \mu\text{g L}^{-1}$) when compared to algorithms including all chlorophyll data, while r^2 dropped 14%

(0.79) and relative error decreased by 6% (59%) (Table 15). When only chlorophyll values between $5 \mu\text{g L}^{-1}$ and $50 \mu\text{g L}^{-1}$ were used, the best algorithms changed little (Table 16; Figures 40, 41). These regressions exhibited an RMS increase of 20% ($5.4 \mu\text{g L}^{-1}$), a drop in r^2 values (0.77), and a 54% decrease in relative error (29%) when compared to regressions using all chlorophyll concentrations (Table 15).

MERIS linear

For algorithms based on MERIS bands using all chlorophyll values, the two best techniques used a single ratio between chlorophyll absorption (either 665 nm or an average of 665 nm and 881 nm) and the scattering peak (709 nm) (Table 14; Figures 40, 42). The average values of the two best algorithms using all chlorophyll values were characterized by an r^2 of 0.89, an RMS of $5.2 \mu\text{g L}^{-1}$, and a relative error of 71% (Table 15). When chlorophyll concentrations above $5 \mu\text{g L}^{-1}$ were used, the same two algorithms were still the best, showing a RMS increase of 17% ($6.1 \mu\text{g L}^{-1}$), slightly higher r^2 values (0.91), and a 54% lower relative error (33%) compared to the algorithms using all chlorophyll concentrations.

The same two algorithms were best suited for when chlorophyll concentrations above $50 \mu\text{g L}^{-1}$ were excluded from the analysis (Table 16; Figures 40, 42). With this chlorophyll range the RMS dropped 8% ($4.8 \mu\text{g L}^{-1}$) when compared to

algorithms including all chlorophyll data, while r-squared dropped to 0.75 and relative error decreased 8% (65%) (Table 15). Algorithms using chlorophyll values between $5 \mu\text{g L}^{-1}$ and $50 \mu\text{g L}^{-1}$ (Table 16; Figures 40, 42) exhibited an RMS increase of 8% ($5.6 \mu\text{g L}^{-1}$), a drop in r-squared values (0.75), and a 58% decrease in relative error (30%) when compared to regressions using all chlorophyll concentrations (Table 15).

MODIS linear

For all algorithms based on MODIS bands using all chlorophyll values, the two best techniques used a single ratio between chlorophyll absorption (either 667 nm or an average of 667 nm and 678 nm) and the simulated scattering peak at 709 nm based on 754 nm band (Table 14; Figures 40, 42). The average values of the two best algorithms using all chlorophyll values were characterized by an r^2 of 0.67, an RMS of $8.9 \mu\text{g L}^{-1}$, and a relative error of 204% (Table 15). When chlorophyll concentrations above $5 \mu\text{g L}^{-1}$ were used the RMS decreased 15% ($7.6 \mu\text{g L}^{-1}$), the r^2 value increased (0.86), at the relative error dropped 76% (49%).

When chlorophyll concentrations above $50 \mu\text{g L}^{-1}$ were excluded from the analysis the RMS dropped 11% ($7.9 \mu\text{g L}^{-1}$) compared to algorithms including all chlorophyll data, while r^2 dropped 52% (0.32) and relative error decreased 22% (160%) (Tables 15, 16; Figures 40, 42). When only chlorophyll values between 5

$\mu\text{g L}^{-1}$ and $50 \mu\text{g L}^{-1}$ were used, the RMS decreased of 17% ($7.4 \mu\text{g L}^{-1}$), the r^2 value was reduced by 15% (0.57), and relative error decreased by 75% (51%) when compared to regressions using all chlorophyll concentrations (Table 15).

Single- and dual-radiometer comparison

When the combined single- and dual-radiometer spectral dataset was evaluated using linear algorithms, all algorithms at all chlorophyll ranges demonstrated higher RMS compared to the same algorithms run using only the dual-radiometer spectra, ranging from 2% to 75% (Table 17). The relative error of each algorithm also increased between algorithms run with the combined data, and those using the dual-radiometer spectra alone. The algorithms least affected by the addition of the single-radiometer spectra were the hyperspectral algorithms using the scattering peak (703 nm, 705 nm, 710 nm). The greatest differences were seen in the MERIS algorithms.

Coefficients for log-log analyses

The coefficients for the best log-log algorithms for New England lakes (Table 9) are listed in Table 16.

APPENDIX D

CHLOROPHYLL ALGORITHMS FOR THE GREAT SALT LAKE

Hyperspectral linear

For algorithms using all chlorophyll values, the best four techniques were 2-band ratios (Table 18; Figures 43, 44). Each of these ratios had one of the bands positioned to detect chlorophyll absorption (665 nm, 673 nm, 675 nm, 677 nm) and the other tuned to monitor the scattering peak (703 nm, 705 nm, 710 nm). The average values of the four best algorithms using all chlorophyll values had a high r^2 (0.92), an RMS of $18.0 \mu\text{g L}^{-1}$, and a high relative error (613%) (Table 19). When only chlorophyll concentrations above $1.5 \mu\text{g L}^{-1}$ were used, the best four algorithms showed an RMS increase of 39% ($24.9 \mu\text{g L}^{-1}$), virtually identical r^2 values (0.91), and a 90% decrease in relative error (59%) compared to the algorithms using all chlorophyll concentrations.

The same four algorithms were best suited when chlorophyll concentrations above $80 \mu\text{g L}^{-1}$ were excluded from the analysis (Table 20; Figures 43, 44). When using this chlorophyll range, the RMS dropped 65% ($6.2 \mu\text{g L}^{-1}$) compared to algorithms including all chlorophyll data, while r^2 changed slightly (0.90) and

relative error decreased 45% (333%) (Table 19). When only chlorophyll values between $1.5 \mu\text{g L}^{-1}$ and $80 \mu\text{g L}^{-1}$ were used, the best algorithms included both 2-band and 3-band methods (Table 20; Figures 43, 44). These regressions exhibited an RMS decrease of 56% ($7.9 \mu\text{g L}^{-1}$), a slight drop in r^2 values (0.89), and a 92% decrease in relative error (50%) compared to regressions using all chlorophyll concentrations (Table 19).

MERIS linear

Linear analysis of algorithms using MERIS resulted in RMS and relative errors nearly identical to those derived with hyperspectral bands. In three out of the four chlorophyll ranges, the best algorithm used an average of the bands centered at 667 nm and 681 nm to assess the chlorophyll absorption maximum, and the scattering peak at 709 nm (Table 18; Figures 43, 45). The average values of the two best algorithms were characterized by high r^2 (0.92), an RMS of $17.9 \mu\text{g L}^{-1}$, and a high relative error (532%) (Table 19). When only chlorophyll concentrations above $1.5 \mu\text{g L}^{-1}$ were used, the same two algorithms still performed the best, showing an RMS increase of 41% ($25.2 \mu\text{g L}^{-1}$), a virtually identical r^2 values (0.91), and a dramatically reduced relative error (50%) compared to the algorithms using all chlorophyll concentrations.

The same two algorithms were best suited when chlorophyll concentrations above $80 \mu\text{g L}^{-1}$ were excluded from the analysis (Table 20, Figures 43, 45). With

this chlorophyll range the RMS dropped 65% ($6.2 \mu\text{g L}^{-1}$) when compared to algorithms including all chlorophyll data, while r^2 changed slightly (0.90) and relative error decreased 32% (364%) (Table 19). When only chlorophyll values between $1.5 \mu\text{g L}^{-1}$ and $80 \mu\text{g L}^{-1}$ were used, the best algorithms included both 2-band and 3-band approaches (Table 20; Figures 43, 45). These regressions exhibited an RMS decrease of 56% ($7.8 \mu\text{g L}^{-1}$), a small drop in r^2 values (0.85), and a 91% decrease in relative error (50%) when compared to regressions using all chlorophyll concentrations (Table 19).

MODIS linear

For algorithms based on MODIS bands using all chlorophyll values, the two best techniques used a single ratio between chlorophyll absorption (either 667 nm or an average of 667 nm and 678 nm) and the scattering peak (709 nm) (Table 18; Figures 43, 45). The average values of those two algorithms were characterized by an r^2 of 0.87, an RMS of $23.1 \mu\text{g L}^{-1}$, and a high relative error (1253%) (Table 19). When chlorophyll concentrations above $1.5 \mu\text{g L}^{-1}$ were used the RMS increased 36% ($31.4 \mu\text{g L}^{-1}$), the r^2 value was virtually unchanged (0.86), and the RMS dropped 93% (88%) compared to the algorithms using all chlorophyll concentrations.

When chlorophyll concentrations above $80 \mu\text{g L}^{-1}$ were excluded from the analysis the RMS dropped 45% ($12.8 \mu\text{g L}^{-1}$) compared to algorithms including all

chlorophyll data, while r^2 dropped 34% (0.57) and relative error decreased 2% (1228%) (Tables 19, 20; Figures 43, 45). When only chlorophyll values between $1.5 \mu\text{g L}^{-1}$ and $80 \mu\text{g L}^{-1}$ were used the RMS decreased of 35% ($15.1 \mu\text{g L}^{-1}$), the r^2 value was reduced by 49% (0.44), and relative error decreased by 91% (118%) when compared to regressions using all chlorophyll concentrations (Table 19).

Coefficients for log-log analyses

The coefficients for the best log-log algorithms for the Great Salt Lake (Table 13) are listed in Table 22.

Table 14. Linear regression models for predicting chlorophyll concentrations in the New England lakes using dual-radiometer spectra sorted by RMS. The number of spectra used for each type of regression analysis: all chlorophyll (n=90), chlorophyll > 5 µg L⁻¹ (n=40).

Type	Algorithm	RMS	Rel Error	r ²
all chl				
Hyper	730/[675-695]	4.5	63%	0.92
	754/[677-703]	4.5	74%	0.92
	710/673	4.6	63%	0.91
	705/675	4.6	61%	0.91
	703/677	4.8	59%	0.91
	710/665	5.5	77%	0.88
	720/670	5.8	115%	0.86
	725/665	6.5	132%	0.83
	740/[671-710]	6.8	152%	0.81
	754/[665-709]	7.3	161%	0.78
735/673	9.7	221%	0.61	
MERIS	709/(665:681)	4.9	66%	0.90
	709/665	5.5	75%	0.88
	754/[665-709]	6.5	133%	0.83
MODIS	709s/(667:678)	8.5	198%	0.71
	709s/667	9.3	211%	0.64
	748/[667-709s]	9.4	222%	0.64
chl > 5				
Hyper	754/[677-703]	5.4	32%	0.93
	710/673	5.6	30%	0.93
	730/[675-695]	5.7	33%	0.92
	705/675	5.7	28%	0.92
	703/677	6.0	30%	0.91
	720/670	6.2	38%	0.91
	710/665	6.5	36%	0.90
	740/[671-710]	6.7	47%	0.89
	725/665	6.9	44%	0.89
	754/[665-709]	7.0	47%	0.88
735/673	8.0	58%	0.85	
MERIS	709/(665:681)	5.8	31%	0.92
	709/665	6.5	35%	0.90
	754/[665-709]	6.5	41%	0.90
MODIS	709s/(667:678)	7.3	46%	0.88
	748/[667-709s]	7.9	51%	0.85
	709s/667	8.3	52%	0.84

Table 15. Comparison of the best linear fit algorithms for New England lakes for each sensor type and chlorophyll range. Data in the Value column represent averages of best algorithms for each category. Number of algorithms averaged varied by sensor type based on obvious break points in regression statistical values. Number of algorithms averaged: Hyperspectral - 4, MERIS - 2, MODIS - 2. Data in the Δ chl column represent the difference between algorithms run with all chlorophyll values, and the algorithms run with restricted chlorophyll values. Chlorophyll values in $\mu\text{g L}^{-1}$.

Type	RMS		Rel Error		r^2	
	Δ all chl	Value	Δ all chl	Value	Δ all chl	Value
Hyperspectral						
all chl	---	4.5	---	63%	---	0.92
chl > 5	+24%	5.6	-52%	30%	+1%	0.93
chl < 50	-2%	4.4	-6%	59%	-14%	0.79
5 < chl < 50	+20%	5.4	-54%	29%	-16%	0.77
MERIS						
all chl	---	5.2	---	71%	---	0.89
chl > 5	+17%	6.1	-54%	33%	+2%	0.91
chl < 50	-8%	4.8	-8%	65%	-16%	0.75
5 < chl < 50	+8%	5.6	-58%	30%	-16%	0.75
MODIS						
all chl	---	8.9	---	204%	---	0.67
chl > 5	-15%	7.6	-76%	49%	+28%	0.86
chl < 50	-11%	7.9	-22%	160%	-52%	0.32
5 < chl < 50	-17%	7.4	-75%	51%	-15%	0.57

Table 16. Coefficients for log-log regressions (Table 9) for relating spectral measurements to chlorophyll concentration in New England lakes (n=90). Factors added to correct otherwise negative values for the predictor variable - ^ - 0.005, * - 0.025, ** - 0.5.

Type	Algorithm	intercept	x	x ²	x ³	x ⁴
Hyper	MCI (677)^	399.8	594.2	295.3	48.90	---
	754/[677-703]**	1.930	2.004	-4.646	---	---
	730/[675-695]*	1.971	1.570	-0.705	---	---
	703/677	0.895	3.409	-2.302	---	---
	MCI (665)^	632.2	937.9	463.6	76.18	---
	754/[665-709]**	2.106	1.410	-10.12	-12.18	---
	705/675	0.926	3.377	-2.359	---	---
	710/673	1.094	2.500	-1.048	---	---
	MCI (681)^	467.1	696.7	346.7	57.37	---
	740/[671-710]**	1.852	2.560	-1.110	-2.100	---
	710/665	1.128	2.892	-1.451	---	---
	720/670	1.236	2.417	-0.429	---	---
	725/665	1.448	2.457	0.170	---	---
	735/673	0.403	0.864	0.000	0.145	---
	MERIS	MCI (665)^	-4623	-9223	-6878	-2273
754/[665-709]**		2.158	0.963	-13.50	-16.41	---
MCI (681)^		-3275	-6594	-4960	-1653	-206.1
OC (489)		0.089	-1.441	3.923	---	---
709/681		1.080	2.928	-1.912	---	---
709/(665:681)		1.095	3.104	-2.105	---	---
OC (510)		0.056	-3.031	4.416	---	---
OC (443)		-0.002	-0.944	1.521	---	---
709/665		1.087	3.184	-1.934	---	---
MODIS	OC (488)	0.053	-1.885	3.604	---	---
	OC (443)	-0.060	-1.315	1.294	---	---
	MCI (678)^	218.7	331.4	168.7	28.64	---
	MCI (667)^	246.8	373.1	189.3	32.02	---
	709s/678	0.762	1.549	1.716	---	---
	709s/(667:678)	0.751	1.510	2.102	---	---
	748/[667-709s]**	1.565	3.428	2.476	---	---
709s/667	0.736	1.441	2.553	---	---	
SeaWiFS	OC (489)	0.069	-1.694	3.987	---	---
	OC (510)	0.046	-3.476	4.161	---	---
	OC (443)	-0.012	-0.991	1.685	---	---

Table 17. Linear regression models for predicting chlorophyll concentrations in New England lakes using dual-radiometer spectra sorted by RMS. The number of spectra used for each type of regression analysis: chlorophyll < 50 $\mu\text{g L}^{-1}$ (n=89), chlorophyll between 5 $\mu\text{g L}^{-1}$ and 50 $\mu\text{g L}^{-1}$ (n=39).

Type	Algorithm	RMS	Rel Error	r^2
chl < 50				
Hyper	703/677	4.3	52%	0.80
	705/675	4.4	59%	0.79
	710/673	4.4	58%	0.79
	730/[675-695]	4.5	68%	0.78
	754/[677-703]	4.6	74%	0.77
	710/665	5.0	69%	0.72
	720/670	5.8	116%	0.63
	740/[671-710]	5.9	116%	0.62
	754/[665-709]	6.0	119%	0.60
	725/665	6.4	128%	0.55
	735/673	9.0	175%	0.12
	MERIS	709/(665:681)	4.6	62%
709/665		5.0	68%	0.72
754/[665-709]		5.6	101%	0.65
MODIS	709s/(667:678)	7.7	160%	0.35
	709s/667	8.1	160%	0.28
	748/[667-709s]	8.3	164%	0.26
5 < chl < 50				
Hyper	703/677	5.3	28%	0.77
	705/675	5.3	27%	0.77
	710/673	5.4	29%	0.77
	754/[677-703]	5.4	32%	0.76
	730/[675-695]	5.6	31%	0.75
	710/665	5.9	33%	0.72
	720/670	6.2	39%	0.69
	740/[671-710]	6.5	47%	0.66
	754/[665-709]	6.5	47%	0.66
	725/665	6.9	45%	0.62
	735/673	8.1	59%	0.48
	MERIS	709/(665:681)	5.3	28%
709/665		5.9	32%	0.72
754/[665-709]		6.3	42%	0.68
MODIS	709s/(667:678)	7.0	48%	0.61
	748/[667-709s]	7.7	53%	0.53
	709s/667	7.7	53%	0.53

Table 18. Comparison of linear algorithms for determining chlorophyll concentrations in New England lakes analyzed with only dual-radiometer spectra (DRS) and a combined data set of single- and dual-radiometer spectra (DRS+RS). Δ RMS indicates the difference between RMS values between the two datasets. Chlorophyll values in $\mu\text{g L}^{-1}$.

Type	Algorithm	Δ RMS	RMS		Rel Error	
			DRS	DRS+RS	DRS	DRS+RS
all chl						
Hyper	710/673	+20%	4.6	5.5	63%	77%
	705/675	+8%	4.6	5.0	61%	66%
	703/677	+5%	4.8	5.0	59%	64%
	710/665	+18%	5.5	6.5	77%	89%
	720/670	+29%	5.8	7.5	115%	130%
MERIS	709/(665:681)	+78%	4.9	8.6	66%	122%
	709/665	+75%	5.5	9.6	75%	132%
chl > 5						
Hyper	710/673	+24%	5.6	6.9	30%	39%
	705/675	+11%	5.7	6.4	28%	32%
	703/677	+7%	6.0	6.4	30%	33%
	720/670	+40%	6.2	8.7	38%	56%
	710/665	+23%	6.5	8.0	36%	49%
MERIS	709/(665:681)	+75%	5.8	10.1	31%	48%
	709/665	+75%	6.5	11.4	35%	56%
chl < 100						
Hyper	703/677	+2%	4.3	4.4	52%	56%
	705/675	+3%	4.4	4.5	59%	62%
	710/673	+13%	4.4	5.0	58%	68%
	710/665	+12%	5.0	5.7	69%	79%
	720/670	+18%	5.8	6.9	116%	123%
MERIS	709/(665:681)	+47%	4.6	6.7	62%	101%
	709/665	+45%	5.0	7.3	68%	108%
5 < chl < 100						
Hyper	703/677	+4%	5.3	5.5	28%	31%
	705/675	+6%	5.3	5.6	27%	31%
	710/673	+14%	5.4	6.1	29%	38%
	710/665	+16%	5.9	6.9	33%	44%
	720/670	+25%	6.2	7.8	39%	55%
MERIS	709/(665:681)	+35%	5.3	7.2	28%	42%
	709/665	+39%	5.9	8.2	32%	49%

Table 19. Linear regression models for predicting chlorophyll concentrations in the Great Salt Lake sorted by RMS. The number of spectra used for each type of regression analysis: all chlorophyll (n=48), chlorophyll > 1.5 $\mu\text{g L}^{-1}$ (n=22).

Type	Algorithm	RMS	Rel Error	r^2
all chl				
Hyper	705/675	17.6	696%	0.92
	703/677	17.8	851%	0.92
	710/673	18.0	480%	0.92
	710/665	18.4	423%	0.92
	730/[675-695]	19.6	343%	0.91
	754/[677-703]	19.6	744%	0.91
	720/670	19.7	317%	0.90
	740/[671-710]	20.2	921%	0.90
	754/[665-709]	20.8	1119%	0.89
	725/665	20.9	477%	0.89
735/673	21.6	821%	0.88	
MERIS	709/(665:681)	17.6	584%	0.92
	709/665	18.1	479%	0.92
	754/[665-709]	20.7	1109%	0.89
MODIS	709s/(667:678)	22.9	1239%	0.87
	709s/667	23.3	1267%	0.87
	748/[667-709s]	23.6	1279%	0.87
chl > 1.5				
Hyper	703/677	23.8	84%	0.92
	705/675	24.2	67%	0.91
	710/673	25.4	44%	0.90
	710/665	26.2	43%	0.90
	754/[677-703]	27.5	39%	0.89
	740/[671-710]	28.0	39%	0.88
	730/[675-695]	28.2	36%	0.88
	720/670	28.3	43%	0.88
	754/[665-709]	28.6	44%	0.88
	725/665	29.8	60%	0.87
735/673	30.3	66%	0.86	
MERIS	709/(665:681)	24.7	55%	0.91
	709/665	25.7	45%	0.90
	754/[665-709]	28.4	44%	0.88
MODIS	709s/(667:678)	31.1	83%	0.86
	709s/667	31.6	93%	0.85
	748/[667-709s]	31.8	112%	0.85

Table 20. Comparison of the best linear fit algorithms for the Great Salt Lake for each sensor type and chlorophyll range. Data in the Value column represent averages of best algorithms for each category. Number of algorithms averaged varied by sensor type based on obvious break points in regression statistical values. Number of algorithms averaged: Hyperspectral - 4, MERIS - 2, MODIS - 2. Data in the Δ chl column represent the difference between algorithms run with all chlorophyll values, and the algorithms run with restricted chlorophyll values. Chlorophyll values in $\mu\text{g L}^{-1}$.

Type	RMS		Rel Error		r^2	
	Δ all chl	Value	Δ all chl	Value	Δ all chl	Value
Hyperspectral						
all chl	---	18.0	---	613%	---	0.92
chl > 1.5	+39%	24.9	-90%	59%	-1%	0.91
chl < 80	-65%	6.2	-46%	333%	-2%	0.90
1.5 < chl < 80	-56%	7.9	-92%	50%	-3%	0.89
MERIS						
all chl	---	17.9	---	532%	---	0.92
chl > 1.5	+41%	25.2	-91%	50%	-1%	0.91
chl < 80	-65%	6.2	-32%	364%	-2%	0.90
1.5 < chl < 80	-56%	7.8	-91%	50%	-8%	0.85
MODIS						
all chl	---	23.1	---	1253%	---	0.87
chl > 1.5	+36%	31.4	-93%	88%	-1%	0.86
chl < 80	-45%	12.8	-2%	1228%	-34%	0.57
1.5 < chl < 80	-35%	15.1	-91%	118%	-49%	0.44

Table 21. Linear regression models for predicting chlorophyll concentrations in the Great Salt Lake sorted by RMS. The number of spectra used for each type of regression analysis: chlorophyll < 80 $\mu\text{g L}^{-1}$ (n=45), chlorophyll between 1.5 $\mu\text{g L}^{-1}$ and 80 $\mu\text{g L}^{-1}$ (n=18).

Type	Algorithm	RMS	Rel Error	r^2	
chl < 80					
Hyper	710/673	6.0	313%	0.90	
	705/675	6.1	332%	0.90	
	703/677	6.2	323%	0.90	
	710/665	6.3	364%	0.90	
	730/[675-695]	6.4	360%	0.89	
	754/[677-703]	6.8	597%	0.88	
	720/670	7.0	312%	0.87	
	740/[671-710]	7.4	749%	0.86	
	754/[665-709]	8.1	888%	0.83	
	725/665	8.5	450%	0.81	
	735/673	10.4	827%	0.71	
MERIS	709/(665:681)	6.2	350%	0.90	
	709/665	6.2	378%	0.90	
	754/[665-709]	8.0	879%	0.83	
MODIS	709s/(667:678)	12.7	1216%	0.57	
	709s/667	12.8	1240%	0.56	
	748/[667-709s]	13.0	1243%	0.55	
1.5 < chl < 80					
Hyper	740/[671-710]	7.6	51%	0.85	
	754/[665-709]	7.6	62%	0.86	
	710/673	8.1	44%	0.84	
	705/675	8.2	43%	0.83	
	710/665	8.2	52%	0.83	
	754/[677-703]	8.3	43%	0.83	
	703/677	8.6	42%	0.82	
	730/[675-695]	8.9	32%	0.80	
	720/670	10.0	40%	0.75	
	725/665	12.0	56%	0.64	
	735/673	13.4	85%	0.56	
	MERIS	754/[665-709]	7.6	62%	0.86
		709/665	8.0	54%	0.84
709/(665:681)		8.2	50%	0.83	
MODIS	709s/(667:678)	15.0	113%	0.44	
	748/[667-709s]	15.1	123%	0.43	
	709s/667	15.2	116%	0.43	

Table 22. Coefficients for log-log regressions (Table 13) relating spectral measurements to chlorophyll concentration in the Great Salt Lake using the restricted dataset (n=31). Factors added to correct otherwise negative values for the predictor variable - ^ - 0.005, * - 0.025, ** - 0.5.

Type	Algorithm	intercept	x	x ²	x ³	x ⁴
Hyper	710/673	1.362	3.492	-9.916	24.80	-21.45
	705/675	1.092	5.475	-15.89	32.37	-24.70
	703/677	0.991	6.311	-19.64	40.96	-31.72
	710/665	1.493	3.582	-9.037	21.64	-20.52
	MCI (665)^	143.6	216.3	110.6	18.94	---
	MCI (681)^	182.2	276.2	141.4	24.23	---
	730/[675-695]*	2.141	0.693	0.873	6.826	---
	MCI (677)^	179.7	274.8	142.4	24.79	---
	754/[677-703]**	-107.8	-3.041	1.690	2.098	2.182
	720/670	1.801	2.654	-4.301	2.578	0.341
	740/[671-710]**	2.587	1.534	-10.13	---	---
	754/[665-709]**	2.733	0.379	-14.25	---	---
	725/665	2.095	2.279	-3.635	---	---
	735/673	2.217	1.585	-2.066	---	---
MERIS	709/(665:681)	1.388	4.120	-11.69	28.47	-26.28
	709/665	1.450	4.760	-10.55	9.083	---
	709/681	1.293	5.197	-11.98	11.41	---
	MCI (665)^	158.7	238.4	121.3	20.68	---
	OC (489)	-3.273	-34.76	-83.15	-66.97	---
	MCI (681)^	212.5	321.1	163.5	27.85	---
	OC (443)	-5.734	-36.18	-60.47	-34.84	---
	754/[665-709]**	2.739	0.272	-14.67	---	---
	OC (510)	-6.300	-86.62	-311.7	-367.2	---
MODIS	OC (488)	-1.778	-23.57	-56.19	-47.24	---
	OC (443)	-4.362	-31.29	-55.56	-34.16	---
	MCI (678)^	-116.8	-173.1	-81.78	-12.45	---
	MCI (667)^	-116.4	-170.7	-79.75	-12.00	---
	709s/678	1.234	4.441	-0.639	-6.318	---
	748/[667-709s]**	1.565	3.428	2.476	---	---
SeaWiFS	709s/667	1.332	3.414	-2.341	---	---
	OC (489)	-2.540	-30.34	-75.22	-63.76	---
	OC (510)	-4.630	-74.32	-291.3	-373.9	---
	OC (443)	-5.013	-34.34	-60.42	-36.73	---

Figure 40. RMS values for linear chlorophyll estimation algorithms for New England lakes. The top graph displays hyperspectral algorithms, and the bottom graph displays MERIS and MODIS algorithms. Light gray bars indicate all chlorophyll, light blue bars indicate chlorophyll > 5 $\mu\text{g L}^{-1}$, cyan bars indicate chlorophyll < 50 $\mu\text{g L}^{-1}$, dark blue bars indicate 5 $\mu\text{g L}^{-1}$ and 50 $\mu\text{g L}^{-1}$ ($n=39$).

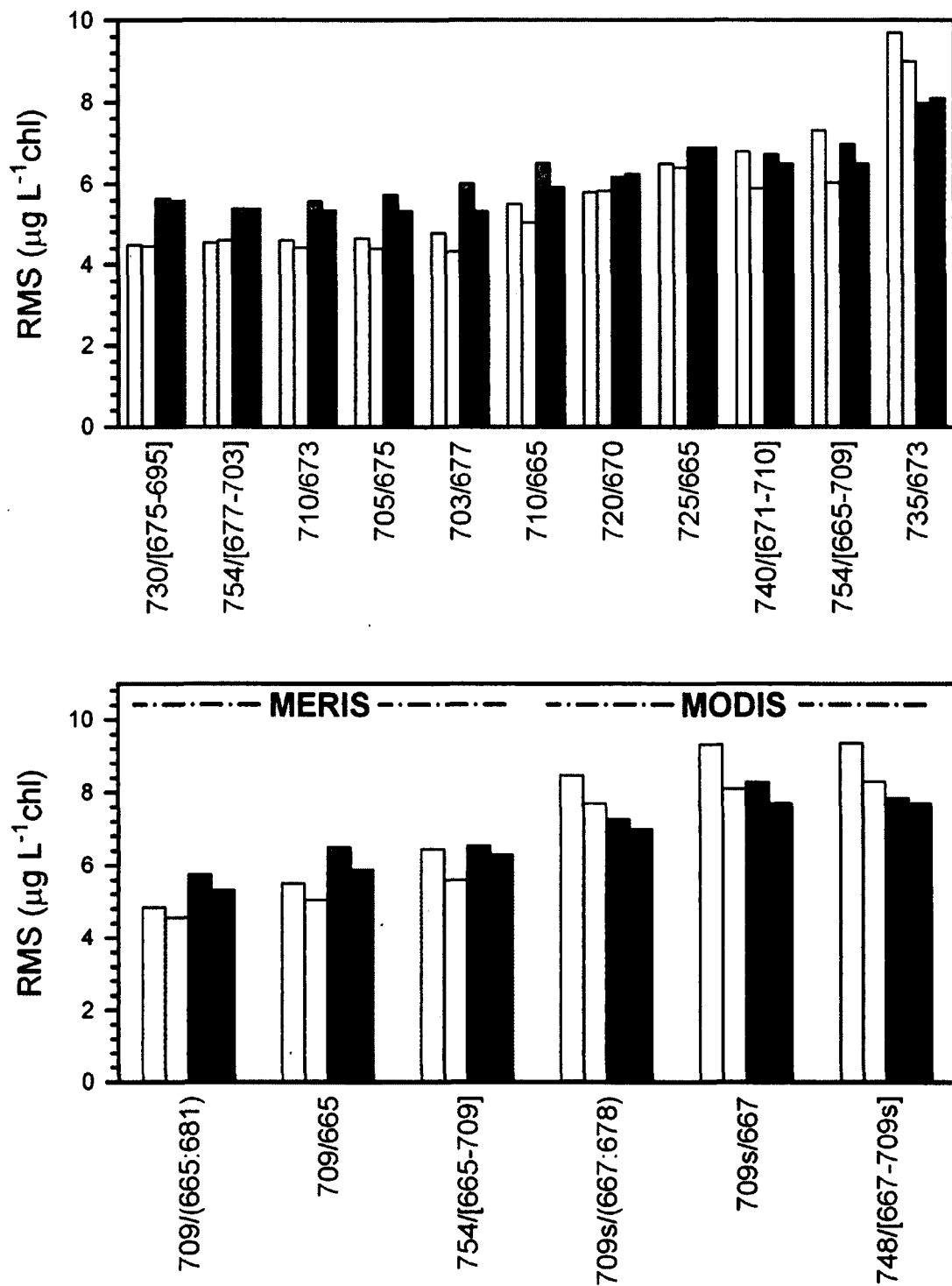


Figure 41. Best linear regression models using hyperspectral bands for predicting chlorophyll concentrations in New England lakes. The green lines represent relationships excluding chlorophyll values of less than 5 $\mu\text{g L}^{-1}$, while the regressions with red lines include all chlorophyll values. The three graphs on the left side include chlorophyll values greater than 50 $\mu\text{g L}^{-1}$, while the graphs on the right exclude chlorophyll values greater than 50 $\mu\text{g L}^{-1}$. The number of spectra used for each type of regression analysis: all chlorophyll (n=90), chlorophyll > 5 $\mu\text{g L}^{-1}$ (n=40), chlorophyll < 50 $\mu\text{g L}^{-1}$ (n=89), chlorophyll between 5 $\mu\text{g L}^{-1}$ and 50 $\mu\text{g L}^{-1}$ (n=39).

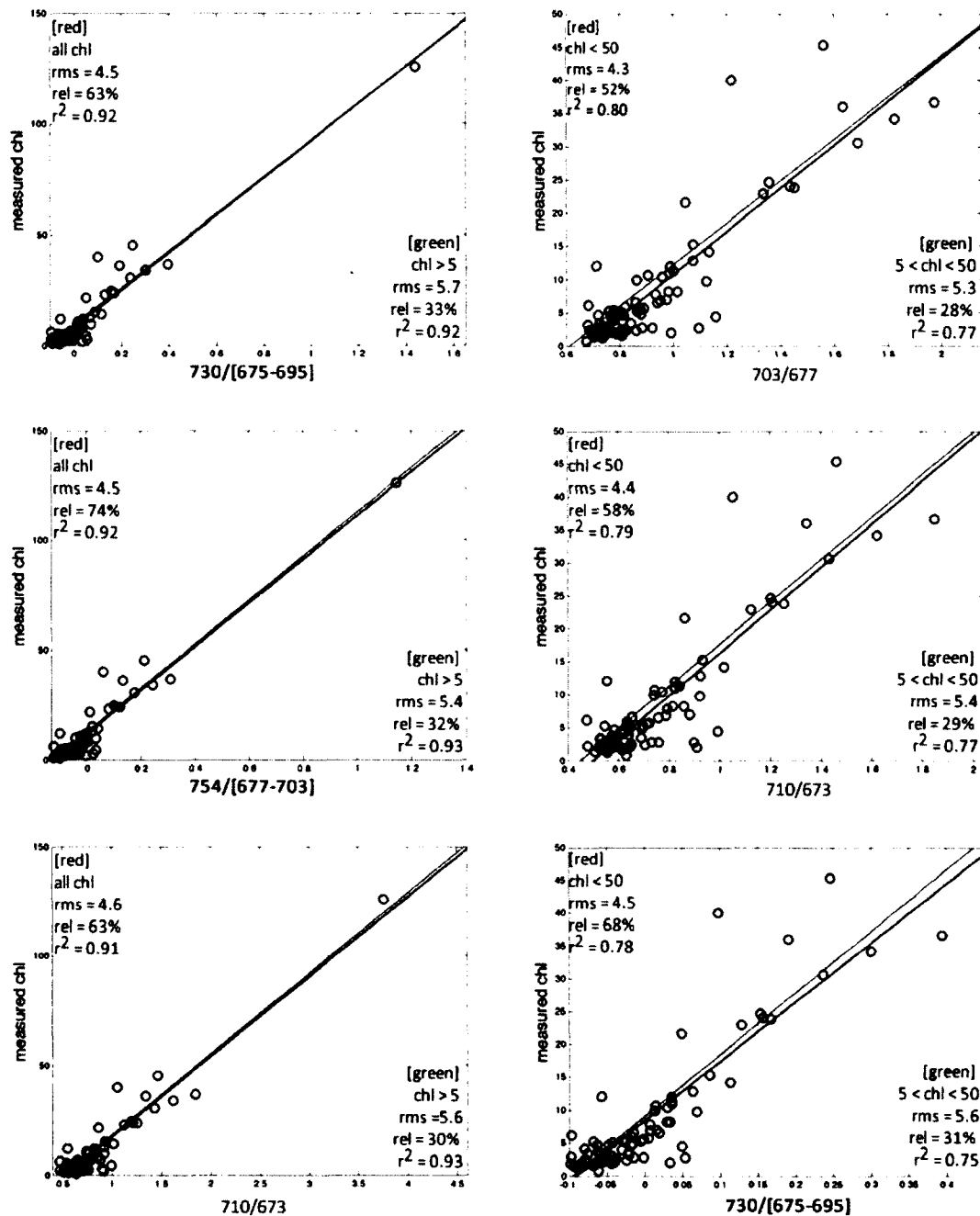


Figure 42. Best linear regression models using satellite sensor bands for predicting chlorophyll concentrations in the New England lakes. The green lines represent relationships excluding chlorophyll values of less than 5 $\mu\text{g L}^{-1}$, while the regressions with red lines include all chlorophyll values. The three graphs on the left side include chlorophyll values greater than 50 $\mu\text{g L}^{-1}$, while the graphs on the right exclude chlorophyll values greater than 50 $\mu\text{g L}^{-1}$. The number of spectra used for each type of regression analysis: all chlorophyll (n=90), chlorophyll > 5 $\mu\text{g L}^{-1}$ (n=40), chlorophyll < 50 $\mu\text{g L}^{-1}$ (n=89), chlorophyll between 5 $\mu\text{g L}^{-1}$ and 50 $\mu\text{g L}^{-1}$ (n=39). Satellite sensors bands used are (A) MERIS and (B) MODIS.

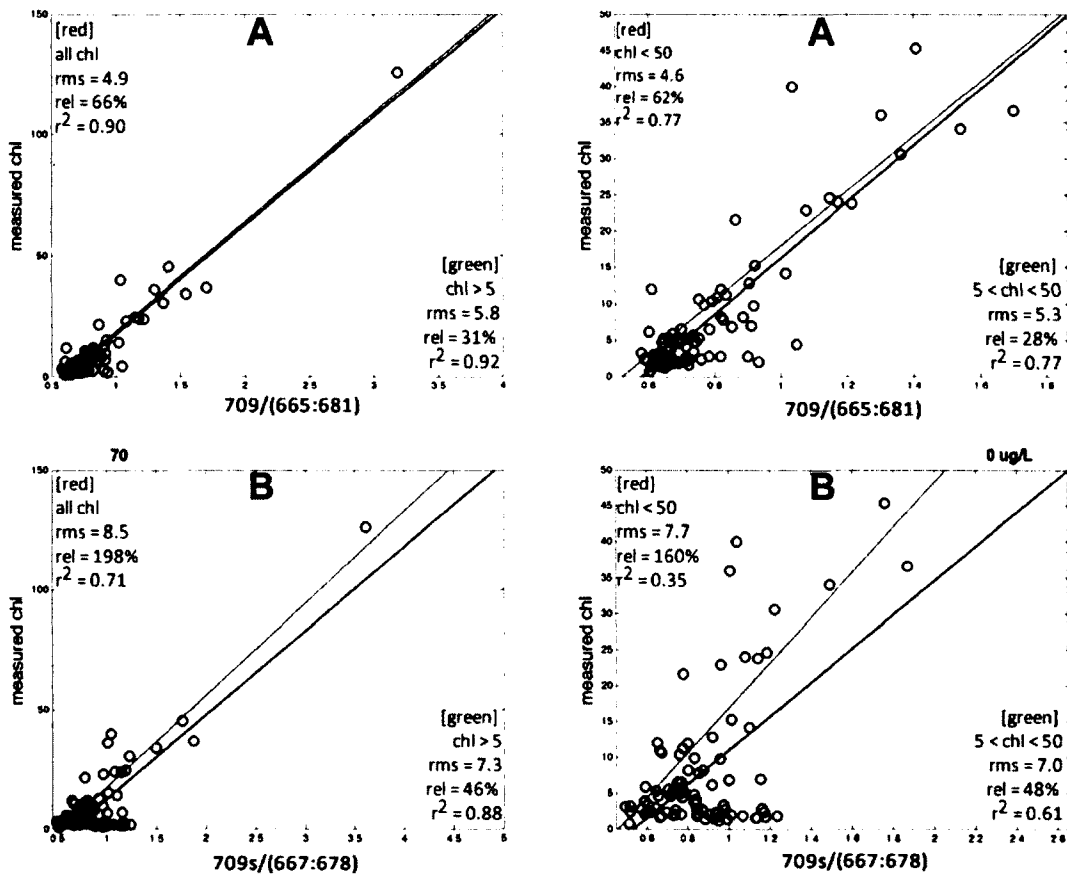


Figure 43. RMS values for linear chlorophyll estimation algorithms for the Great Salt Lake. The top graph displays hyperspectral algorithms, and the bottom graph displays MERIS and MODIS algorithms. Light gray bars indicate all chlorophyll, light blue bars indicate chlorophyll > 1.5 $\mu\text{g L}^{-1}$, cyan bars indicate chlorophyll < 80 $\mu\text{g L}^{-1}$, dark blue bars indicate 1.5 $\mu\text{g L}^{-1}$ and 80 $\mu\text{g L}^{-1}$ ($n=39$).

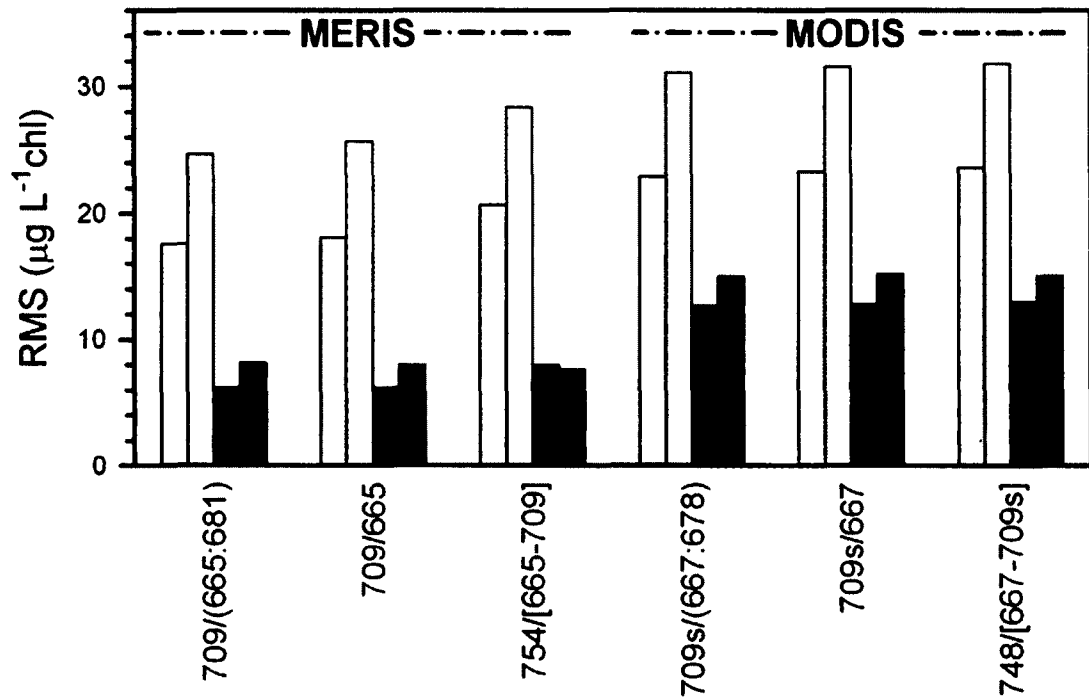
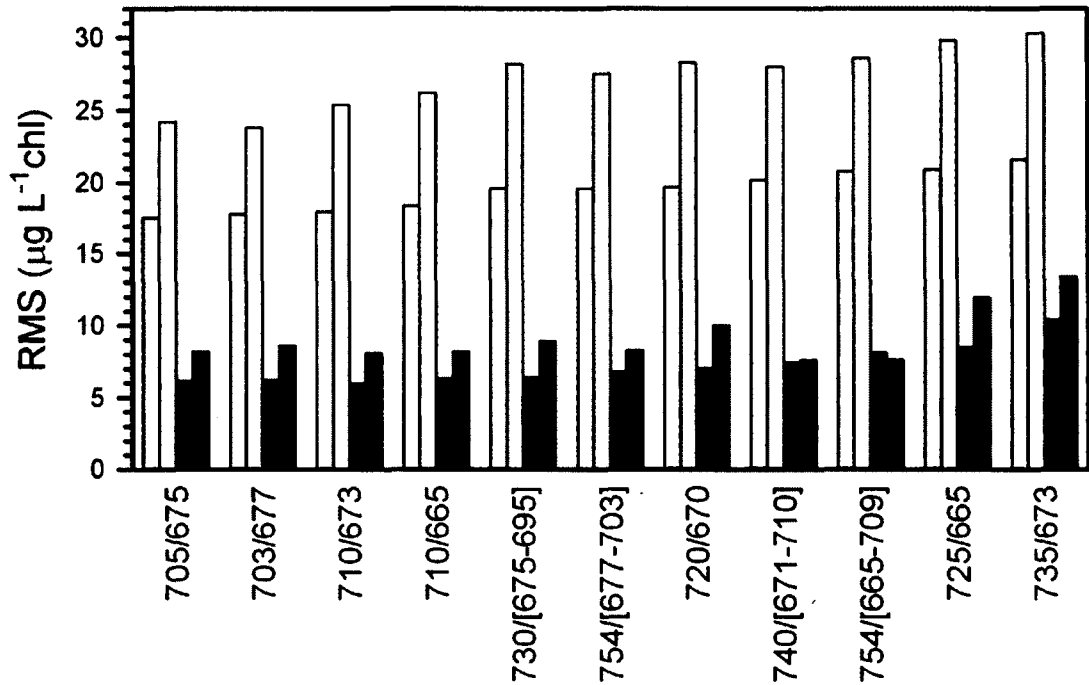


Figure 44. Best linear regression models using hyperspectral bands for predicting chlorophyll concentrations in the Great Salt Lake. The green lines represent relationships excluding chlorophyll values of less than $1.5 \mu\text{g L}^{-1}$, while the regressions with red lines include all chlorophyll values. The three graphs on the left side include chlorophyll values greater than $80 \mu\text{g L}^{-1}$, while the graphs on the right exclude chlorophyll values greater than $80 \mu\text{g L}^{-1}$. The number of spectra used for each type of regression analysis: all chlorophyll ($n=48$), chlorophyll $> 1.5 \mu\text{g L}^{-1}$ ($n=22$), chlorophyll $< 80 \mu\text{g L}^{-1}$ ($n=45$), chlorophyll between $1.5 \mu\text{g L}^{-1}$ and $80 \mu\text{g L}^{-1}$ ($n=18$).

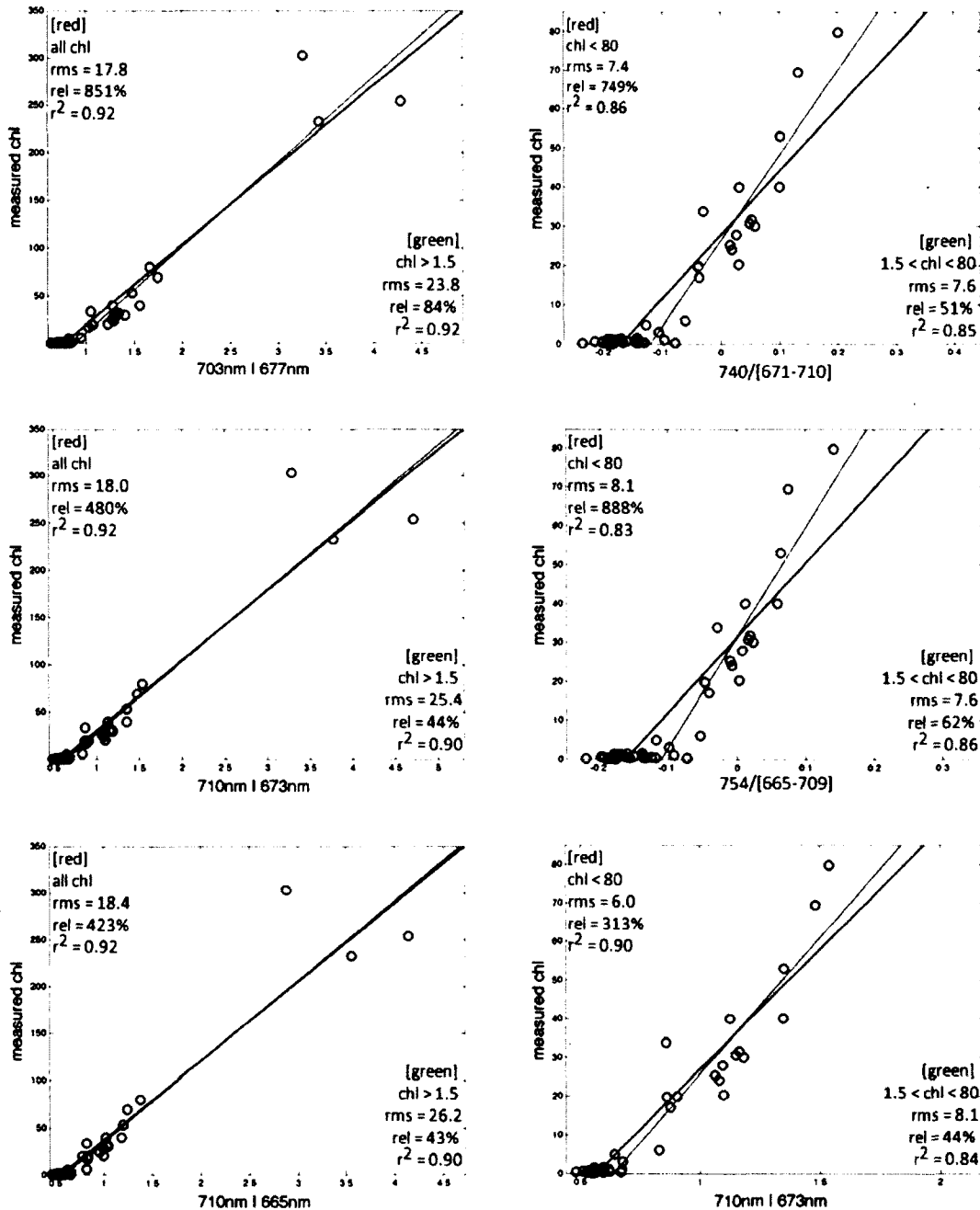
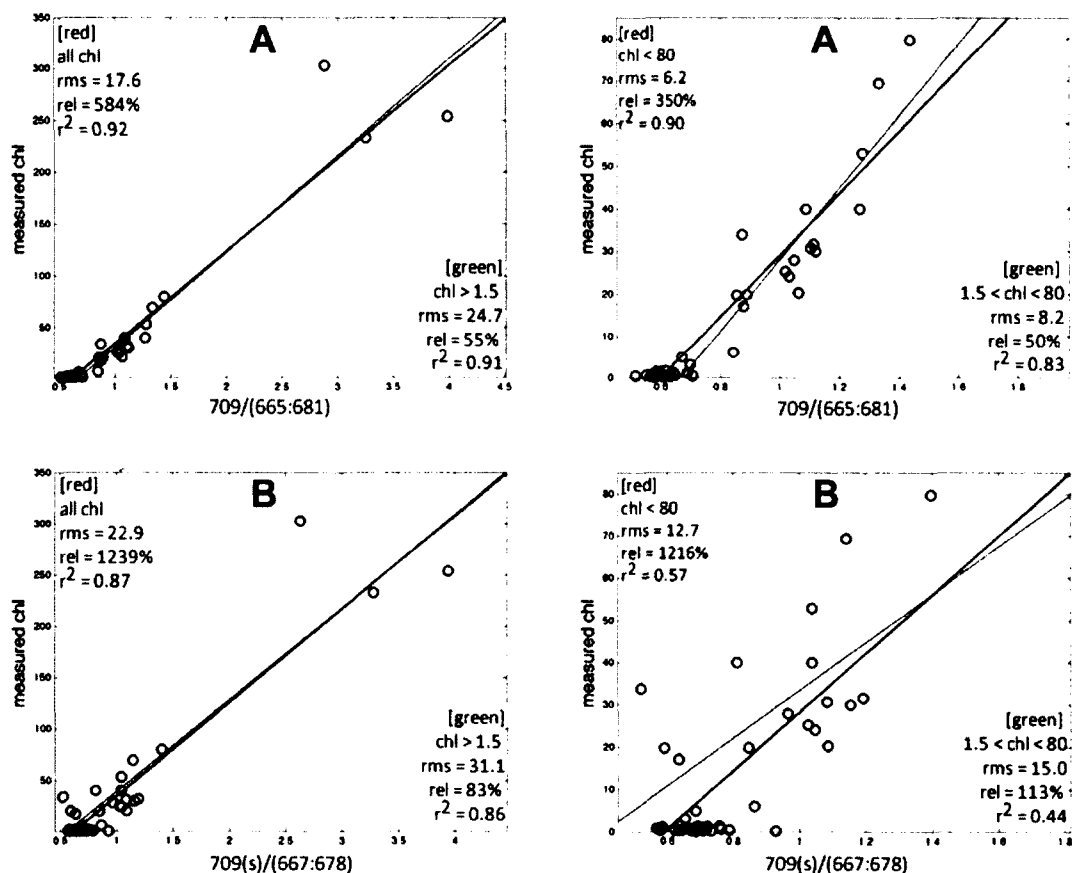


Figure 45. Best linear regression models using satellite sensor bands for predicting chlorophyll concentrations in the Great Salt Lake. The green lines represent relationships excluding chlorophyll values of less than $1.5 \mu\text{g L}^{-1}$, while the regressions with red lines include all chlorophyll values. The three graphs on the left side include chlorophyll values greater than $80 \mu\text{g L}^{-1}$, while the graphs on the right exclude chlorophyll values greater than $80 \mu\text{g L}^{-1}$. The number of spectra used for each type of regression analysis: all chlorophyll ($n=48$), chlorophyll $> 1.5 \mu\text{g L}^{-1}$ ($n=22$), chlorophyll $< 80 \mu\text{g L}^{-1}$ ($n=45$), chlorophyll between $1.5 \mu\text{g L}^{-1}$ and $80 \mu\text{g L}^{-1}$ ($n=18$). Satellite sensors bands used are (A) MERIS and (B) MODIS.



LITERATURE CITED

- Ahn, Y.-H., and P. Shanmugam. 2006. Detecting the red tide algal blooms from satellite ocean color observations in optically complex Northeast-Asia Coastal waters. *Remote Sensing of Environment* **103**: 419–437.
- Anderson, D. M. 2009. Approaches to monitoring, control and management of harmful algal blooms (HABs). *Ocean and Coastal Management* **52**: 342–347
- APHA, WPCF, AWWA. 1998. *Standard Methods for the Examination of Water and Wastewater*, 20th ed. L.S. Clesceri, A.E. Greenberg, and A.D. Eaton [eds.]. American Public Health Association.
- Banack, S. A., T. A. Caller, and E. W. Stommel. 2010. The cyanobacteria derived toxin beta-N-methylamino-L-alanine and amyotrophic lateral sclerosis. *Toxins* **2**: 2837–2850.
- Behrenfeld, M. J., R. T. O'Malley, D. A. Siegel, C. R. McClain, J. L. Sarmiento, G. C. Feldman, A. J. Milligan, P. G. Falkowski, R. M. Letelier, and E. S. Boss. 2006. Climate-driven trends in contemporary ocean productivity. *Nature* **444**: 752–755
- Binding, C. E., T. A. Greenberg, and R. P. Bukata. 2011. Time series analysis of algal blooms in Lake of the Woods using the MERIS maximum chlorophyll index. *Journal of Plankton Research* **33**: 1847–1852
- Binding, C. E., T. A. Greenberg, R. P. Bukata, D. E. Smith, and M. R. Twiss. 2012. The MERIS MCI and its potential for satellite detection of winter diatom blooms on partially ice-covered Lake Erie. *Journal of Plankton Research* **34**: 569–573
- Bradt, S. R., W. A. Wurtsbaugh, D. L. Naftz, T. Moore, and J. F. Haney. 2008. The use of remote sensing to track phytoplankton in the Great Salt Lake, Utah, USA. *The 10th International Conference on Salt Lake Research*.

- Burgess, C. 2001. A wave of momentum for toxic algae study. *Environ. Health Perspect.* **109**: A160–1.
- Carlson, R. E. 1977. A trophic state index for lakes. *Limnology and Oceanography* **22**: 361–369.
- Carmichael, W. W. 2001. Health Effects of Toxin-Producing Cyanobacteria: “The CyanoHABs.” *Human and Ecological Risk Assessment: An International Journal* **7**: 1393–1407
- Chorus, I., I. R. Falconer, H. J. Salas, and J. Bartram. 2000. Health risks caused by freshwater cyanobacteria in recreational waters. *Journal of Toxicology and Environmental Health, Part B* **3**: 323–347
- Codd, G. 1995. Cyanobacterial toxins: occurrence, properties and biological significance. *Water Science & Technology* **32**: 149–156.
- Codd, G. A., L. F. Morrison, and J. S. Metcalf. 2005. Cyanobacterial toxins: risk management for health protection. *Toxicology and Applied Pharmacology* **203**: 264–272
- Cooper, S. D., D. W. Winkler, and P. H. Lenz. 1984. The Effect of Grebe Predation on a Brine Shrimp Population. *J Anim Ecol* **53**: 51–64.
- Dall’Olmo, G., and A. A. Gitelson. 2005. Effect of bio-optical parameter variability on the remote estimation of chlorophyll-a concentration in turbid productive waters: experimental results. *Applied Optics* **44**: 412–422
- Dall’Olmo, G., and A. A. Gitelson. 2006. Effect of bio-optical parameter variability and uncertainties in reflectance measurements on the remote estimation of chlorophyll-a concentration in turbid productive waters: modeling results. *Applied Optics* **45**: 3577–3592.
- Doxaran, D., R. C. N. Cherukuru, and S. J. Lavender. 2005. Use of reflectance band ratios to estimate suspended and dissolved matter concentrations in estuarine waters. *International Journal of Remote Sensing* **26**: 1763–1769

- Duan, H., R. Ma, Y. Zhang, S. A. Loiselle, J. Xu, C. Zhao, L. Zhou, and L. Shang. 2010. A new three-band algorithm for estimating chlorophyll concentrations in turbid inland lakes. *Environ. Res. Lett.* **5**: 044009
- EPA, U. S. 2009. National Lakes Assessment. EPA 841-R-09-001. EPA 841-R-09-001 U.S. Environmental Protection Agency, Office of Water and Office of Research and Development.
- Falconer, I. R. 1996. Tumour promotion by cyanobacterial toxins. *Phycologia*.
- Gilerson, A., J. Zhou, S. Hlaing, I. Ioannou, J. Schalles, B. Gross, F. Moshary, and S. Ahmed. 2007. Fluorescence component in the reflectance spectra from coastal waters. Dependence on water composition. *Optics Express* **15**: 15702–15721.
- Gitelson, A. 1992. The peak near 700 nm on radiance spectra of algae and water: relationships of its magnitude and position with chlorophyll concentration. *International Journal of Remote Sensing* **13**: 3367–3373.
- Gitelson, A. A., B.-C. Gao, R.-R. Li, S. Berdnikov, and V. Sapygin. 2011a. Estimation of chlorophyll-a concentration in productive turbid waters using a Hyperspectral Imager for the Coastal Ocean—the Azov Sea case study. *Environ. Res. Lett.* **6**: 024023
- Gitelson, A. A., D. Gurlin, W. J. Moses, and T. Barrow. 2009. A bio-optical algorithm for the remote estimation of the chlorophyll-a concentration in case 2 waters. *Environ. Res. Lett.* **4**: 045003
- Gitelson, A. A., J. F. Schalles, and C. M. Hladik. 2007. Remote chlorophyll-a retrieval in turbid, productive estuaries: Chesapeake Bay case study. *Remote Sensing of Environment* **109**: 464–472
- Gitelson, A. A., J. F. Schalles, D. C. Rundquist, F. R. Schiebe, and Y. Z. Yacobi. 1999. Comparative reflectance properties of algal cultures with manipulated densities. *Journal of Applied Phycology* **11**: 345–354.

- Gitelson, A. A., Y. Z. Yacobi, J. F. Schalles, D. C. Rundquist, L. Han, R. Stark, and D. Etzion. 2000. Remote estimation of phytoplankton density in productive waters. *Arch. Hydro. Spec. Issues Advanc. Limnol.* **55**: 121–136.
- Gitelson, A., D. Gurlin, W. Moses, and Y. Yacobi. 2011b. Remote Estimation of Chlorophyll-a Concentration in Inland, Estuarine, and Coastal Waters, p. 449–478. *In Advances in Environmental Remote Sensing, Sensors: Algorithms, and applications.* CRC Press, Taylor and Francis Group.
- Gons, H. J., M. T. Auer, and S. W. Effler. 2008. MERIS satellite chlorophyll mapping of oligotrophic and eutrophic waters in the Laurentian Great Lakes. *Remote Sensing of Environment* **112**: 4098–4106
- Gower, J. 1980. *Boundary-Layer Meteorology*, Volume 18, Number 3 - SpringerLink. *Boundary-Layer Meteorology*.
- Gower, J. F. R., R. Doerffer, and G. A. Borstad. 1999. Interpretation of the 685nm peak in water-leaving radiance spectra in terms of fluorescence, absorption and scattering, and its observation by MERIS. *International Journal of Remote Sensing* **20**: 1771–1786
- Gower, J., C. Hu, G. Borstad, and S. King. 2006. Ocean color satellites show extensive lines of floating sargassum in the Gulf of Mexico. *IEEE T Geosci Remote* **44**: 3619–3625
- Gower, J., S. King, and P. Goncalves. 2008. Global monitoring of plankton blooms using MERIS MCI. *International Journal of Remote Sensing* **29**: 6209–6216
- Gower, J., S. King, G. Borstad, and L. Brown. 2005a. Detection of intense plankton blooms using the 709 nm band of the MERIS imaging spectrometer. *International Journal of Remote Sensing* **26**: 2005–2012
- Gower, J., S. Kings, G. Borstad, and L. Brown. 2005b. Use of the 709 nm band of MERIS to detect intense plankton blooms and other conditions in coastal waters. *Proceedings of the Proc. of the 2004 Envisat & ERS Symposium.* 1–4.

- Gurlin, D., A. A. Gitelson, and W. J. Moses. 2011. Remote estimation of chl-a concentration in turbid productive waters — Return to a simple two-band NIR-red model? *Remote Sensing of Environment* **115**: 3479–3490
- Han, L., and D. Rundquist. 1997. Comparison of NIR/RED ratio and first derivative of reflectance in estimating algal-chlorophyll concentration: A case study in a turbid reservoir. *Remote Sensing of Environment* **33**: 253–261.
- Harbinson, J., and E. Rosenqvist. 2003. An Introduction to Chlorophyll Fluorescence, p. 1–29. *In* J. DeEll and P. Toivonen [eds.], *Practical Applications of Chlorophyll Fluorescence in Plant Biology*. Springer.
- He, M. X., Y. Wang, L. Hu, Q. Yang, S. HE, and C. Hu. 2008. Detection of red tides using MERIS 681 nm and 709 nm bands in the East China Sea: A case study. *Proc Dragon*.
- Hu, C. 2009. A novel ocean color index to detect floating algae in the global oceans. *Remote Sensing of Environment* **113**: 2118–2129
- Hu, C. M., F. E. Muller-Karger, C. Taylor, K. L. Carder, C. Kelble, E. Johns, and C. A. Heil. 2005. Red tide detection and tracing using MODIS fluorescence data: A regional example in SW Florida coastal waters. *Remote Sensing of Environment* **97**: 311–321
- Hu, C., Z. Lee, R. Ma, K. Yu, D. Li, and S. Shang. 2010. Moderate Resolution Imaging Spectroradiometer (MODIS) observations of cyanobacteria blooms in Taihu Lake, China. *J. Geophys. Res.* **115**
- Irwin, A. J., and M. J. Oliver. 2009. Are ocean deserts getting larger? *Geophysical Research Letters* **36**: L18609
- Izaguirre, G., C. J. Hwang, S. W. Krasner, and M. J. McGuire. 1983. Production of 2-Methyliso-Borneol by Two Benthic Cyanophyta. *Water Science & Technology* **15**.
- Jacoby, J. M., and J. Kann. 2007. The occurrence and response to toxic cyanobacteria in the Pacific Northwest, North America. *Proceedings of the Lake and Reservoir Management*. 123–143.

- Jones, G., and I. Chorus. 2001. Toxic cyanobacteria--towards a global perspective. Proceedings of the Fifth International Conference on Toxic Cyanobacteria. 456–571.
- Letelier, R., and M. Abbott. 1996. An analysis of chlorophyll fluorescence algorithms for the moderate resolution imaging spectrometer (MODIS). *Remote Sensing of Environment* **58**: 215–223.
- Lind, O. T. 1985. Handbook of common methods in limnology, 2nd ed. Iowa: Kendall Hunt.
- Maritorena, S., D. Siegel, and A. Peterson. 2002. Optimization of a semianalytical ocean color model for global-scale applications. *Applied Optics* **41**: 2705–2714.
- Mobley, C. 1999. Estimation of the remote-sensing reflectance from above-surface measurements. *Applied Optics* **38**: 7442–7455.
- Mobley, C. 2004. *Light and Water*. 1–39.
- Morel, A., and L. Prieur. 1977. Analysis of variations in ocean color. *Limnology and Oceanography* 709–722.
- Moses, W. J., A. A. Gitelson, R. L. Perk, D. Gurlin, D. C. Rundquist, B. C. Leavitt, T. M. Barrow, and P. Brakhage. 2012. Estimation of chlorophyll-a concentration in turbid productive waters using airborne hyperspectral data. *Water Research* **46**: 993–1004
- O'Reilly, J. E., S. Maritorena, M. C. O'Brien, D. A. Siegel, D. Toole, D. Menzies, R. C. Smith, J. L. Mueller, B. G. Mitchell, M. Kahru, F. P. Chavez, P. Strutton, G. F. Cota, S. B. Hooker, C. R. McClain, K. L. Carder, F. Müller-Karger, L. Harding, A. Magnuson, D. Phinney, G. F. Moore, J. Aiken, K. R. Arrigo, R. Letelier, and M. Culver. 2000. SeaWiFS Postlaunch Technical Report Series. NASA Technical Memo 2000-206892. NASA Technical Memo 2000-206892 NASA Goddard Space Flight Center.

- O'Reilly, J., S. Maritorena, B. Mitchell, D. Siegel, K. Carder, S. Garver, M. Kahru, and C. McClain. 1998. Ocean color chlorophyll algorithms for SeaWiFS. *J Geophys Res-Oceans* **103**: 24937–24953.
- Oki, T., and S. Kanae. 2006. Global Hydrological Cycles and World Water Resources. *Science* **313**: 1068–1072
- Ouellette, A., S. M. Handy, and S. W. Wilhelm. 2006. *Microbial Ecology*, Volume 51, Number 2 - SpringerLink. Microbial ecology.
- Paerl, H. W., and V. J. Paul. 2012. Climate change: Links to global expansion of harmful cyanobacteria. *Water Research* **46**: 1349–1363
- Pauly, K., R. Goossens, and O. De Clerck. 2011. Mapping coral-algal dynamics in a seasonal upwelling area using spaceborne high resolution sensors. *ESA Special Publications* **686**.
- Polovina, J. J., E. A. Howell, and M. Abecassis. 2008. Ocean's least productive waters are expanding. *Geophysical Research Letters* **35**: L03618
- Quan, X., and E. S. Fry. 1995. Empirical equation for the index of refraction of seawater. *Applied Optics* **34**: 3477–3480.
- Repavich, W. M., W. C. Sonzogni, J. H. Standridge, R. E. Wedepohl, and L. F. Meisner. 1990. Cyanobacteria (Blue-Green-Algae) in Wisconsin Waters: Acute and Chronic Toxicity. *Water Research* **24**: 225–231.
- Rundquist, D., L. Han, J. Schalles, and J. Peake. 1996. Remote measurement of algal chlorophyll in surface waters: The case for the first derivative of reflectance near 690 nm. *Photogramm Eng Rem S* **62**: 195–200.
- Schalles, J., A. Gitelson, Y. Yacobi, and A. Kroenke. 1998. Estimation of chlorophyll a from time series measurements of high spectral resolution reflectance in an eutrophic lake. *Journal of Phycology* **34**: 383–390.
- Sivonen, K., S. I. Niemela, R. M. Niemi, L. Lepisto, T. H. Luoma, and L. A. Rasanen. 1990. Toxic Cyanobacteria (Blue-Green-Algae) in Finnish Fresh and Coastal Waters. *Hydrobiologia* **190**: 267–275.

- Slatkin, D. N., R. D. Stoner, W. H. Adams, J. H. Kycia, and H. W. Siegelman. 1983. Atypical Pulmonary Thrombosis Caused by a Toxic Cyanobacterial Peptide. *Science* **220**: 1383–1385.
- Smith, V. H., J. Sieber-Denlinger, F. deNoyelles Jr., S. Campbell, S. Pan, S. J. Randtke, G. T. Blain, and V. A. Strasser. 2002. Managing Taste and Odor Problems in a Eutrophic Drinking Water Reservoir. *Lake and Reservoir Management* **18**: 319–323
- Stephens, D. W. 1990. Changes in lake levels, salinity and the biological community of Great Salt Lake (Utah, USA), 1847–1987. *Hydrobiologia* **197**: 139–146
- Stewart, I., P. M. Webb, P. J. Schluter, and G. R. Shaw. 2006. Recreational and occupational field exposure to freshwater cyanobacteria – a review of anecdotal and case reports, epidemiological studies and the challenges for epidemiologic assessment. *Environ Health* **5**: 6
- Strayer, D. L., and D. Dudgeon. 2010. Freshwater biodiversity conservation: recent progress and future challenges. *J N Am Benthol Soc* **29**: 344–358
- Tedesco, M., and N. Steiner. 2011. In-situ multispectral and bathymetric measurements over a supraglacial lake in western Greenland using a remotely controlled watercraft. *The Cryosphere* **5**: 445–452
- Turner, P. C., A. J. Gammie, K. Hollinrake, and G. A. Codd. 1990. Pneumonia associated with contact with cyanobacteria. *BMJ* **300**: 1440–1441.
- Ueno, Y., S. Nagata, T. Tsutsumi, A. Hasegawa, M. F. Watanabe, H. D. Park, G. C. Chen, G. Chen, and S. Z. Yu. 1996. Detection of microcystins, a blue-green algal hepatotoxin, in drinking water sampled in Haimen and Fusui, endemic areas of primary liver cancer in China, by highly sensitive immunoassay. *Carcinogenesis* **17**: 1317–1321.
- USEPA. 2010. Gauging the Health of New England's Lakes and Ponds. US Environmental Protection Agency.

- Vadeboncoeur, Y., P. B. McIntyre, and M. J. Vander Zandan. 2011. Borders of Biodiversity: Life at the Edge of the World's Large Lakes. *BioScience* **61**.
- Watson, S. B. 2004. AQUATIC TASTE AND ODOR: A PRIMARY SIGNAL OF DRINKING-WATER INTEGRITY. *Journal of Toxicology and Environmental Health, Part A* **67**: 1779–1795
- Welschmeyer, N. A. 1994. Fluorometric analysis of chlorophyll a in the presence of chlorophyll b and pheopigments. *Limnology and Oceanography* **39**.
- Wetzel, R. G. 1983. *Limnology*, W.B. Saunders Co.
- White, P., K. Robinette, and F. Howe. 1992. 1992 Great Salt Lake eared grebe survey
 . Unpublished Report, Utah Division of Wildlife Resources.
- Williams, W. D. 1998. *Hydrobiologia*, Volume 381, Numbers 1-3 - SpringerLink. *Hydrobiologia*.
- Williamson, C. E., J. E. Saros, W. Vincent, and J. P. Smold. 2009. Lakes and reservoirs as sentinels, integrators, and regulators of climate change. *Limnology and Oceanography* **54**.
- Wurtsbaugh, W. A. 1992. Food-Web Modification by an Invertebrate Predator in the Great-Salt-Lake (Usa). *Oecologia* **89**: 168–175.
- Xing, X., D. Zhao, Y. Liu, J. Yang, and P. Xiu. 2007. An Overview of Remote Sensing of Chlorophyll Fluorescence. *Ocean Science Journal* **42**: 49–59.
- Yacobi, Y. Z., W. J. Moses, S. Kaganovsky, B. Sulimani, B. C. Leavitt, and A. A. Gitelson. 2011a. NIR-red reflectance-based algorithms for chlorophyll-a estimation in mesotrophic inland and coastal waters: Lake Kinneret case study. *Water Research* **45**: 2428–2436
- Yacobi, Y., W. Wesley, S. Kaganovsky, B. Sulimani, B. Leavitt, and A. Gitelson. 2011b. Chlorophyll a in turbid productive waters: testing the limits of NIR-Red algorithms. *Proceedings of the ESA Living Planet Symposium*. 1–7.